HEAT-FLOW MEASUREMENTS AT SHOT POINTS ALONG THE 1978 SAUDI ARABIAN SEISMIC DEEP-REFRACTION LINE, PART 1: RESULTS OF THE MEASUREMENTS

by

M. E. Gettings and A. Showail

U.S. Geological Survey
Open-File Report 82-793

Report prepared for the
Ministry of Petroleum and Mineral Resources
Deputy Ministry for Mineral Resources
Jiddah, Kingdom of Saudi Arabia
1402 AH 1982 AD

1982

CONTENTS

ILLUSTRATIONS

Page

Figures 10-58. Observed temperature versus depth profile for-Continued

TABLES

HEAT-FLOW MEASUREMENTS AT SHOT POINTS ALONG THE 1978 SAUDI ARABIAN SEISMIC DEEP-REFRACTION LINE, PART 1: RESULTS OF THE MEASUREMENTS

by

M. E. Gettings and A. Showail

ABSTRACT

Heat-flow measurements were made at five onland shot points of the 1978 Saudi Arabian seismic deep-refraction line, which sample major tectonic elements of the Arabian Shield along a profile from Ar Riyad to the Farasan Islands. Because of the pattern drilling at each shot point, several holes (60 m deep) could be logged for temperature at each site and thus allow a better estimate of the geothermal gradient. Each site was mapped and sampled in detail, and modal and chemical analyses of representative specimens were made in the laboratory. Thermal conductivities were computed from the modal analyses and single-mineral conductivity data.

The resulting heat-flow values, combined with published values for the Red Sea and coastal plain, indicate a three-level pattern, with a heat flow of about 4.5 heat-flow unit (HFU) over the Red Sea axial trough, about 3.0 HFU over the shelf and coastal plain, and an essentially constant 1.0 HFU over the Arabian Shield at points well away from the suture zone with the oceanic crust. At three sites where the rocks are granitic, gamma-ray spectrometry techniques were employed to estimate thorium, potassium, and uranium concentrations. The resulting plot of heat generation versus heat flow suggests that in the Arabian Shield the relationship between heat flow and heat production is not linear. More heat-flow data are essential to establish or reject this conclusion.

INTRODUCTION

With the single exception of Mansiyah I, lat 17.22° N., long 42.37° E. (Girdler, 1970), heat-flow measurements in the Kingdom of Saudi Arabia have not been published. The field-operations phase of the seismic deep-refraction line across the Precambrian Saudi Arabian Shield (Blank and others, 1979) was carried out in January and February of 1978. Geothermal-gradient measurements were obtained from several drill holes at five shot points (SP1-SP5), each about 200 km apart, across the southern Shield. The locations of the shot points and the generalized geology are shown in figure 1.

Shot point 1, (SP1) the only shot point not in Precambrian rocks, is located on Permian or Triassic shales of the Phanerozoic platform about 40 km from the eastern edge of the Shield. The rocks of the platform are essentially undeformed and dip gently (1°-2°) east. The sedimentary

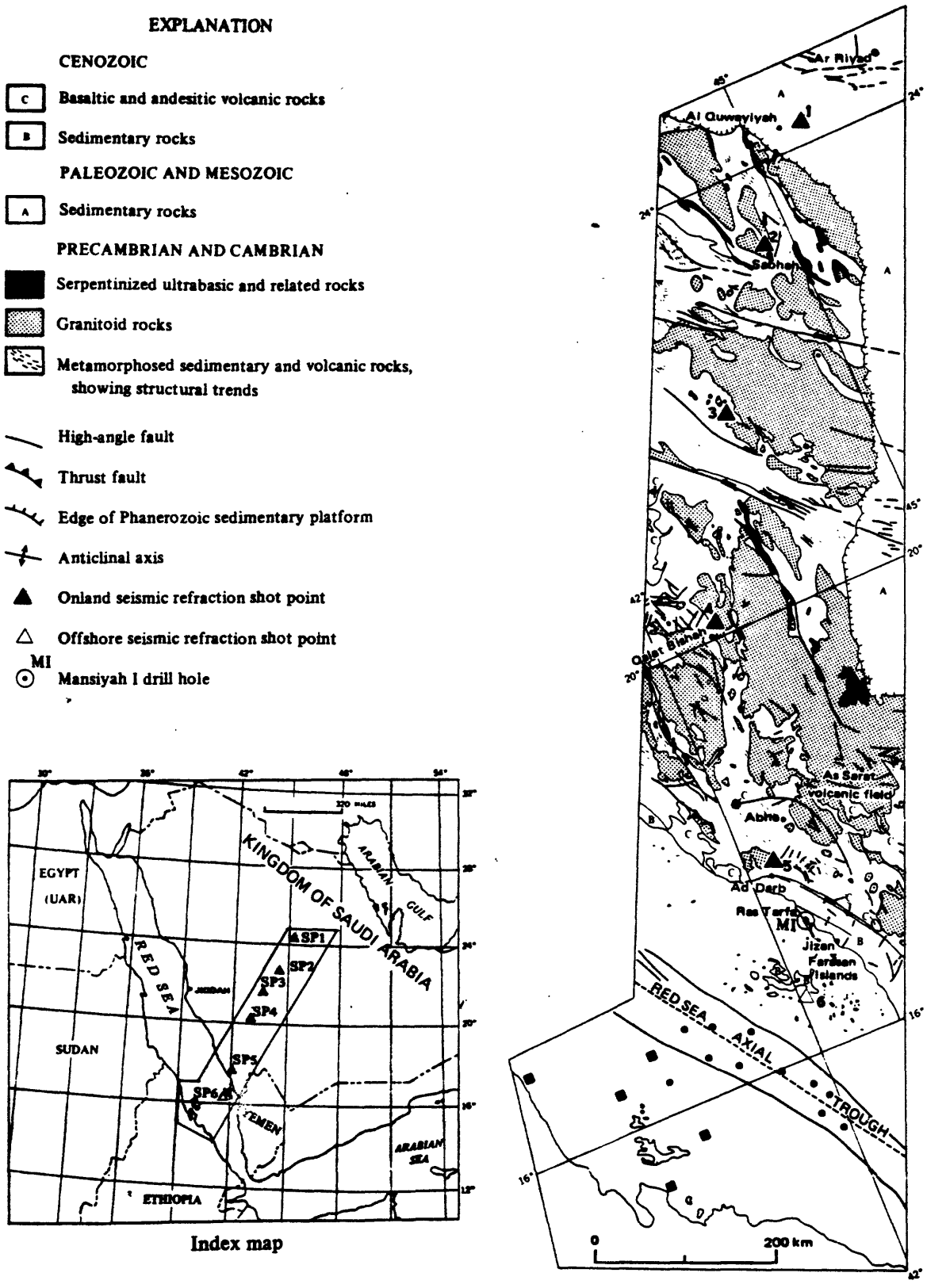

Figure 1.–Generalized geologic map showing the locations of the shot points of the 1978 seismic deep-refraction line (numbered points) and the locations of other heat-flow observations on the coastal plain and in the Red Sea. Coastal plain and Red Sea heat-flow data are from Girdler and Evans (1977), and geologic data is generalized from Brown (1972). In the Red Sea, square symbols are shallow-water (shelf) observations, and round symbols are deep-water (> 1 km) measurements. Point labeled "MI" is the 4 km-deep, petroleum exploration drill hole Mansiyah I. Dashed line in the Red Sea is an arbitrarily defined axis of the deep-water trough, chosen as a single straight line through the deepest water south of lat 20°N.

rocks of the platform overlying the Shield are about 500 m thick at this locality (Brown, 1972).

Shot point 2 (SP2) is located on calcareous chlorite and sericite schist and greenstone near the edge of a large, postorogenic (490-600 million years (m.y.) old) granite intrusion (Brown, 1972). The schist is highly deformed and commonly exhibits chevron folding.

Shot point 3 (SP3) is located in a large, postorogenic granitic intrusion, which contains several large xenoliths of Halaban andesite (Schmidt and others, 1979). This locality is in the central part of the left- lateral strike-slip Najd fault system, a major tectonic feature that strikes northwest across the Arabian Shield.

Shot point 4 (SP4) is located on late-orogenic, metamorphosed gneissic granite, probably 600-650 m.y. in age (Brown, 1972). This locality, together with SP2 and SP3, is in the "Halaban crust" of Schmidt and others (1979), whereas SP1 is in the sedimentary rocks overlying the "allochthonus continent" (Schmidt and others, 1979).

Shot point 5 (SP5) is located on chlorite-sericite schist of the Ablah formation (G. M. Fairer, oral commun., 1979) in the "Jiddah crust" of Schmidt and others (1979). This site is about 5 km east of the eastern edge of the Miocene Tihamat Asir ophiolite (Coleman and others, 1979), which is thought to represent the eastern edge of oceanic crust formed during the opening of the Red Sea in Tertiary time. The single previously reported heat-flow measurement for Saudi Arabia was made on the Red Sea coast at the head of the bay behind Ras Tarfa (fig. 1). At this site six bottom-hole temperature measurements from a 4-km-deep drill hole in Tertiary sedimentary rocks yielded a heat flow of 2.7 HFU (heat-flow unit, equal to 1E-6 cal-cm^{-2}-s^{-1} or 4.1868E-2 Wm^{-2}) (Girdler, 1970).

These six sites thus sample the major tectonic elements of the southern Saudi Arabian Shield. In this report we present the results of thermal-gradient measurements at the shot points, heat-flow values derived from them together with estimates of thermal conductivity, detailed geologic information at the shot points, and the results of heat-production measurements of the granitic rocks. Although the drill holes at the shot points were shallow (~60 m), temperature-profile measurements of several holes in the grid pattern, together with interpretation of detailed geologic relationships observed at each site, result in a reasonably reliable value for the geothermal gradient.

We would like to thank G. M. Fairer for assistance during the geologic fieldwork and D. B. Stoeser, A. H. El Bazli, F. Elsass, J. J. Matzko, and I. M. Naqvi, all of the U.S. Geological Survey (USGS) Saudi Arabian Mission, for their work in mineral identification. The temperature logger was loaned to us by the U.S. Geological Survey, Menlo Park, California. Chemical analyses were carried out by the Directorate General of Mineral Resources (DGMR)-USGS geochemistry laboratory, Jiddah. This work was completed as part of a work agreement between the U.S. Geological Survey and the Ministry of Petroleum and Mineral Resources, Kingdom of Saudi Arabia.

LOCATION, TOPOGRAPHY, AND GEOLOGY OF THE SHOT POINTS

During preliminary reductions of the temperature-depth data at the shot points, discrepancies between the general geologic descriptions (see Blank and others, 1979, p. 7-14) and the geothermal gradients became obvious (discussed below). In an effort to resolve these ambiguities, G. M. Fairer and M. E. Gettings mapped in detail the geology around SP2, SP3, SP4, and SP5, and estimated the topographic relief during April 21-23, 1978. Enlargements of existing 1:60,000-scale aerial photographs were used as a base. A tripod-mounted Brunton compass was used to survey topography of the shot-point areas. The base line, accurately pinpricked on the photographs, and distances between the drill holes at each shot point were measured using a 30-m-long tape in order to establish the drilling pattern. Approximately one-half of a day was spent at each shot point for a total of four man-days. Gettings compiled maps of the geology by using photogeologic methods to supplement results of the fieldwork.

Modal analyses and X-ray diffraction mineral determinations were carried out on selected samples. Modes were determined by point counts on thin sections, stained slabs, and acid-etched slabs. Modes of thin sections utilized 300 to 400 total counts and are probably accurate to ±20 percent. Stained-slab point counts utilized about 500 points and are probably accurate to ±15 percent. Plagioclase compositions were determined by X-ray diffraction techniques and measurement of extinction angles of twinned crystals. Quartz contents were determined by Elsass and Naqvi by quantitative X-ray diffraction methods and are accurate to ±5 percent. Modal mineral compositions are given in table 1, chemical analyses of the granitic rocks in table 2.

Shot-point locations given in this report are accurate to about ±3" in latitude and longitude; altitudes are accurate to ±5 m (D. J. Faulkender, oral commun., 1979).

Shot point 1

Shot point 1 (SP1) is at lat 26°16'12" N., long 45°35'57" E., 43 km northeast of the village of Al Quwayiyah on the eastern side of the Nafud as Sirr, at an altitude of 692 m. The site is approximately 1 km north of the paved road and about 150 m from the edge of the sand dunes. The immediate area is covered entirely by unconsolidated material and desert pavement, although shale crops out about 1 km to the northeast (fig. 2). Drilling chips show that bedrock is predominantly green shale, with some red shale and sandy and pebbly lenses or interbeds. The rocks belong to the Sudair Shale formation of Powers and others (1966).

A total of 18 holes, having an average depth of about 65 m, were drilled at SP1 (fig. 2); 12 holes were logged for temperature, and two were electrically logged for self-potential (SP) and single-point resistivity. The hole designations used in this report refer to the labels on the temperature logs and may not be the same as those given in the reports of the seismic refraction work.

Table 2.--*Major-element analyses and CIPW normative mineral compositions for igneous rock samples from drill holes at shot points 2, 3, and 4*
[In sample ID, number before hyphen refers to shot point, number after hyphen to sample locality (see figs. 2, 4, 6-8]

#	132049	132050	132051	132052	132053	132054	132055
ID	SP2- 5	SP3-10	SP3-11	SP3-12	SP4-6B	SP4-8A	SP4-8B
SIO2	66.30	76.90	71.00	71.90	74.50	75.80	74.20
AL203	14.60	12.10	14.10	14.40	14.00	13.00	13.70
FE203	4.23	1.08	2.11	1.28	0.32	0.38	0.47
FEO	0.77	0.22	0.19	0.62	0.15	0.26	0.43
MGO	2.66	0.08	0.30	0.20	0.10	0.10	0.19
CAO	3.44	0.48	0.77	0.56	0.95	1.35	0.92
NA2O	4.12	3.67	5.20	4.60	4.80	3.90	3.95
K2O	1.46	4.40	4.01	4.40	4.06	4.20	4.72
H2O	2.32	1.30	2.30	1.90	0.40	0.40	0.90
TIO2	0.42	0.13	0.23	0.16	0.18	0.10	0.13
P2O5	0.18	0.05	0.15	0.11	0.04	0.03	0.06
TOTAL	100.50	100.41	100.36	100.13	99.50	99.52	99.67
Q	25.791	37.554	23.649	27.082	29.117	34.453	31.094
C	0.416	0.545	0.164	1.314	0.078		0.566
OR	8.585	25.895	23.611	25.967	24.112	24.939	27.984
AB	34.689	30.928	43.843	38.873	40.820	33.160	33.534
AN	15.811	2.046	2.830	2.057	4.474	5.588	4.186
WO						0.394	
EN	6.592	0.198	0.744	0.497	0.250	0.250	0.475
FS							0.187
MT	1.258	0.331		1.532		0.551	0.684
HM	3.341	0.847	2.102	0.221	0.322	0.002	
IL	0.794	0.246	0.400	0.303	0.318	0.191	0.248
RU			0.019		0.013		
AP	0.424	0.118	0.354	0.260	0.095	0.071	0.143
TOTAL	97.701	98.708	97.716	98.108	99.600	99.600	99.100
SALIC	85.292	96.967	94.097	95.293	98.601	98.140	97.364
FEMIC	12.409	1.741	3.619	2.815	0.999	1.460	1.736

Table 1.--*Modal mineral compositions in percent for selected rock specimens from shot points 2. 3. 4. and 5*

[Modes for all specimens except SP5-8 and SP5-14 were determined by counting 300 points in thin section. Alkali feldspar modes were determined by 200-700 point counts on stained slabs. All quartz modes were determined by quantitative X-ray diffraction. Plagioclase compositions were determined by X-ray diffraction and measurement of Carlsbad twin extinction angles in thin section. Modes (except quartz) for specimens SP5-8 and SP5-14 were estimated visually because the rock is a very fine grained schist and point counting was difficult. Rows "Q/Q+A+P)" and "P/(A+P)" are the variables that determine the igneous rock classification under the International Union of Geological Sciences (IUGS) system (IUGS Subcommission on the Systematics of Igneous Rocks, 1973). "-" indicates mineral not observed in sample]

	SP2-1B	SP2-1E	SP2-3	SP2-5	SP3-4567	SP3-12	SP3-12A	SP3-13	SP4-4	SP4-6B	SP4-8A	SP4-8B	SP5-8	SP5-14
Rock type	Quartz-sericite schist	Quartz-sericite schist	Quartz-rich granitoid	Quartz-rich granitoid	Granite	Granite	Granite	Diorite	Granite	Granite	Granite	Granite	Quartz-mica phyllite	Quartz-mica phyllite
Mineral														
Quartz	22	13	35	27	-	35	27	39	-	36	36	30	34	37
Alkali feldspar	-	20	-	8.5	-	49.5	45	39.8	-	42	42	41	-	-
Plagioclase	39.3 (Ab)	38.7 (Ab)	15.3 (Ab)	7.2 (Ab)	35.3 (An_{15})	5.8 (An_{15})	12.3 (Ab)	15.5 (An_{15})	46 (An_{15})	7 (An_{15})	18.3 (An_{15})	21 (An_{15})	Minor	Minor
Calcite	14	13.7	3.7	-	-	-	-	-	-	-	-	-	-	-
Muscovite	5.7	8.6	3	3	-	-	tr	-	-	-	-	-	16	13
Biotite	14	-	11.3	-	-	4	-	3.7	-	14	2.3	6.7	-	-
Hornblende	-	-	-	-	56 (titanian)		11.3	0.7	52.6	-	-	-	-	-
Chlorite	4	6	8.7	35.3	-	-	2.7	-	-	-	-	-	47	47
Epidote	-	-	10	11.7	-	-	-	-	-	-	-	-	-	-
Sphene	-	-	-	-	-	1.7	1	-	-	-	-	-	-	-
Opaques	1	-	13	7.3	8.7	1	0.7	1.3	1.4	1	1.4	1.3	3	3
Q/(Q+A+P)	-	-	0.70	0.63	-	0.39	.32	.41	0.0	0.42	0.37	0.33	-	-
P/(A+P)	-	-	1.00	.46	-	.10	.21	.28	1.0	.14	.30	.34	-	-

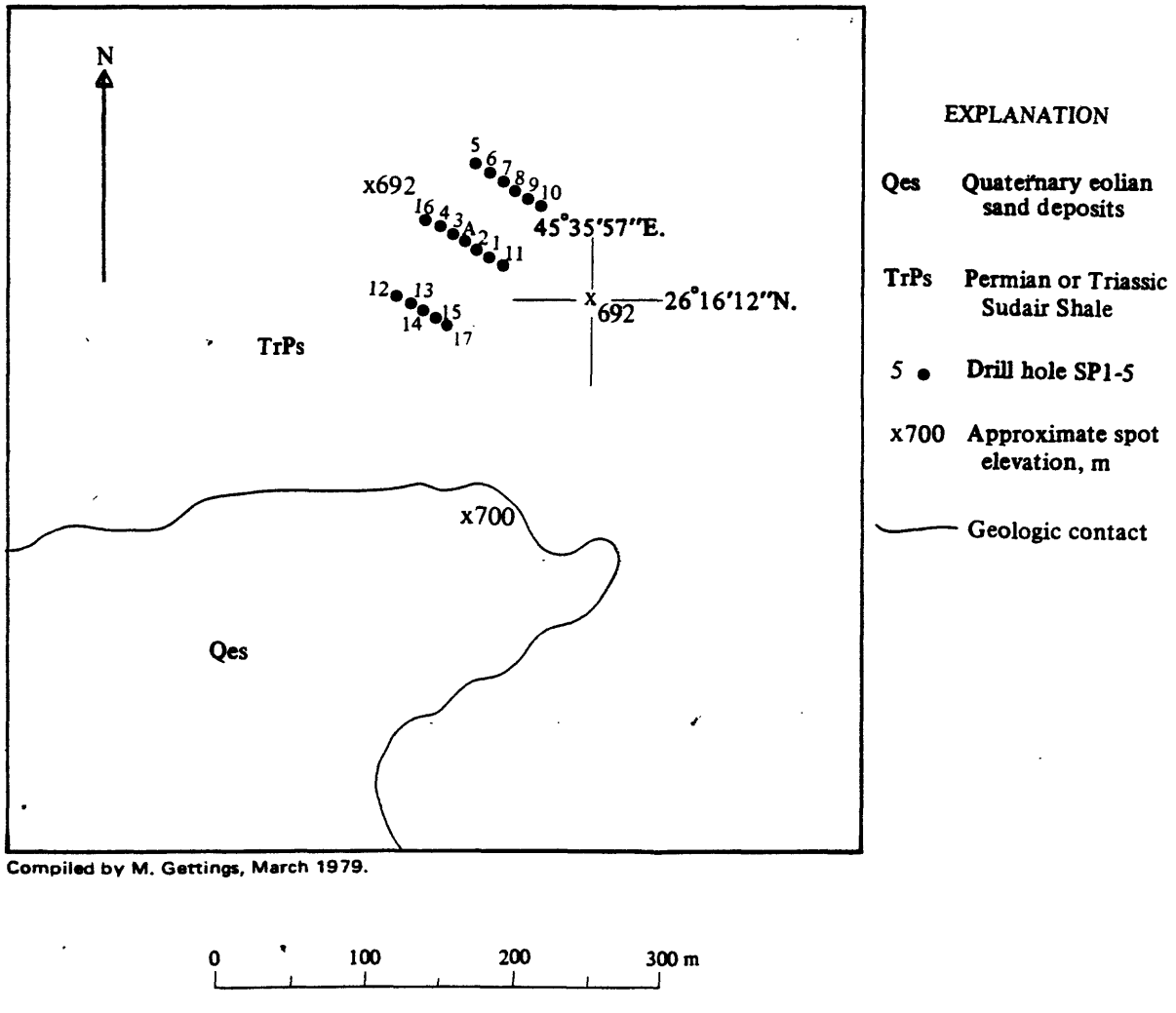

Figure 2.–Generalized geologic map of the shot point 1 area.

The electric logs were measured on February 1, 1978, with a Neltronic Instrument Corporation model 1K type D logger. The logger operation and calibration were checked prior to logging operations. The logs of drill hole SP1-3 are shown in figure 3; hole SP1-12 was also logged, but because the results were identical within experimental error only the logs for SP1-3 are illustrated. Both holes were logged twice with identical results. The logs are monotonous, and only the SP log shows small variations. Large-scale lithologic changes are not implied by the logs; the small variations suggest units or beds of shale 1 to 5 m thick having slightly different SP properties. The approximately linear increase in the SP response from 33 to 14 m depth is a commonly observed phenomenon in SP logs and probably represents a zone of changing oxidation state as the water table is approached. For comparison, the thermal gradient (discussed later) for drill hole SP1-3 is also plotted in figure 3. The sharp decrease in thermal gradient at a depth of about 48 m corresponds with a slight change in character of the SP log from variable below 48 m to essentially constant above. This depth may mark the base of a zone of water circulation that accounts for the very low thermal gradients above 48 m.

Shot point 2

Shot point 2 (SP2) is at lat 23°17'28" N., long 44°40'55" E. at an altitude of 887 m. The site is about 5 km northeast of the village of Sabhah in a terrane predominantly of quartz-sericite schist. The nearest outcrops of the posttectonic Jabal Sabhah granite are 1.7 km to the southwest, although parts of the intrusion may be much nearer and concealed beneath alluvial cover.

Ten holes, having an average depth of 62 m, were drilled at shot point 2 (fig. 4). Maximum topographic relief within 250 m of the drill holes does not exceed 10 m.

The rocks at shot point 2 are principally calcareous quartz-sericite schist and a small foliated and folded, quartz-rich granitoid (figs. 4 and 5). The schist is severely deformed by pervasive chevron folding; quartz "rods" are commonly observed in the noses of larger (~10 m half-wavelength) folds. Foliation generally strikes northeast and dips 40° to 70° SE. Fold axes of both chevron and larger folds plunge steeply (~70°) southeast. Modal compositions of the schist indicate a pelitic assemblage. This unit is probably part of the Abt schist (Fitch, 1978), which has been mapped a short distance to the northeast and south (Vincent, 1968). The granitoid is holocrystalline and, in thin section, is seen to have had a complex history of deformation and metamorphism. Plagioclase is recrystallized, and retrograde metamorphism is suggested by the conversion of biotite to chlorite. The original rock was probably a tonalite in composition. Where exposed, the contact between the granitoid and the schist appears to be a fault because the folding in the granitoid is truncated at the contact.

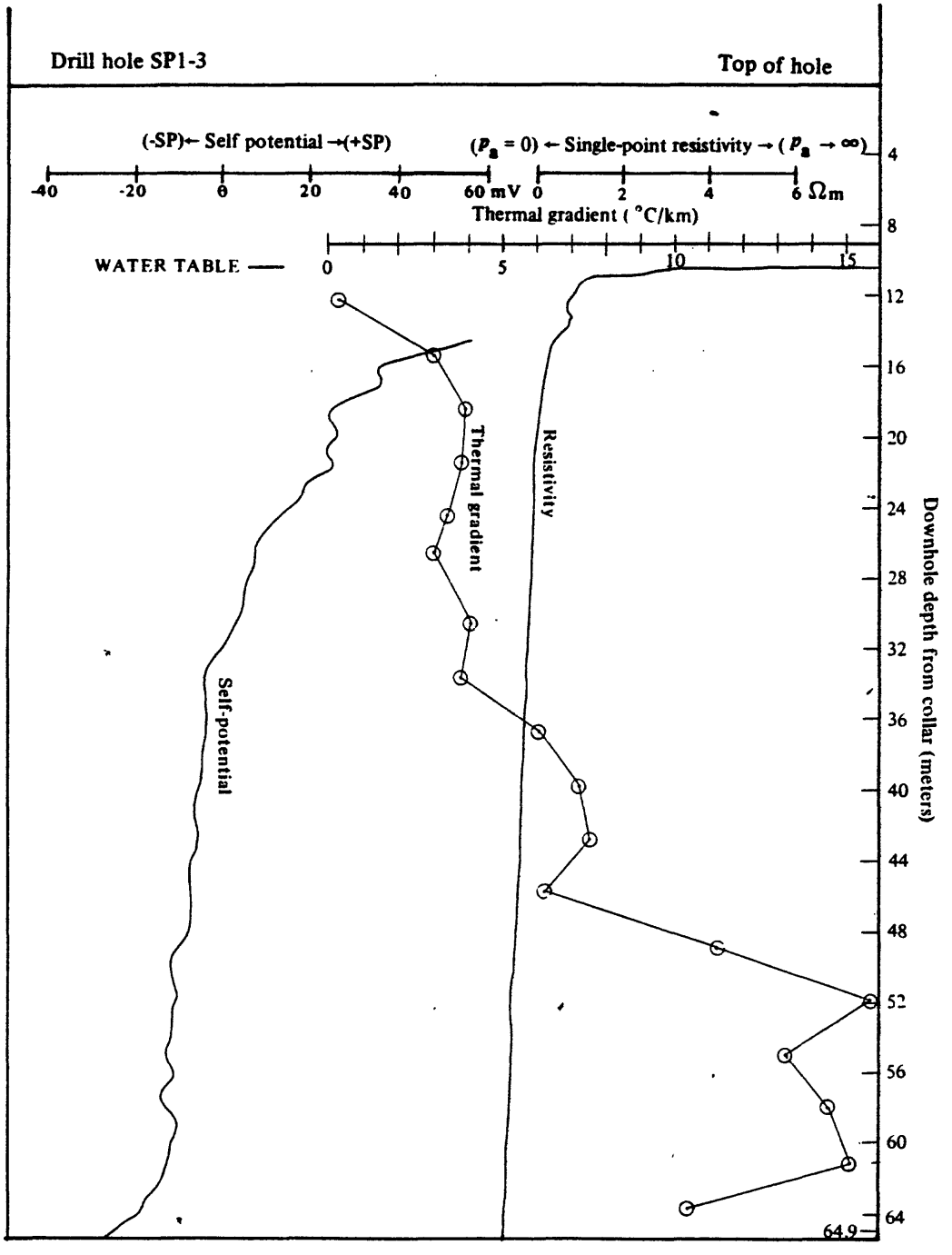

Figure 3.–Self-potential and single-point resistivity log of drill hole SP1-3, shot point 1. The observed thermal gradient is also shown for correlation purposes.

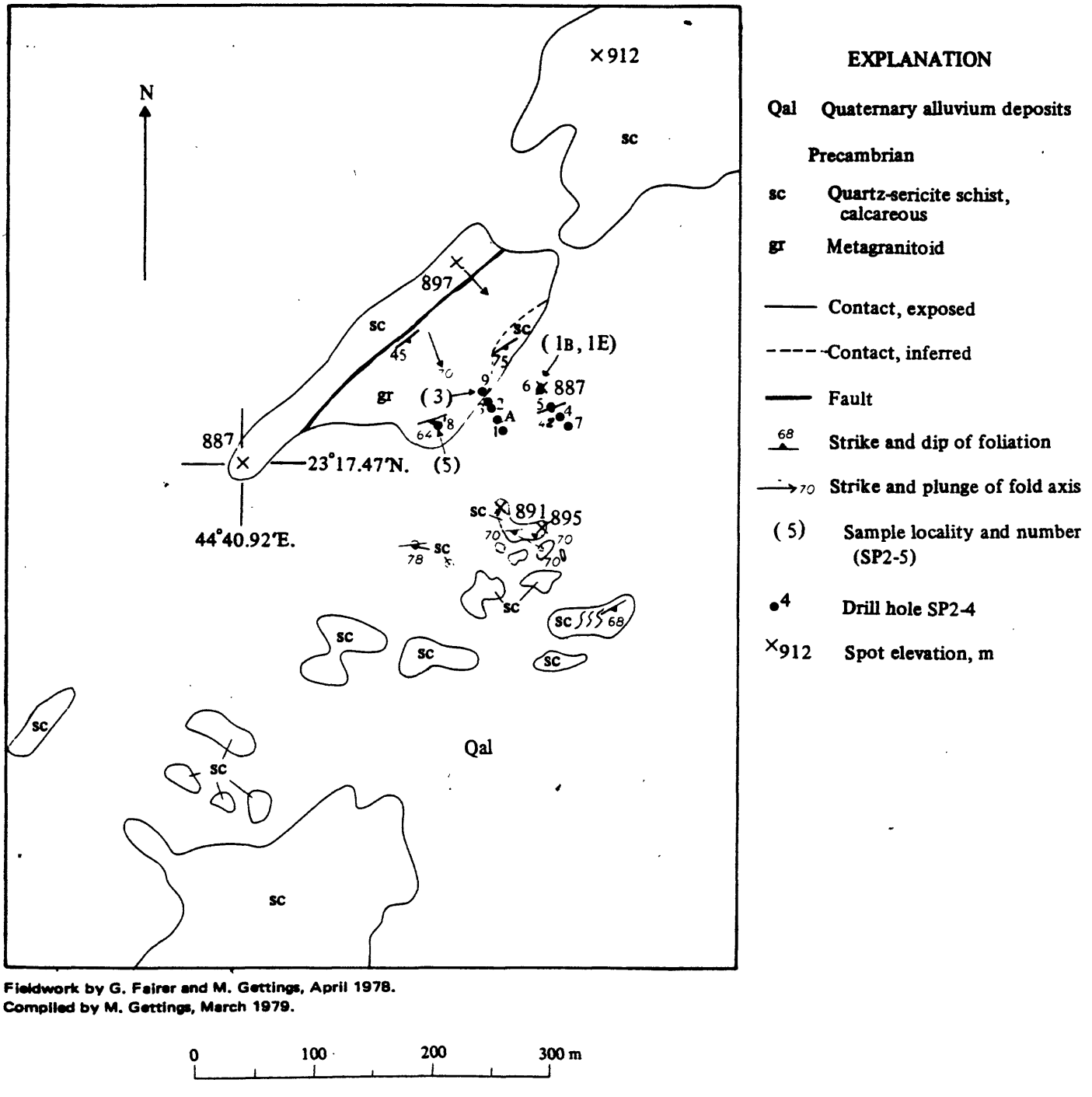

Figure 4.–Generalized geologic map of the shot point 2 area.

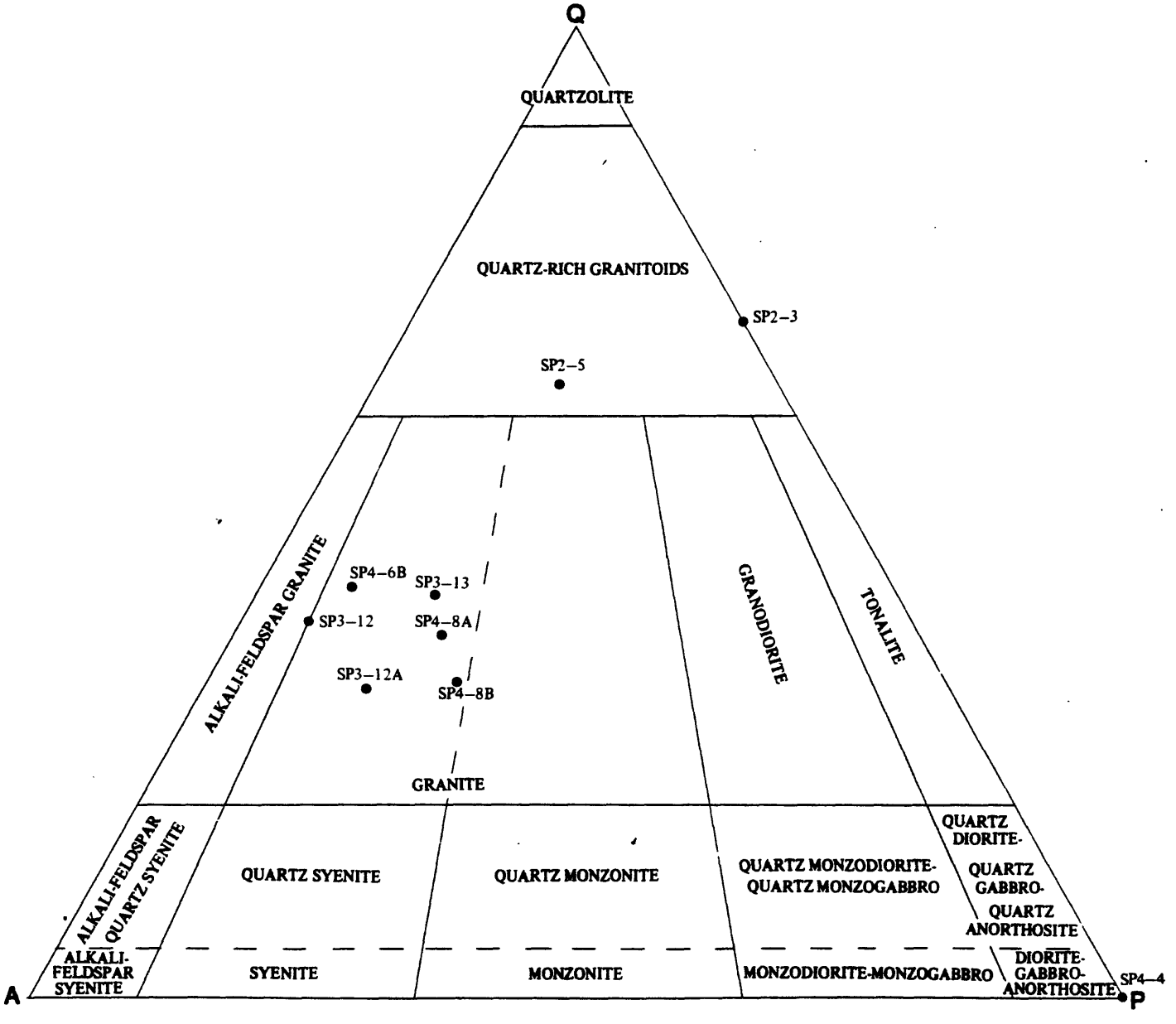

Figure 5.–Analysed plutonic rocks plotted on the classification diagram of the IUGS Subcommission Streckeisen, 1973). Classification and nomenclature according to modal mineral content (measured in volume percent). Q = quartz, A = alkali feldspars, P = plagioclase (An_{05-100}); Q+A+P = 100.

As can be seen in figure 4, hole 8 is in the granitoid, holes A, 1, 2, and 3 are in schist near the granitoid-schist contact, and holes 4, 5, 6, and 7 are in the schist at some distance from the granitoid. Since the granitoid and schist have quite different mineral compositions, different geothermal gradients should exist among the three groups of holes.

Shot point 3

Shot point 3 (SP3) is at lat 21°56'44" N., long 43°34'16" E., on a large plain at an altitude of 946 m, about 550 m northeast of a small granite peak that surmounts a large granite intrusion. The terrain is extremely flat, with less than 5 m relief within 500 m of the site.

Eleven holes, having an average depth of 60 m, were drilled at shot point 3 (fig. 6). Holes 1, 2, 3, 4, 5, and 10, which include the hole of the test drilling program (Blank and others, 1979), were drilled in a greenstone xenolith (probably Halaban andesite), and the others were drilled in granite. Modal analyses of greenstone and granite are given in table 1, modes of the three granites are plotted in figure 5, and chemical analyses and CIPW norms of the granites are given in table 2. The granite is not foliated and shows no evidence of deformation or tectonism. The only notable feature of the greenstone is that its dominant mineral (56 percent) is titanian hornblende (kaersutite).

Shot point 4

Shot point 4 (SP4) is at lat 20°05'13" N., long 42°39'04" E., at an altitude of 1,144 m, on a flat approximately 400 m in diameter surrounded by low, rolling hills. The locality is approximately 11 km northeast of Qalat Bishah and 4 km east of Wadi Bishah. The rock is mainly gneissic granite, which contains several large metadiorite xenoliths. Topographic relief is low, and the maximum relief within 300 m of the drill holes is only 10 m.

Nine holes, with an average depth of 51 m, were drilled at shot point 4 (fig. 7). Examination of drilling chips and fragments blown out by the shots indicate that the holes penetrated dominantly or wholly the gneissic granite.

This granite (tables 1 and 2; fig. 5) is similar to that at shot point 3 but has a well-developed gneissic layering that strikes northeast and dips 15° to 30° NW. In the easternmost outcrops shown in figure 7, the granite has alternating leucocratic and melanocratic layers 1 to 5 m thick. It varies in grain size from fine to coarse and weathers both pink and gray. Metamorphosed diorite crops out as xenoliths in the granite. The diorite is coarse grained, holocrystalline, and rhythmically layered. Where contacts are visible, structures and small mafic dikes in the diorite are truncated by the granite and veinlets of granite fill fractures in the diorite at the contact. Several younger, northeast-trending mafic dikes were observed in the area.

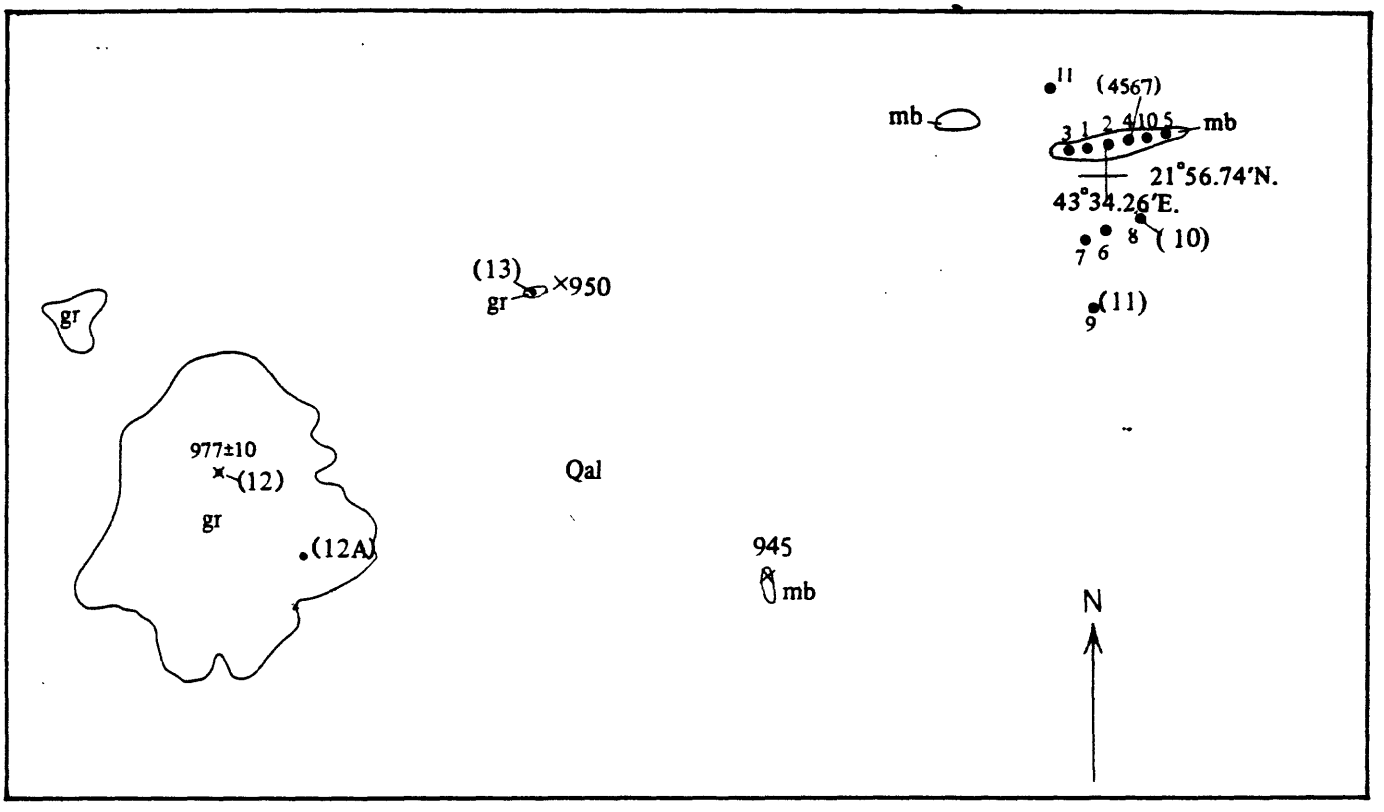

Fieldwork by G. Fairer and M. Gettings, April 1978.
Compiled by M. Gettings, March 1979.

0 100 200 300 m

EXPLANATION

Qal	Quaternary alluvium deposits	——	Geologic contact
	Precambrian	•(12A)	Sample locality and number (SP3–12A)
gr	Granite	•1	Drill hole SP4–1
mb	Metabasalt (greenstone)	× 912	Spot elevation, m

Figure 6.–Generalized geologic map of the shot point 3 area.

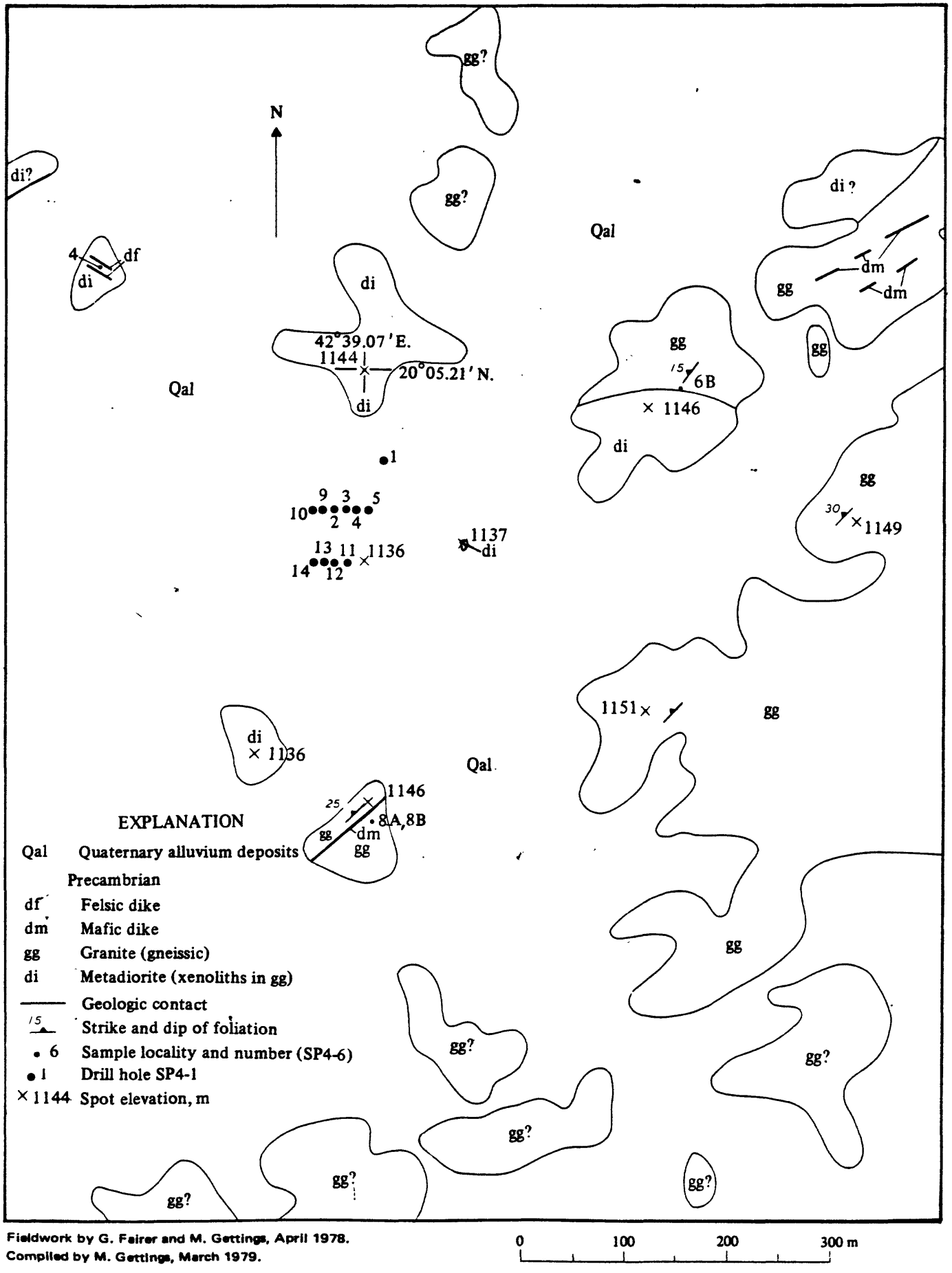

Figure 7.–Generalized geologic map of the shot point 4 area.

Shot point 5

Shot point 5 (SP5) is at lat 17°46'36" N., long 42°20' 47" E., at an altitude of 179 m, on the western side of a meander of Wadi Itwad, 11 km northeast of the village of Ad Darb. The wadi channel is about 15 m deep and represents the only significant topographic relief in the shot point area. The area is within an extensive gravel-covered plain on phyllitic schist.

Seven holes were drilled at shot point 5 (fig. 8), having an average depth of 60 m. Chips from all the holes indicate that they penetrated a uniform quartz-mica phyllite. The rock is fine grained and bluish-gray and has well-developed slaty cleavage striking north-northwest and dipping about 35° NE. Veins and pods of quartz, usually striking parallel with the phyllite, are common. Modal analyses for two specimens are given in table 1.

Examination of aerial photographs of the region shows a large regional fault or fault zone trending about 080° NE through shot point 5 (fig. 8). The fault was not detected in reconnaissance examination of the west wall of Wadi Itwad, where large areas are covered with talus debris and vegetation.

THERMAL-GRADIENT MEASUREMENTS

Temperature logs of most of the holes at each shot point were recorded, generally only below the water table. All measurements were performed with a lightweight, portable borehole-temperature logger consisting of a Data Precision Corporation digital multimeter model 2530AZ, USGS thermistor probe assembly (number F1295, calibrated 05/10/71), USGS cable assembly (number 125), and associated winch, depth counter, and accessories. The entire unit is packaged in four small suitcase-style instrument cases and is highly portable and easily used by one person. The digital multimeter is operated from rechargeable batteries and displays the cable-thermistor resistance on a digital readout. The resistance is recorded by the operator, along with the probe depth and any other pertinent information at each selected depth in the borehole. This system is capable of measuring successive temperature differences (that is, temperature gradients) precise to 1E-3°C and probably has a maximum error in absolute temperature no greater than 0.2°C (Sass and others, 1971b). All temperature logs were made by Showail.

After several experimental runs in drill hole SP1-3, the following procedure was established. First, the probe was inserted in the hole near the surface and allowed to stabilize to give an air-temperature reading. Next, it was lowered to a depth of about 30 m and allowed to stabilize, and a reading was taken; this process was repeated at a depth of 45 m. The probe was then lowered to the bottom of the hole (60 m in most cases) and allowed to stabilize at least 5 minutes. Temperatures in the hole were then logged upward at approximately 3-m intervals, with at least a 3-minute stabilization time at each measurement level. Two test logs of SP1-3 on successive days, one in the morning and one in the early evening and both using this procedure, gave two temperature-depth

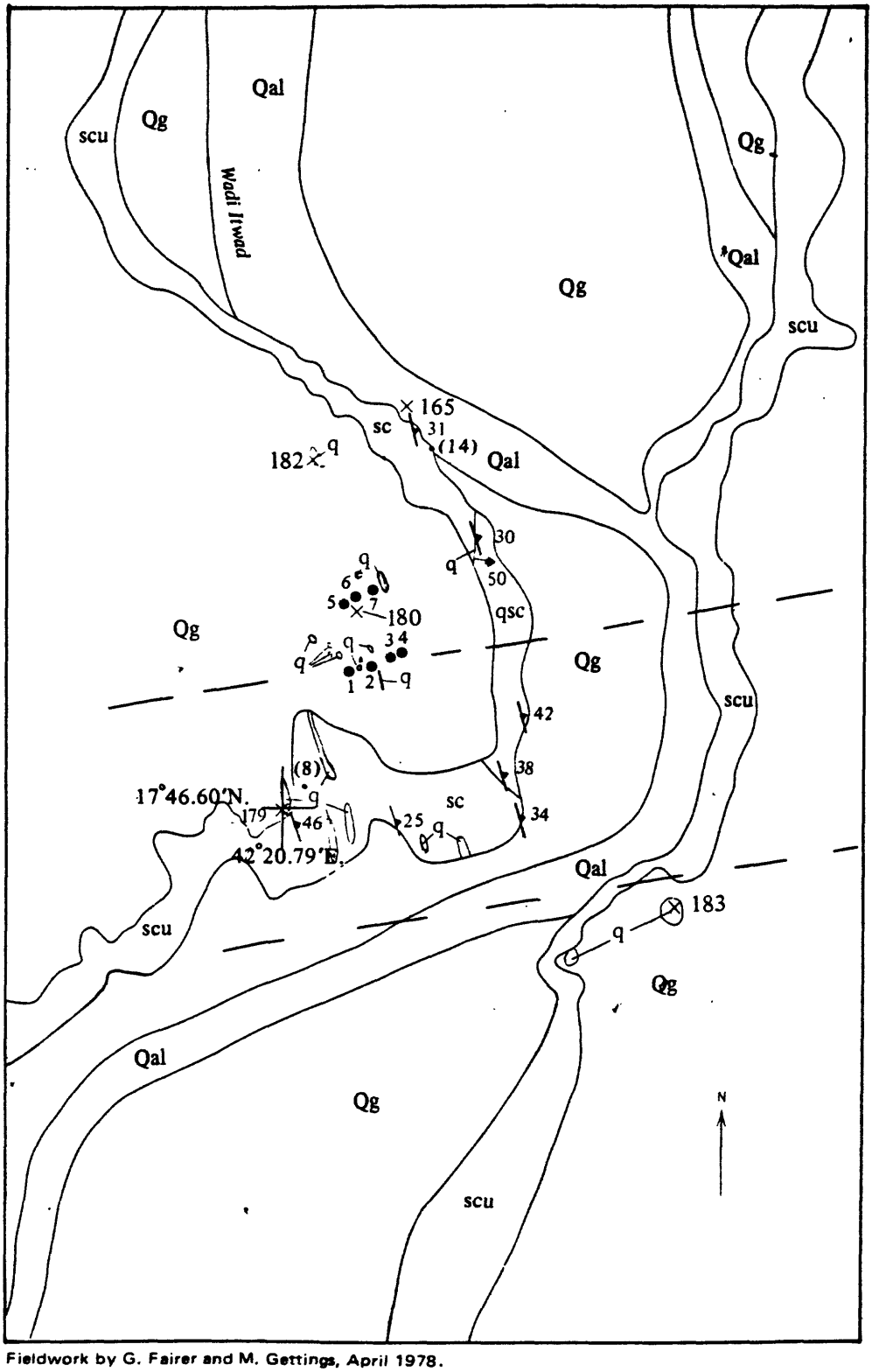

Fieldwork by G. Fairer and M. Gettings, April 1978.
Compiled by M. Gettings, March 1979.

0 100 200 300 m

EXPLANATION

Quaternary

Qal Wadi alluvium deposits

Qg Gravel, talus, and lag deposits

Precambrian

scu Sericite schist, undivided

sc Sericite schist

qsc Quartz-sericite schist

q Quartz veins and pods

Geologic contact

Fault zone boundary

q 50 Strike and dip of quartz vein

31 Strike and dip of foliation

(8) Sample locality and number (SP5-8)

2 Drill hole SP5-2

×180 Spot elevation, m

Figure 8.–Generalized geologic map of the shot point 5 area.

profiles whose mean discrepancy was 0.0011°C, with a standard deviation of ±0.0027° C. These profiles, together with a profile of an earlier log that was done with shorter stabilization times, are shown in figure 9. In this figure, the temperature gradient is plotted against temperature, rather than temperature versus depth. The resulting plot is very error sensitive and shows quite clearly the agreement of the two later profiles, as well as the disagreement of the earlier one. One and one-half to two hours were required to log a hole using this procedure.

Thermal gradient measurements were logged for most of the drill holes at the five shot points at different times. Eighteen shot point 1 drill holes (SP1-A, SP1-1 - SP1-17) were logged during the period January 25-28, 1978, and January 31-February 3, 1978; ten shot point 2 holes (SP2-A, SP2-1 - SP2-9) were logged in the period January 29-31, 1978; eight shot point 3 holes (SP3-1, - SP3-8) were logged in the period February 5-6, 1978; six shot point 4 holes (SP4-1, SP4-3 - SP4-5, SP4-9 - SP4-10) were logged on February 11, 1978; and seven shot point 5 holes (SP5-1 - SP5-7) were logged in the period February 16-17, 1978. The holes at shot point 5 were the last to be drilled and were completed by midsummer 1977 (Blank and others, 1979); thus all holes were drilled at least 5 months before the temperature measurements were made. About a month before the measurements, a drill was used to clean the holes; however all holes were found to be open, and no actual drilling was done.

Data reduction was effected using the resistance-temperature conversion table at 0.1°C intervals provided by USGS with the instrument and an interpolation program executed in the DGMR PDP-11/45 computer. The program uses a cubic polynomial interpolater fitted exactly to four points of the calibration table such that two points fall on each side of the observation value. The temperature-depth profiles for all holes logged are presented in figures 10-58, and the numerical values are listed in the appendix.

Each of the profiles was visually inspected to determine segments that appeared to form straight lines. Observed values within these segments were then fitted with straight lines by least-squares techniques using a computer program written for the purpose. The resulting thermal gradients for corresponding depth intervals of all holes at each shot point were then averaged to yield a preliminary gradient and standard deviation. This procedure yielded satisfactory results only at shot point 4, for which we accept 12.43±0.64°C/km as the best estimate of the geothermal gradient. Treatments that take into account the various geologic factors at the other shot points were carried out as described below.

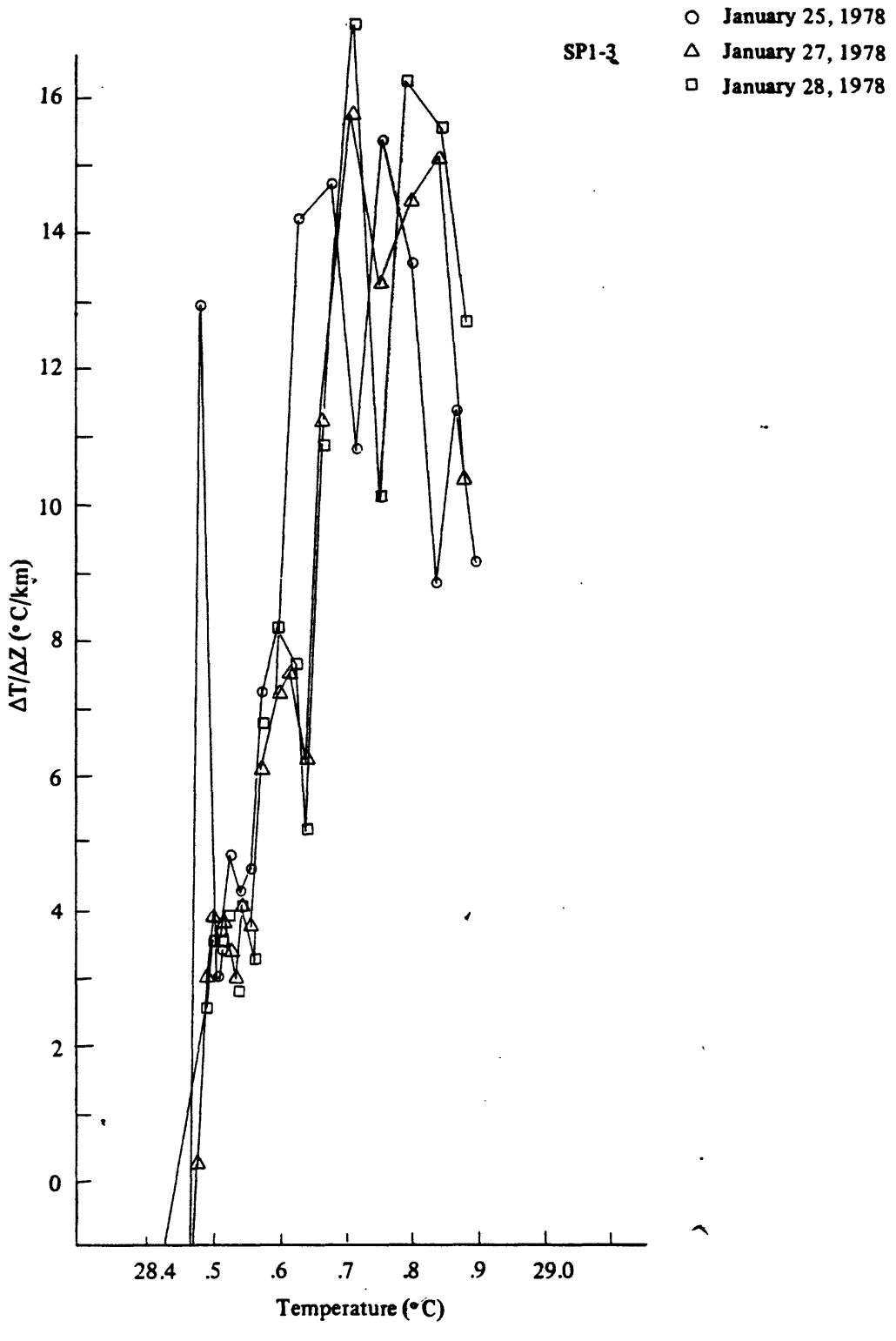

Figure 9.–Plot of thermal gradient versus temperature for three logs of drill hole SP1-3. Individual temperature versus depth logs shown on figures 13-15.

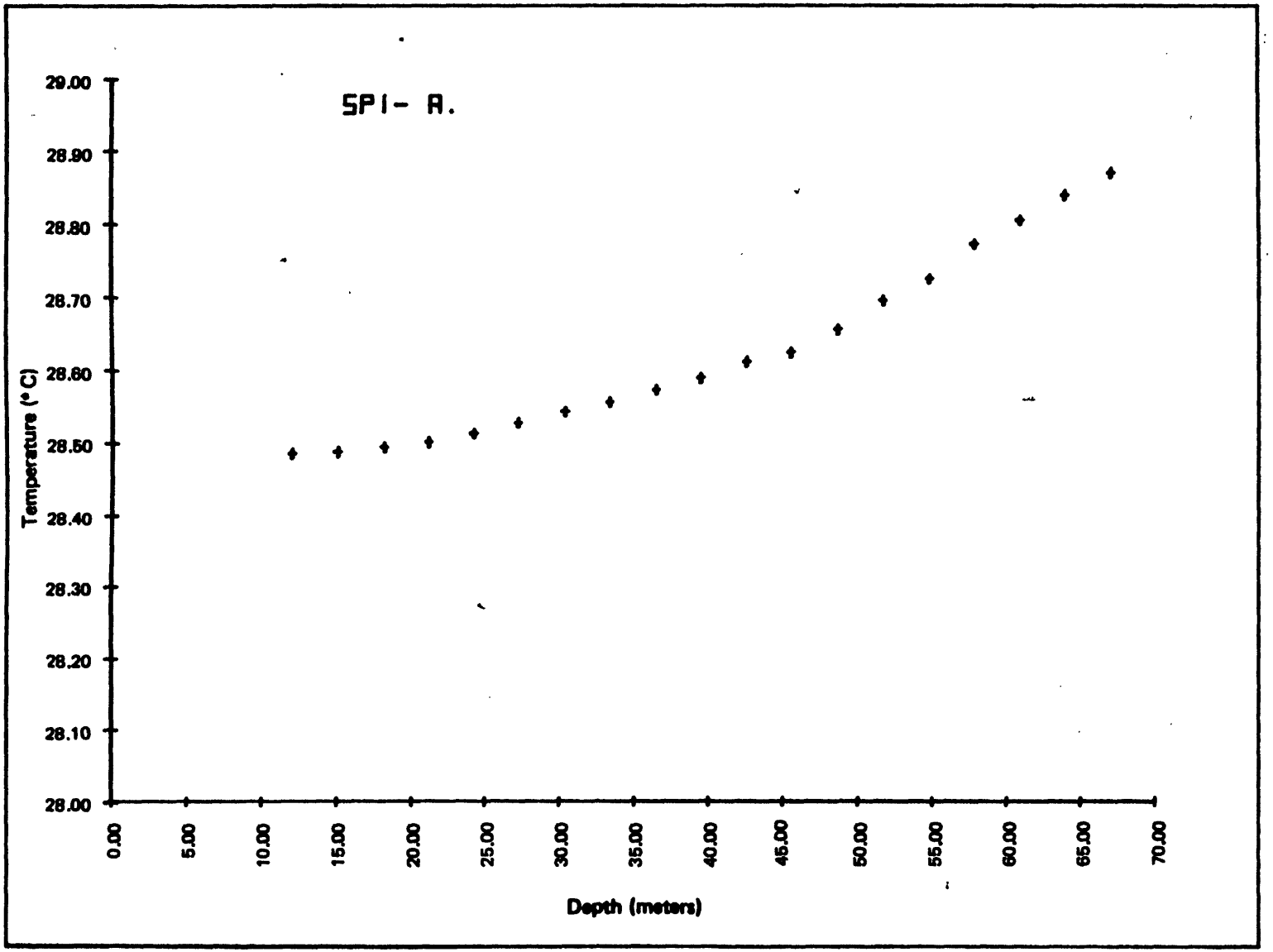

Figure 10.–Observed temperature versus depth profile for drill hole SP1-A.

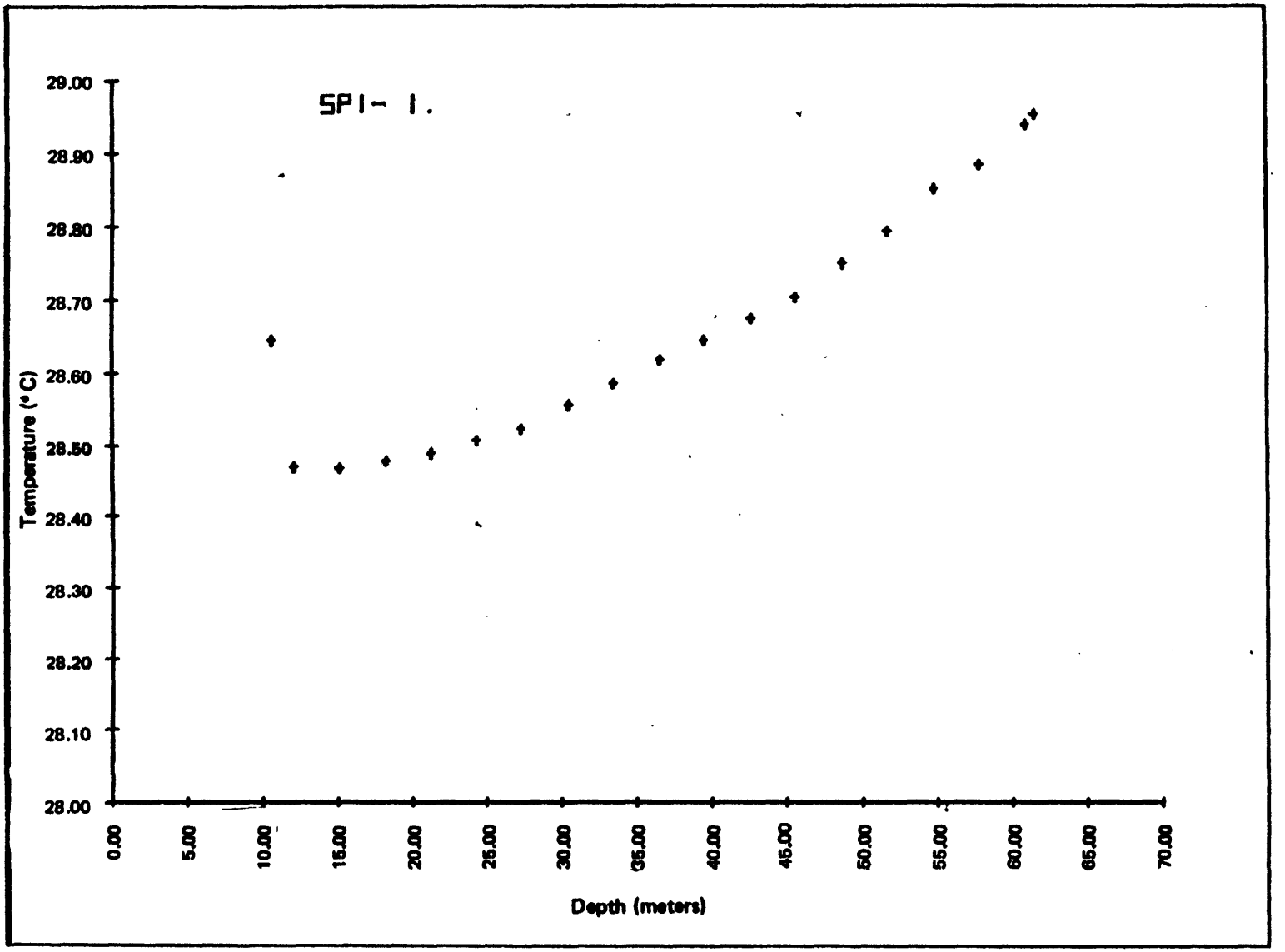

Figure 11.–Observed temperature versus depth profile for drill hole SP1-1.

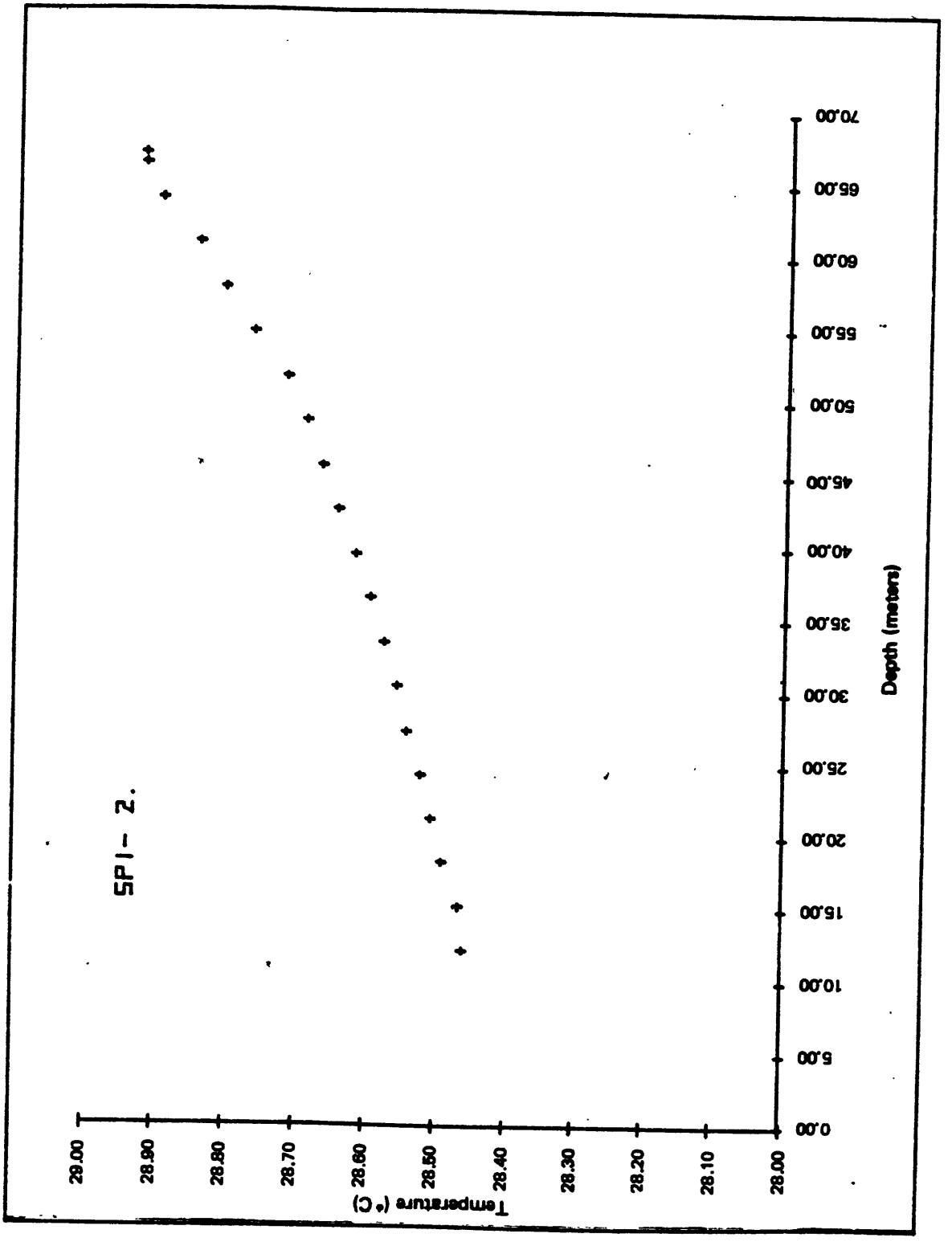

Figure 12.–Observed temperature versus depth profile for drill hole SP1-2.

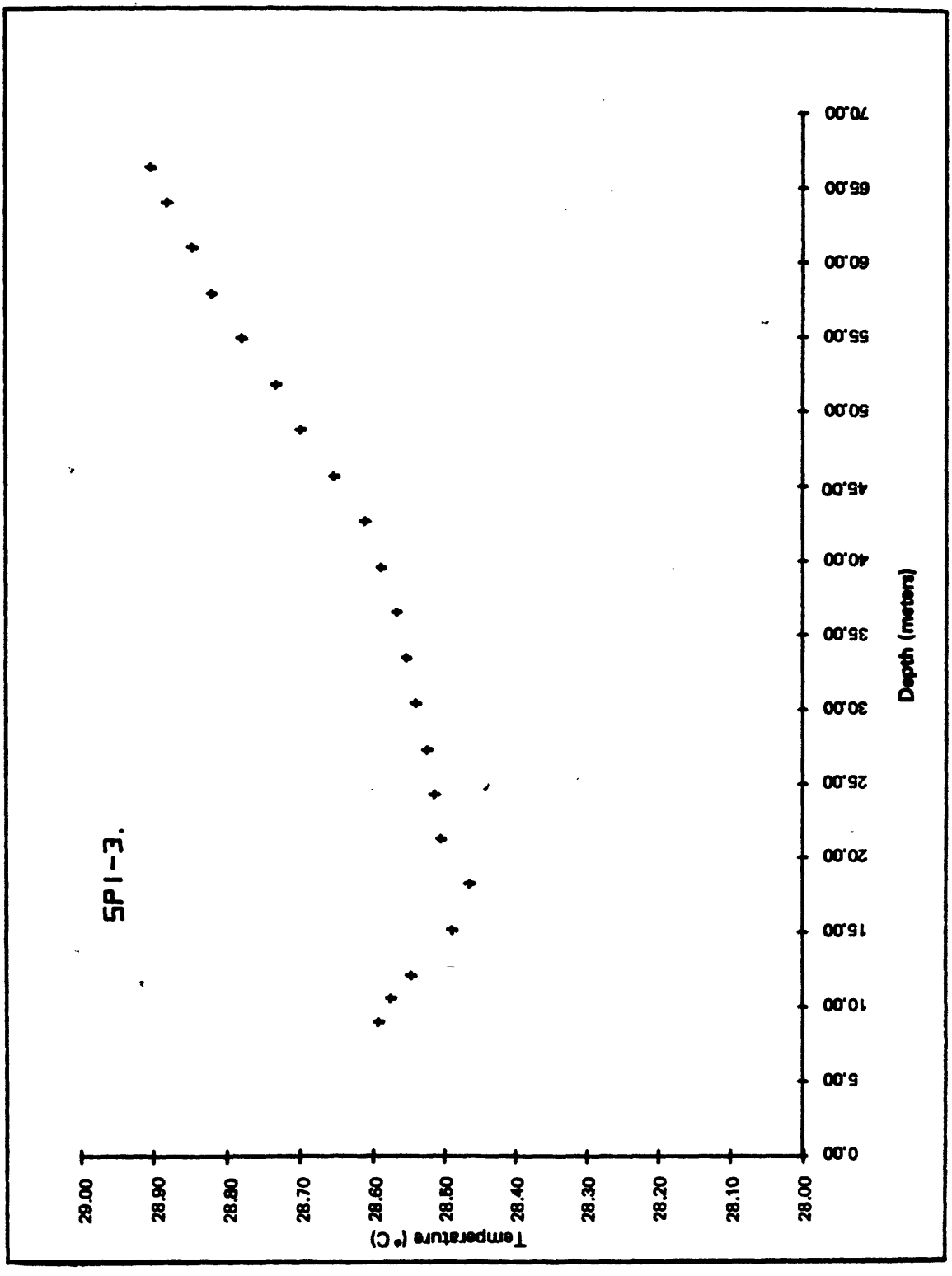

Figure 13.–Observed temperature versus depth profile for drill hole SP1-3, logged January 25, 1978.

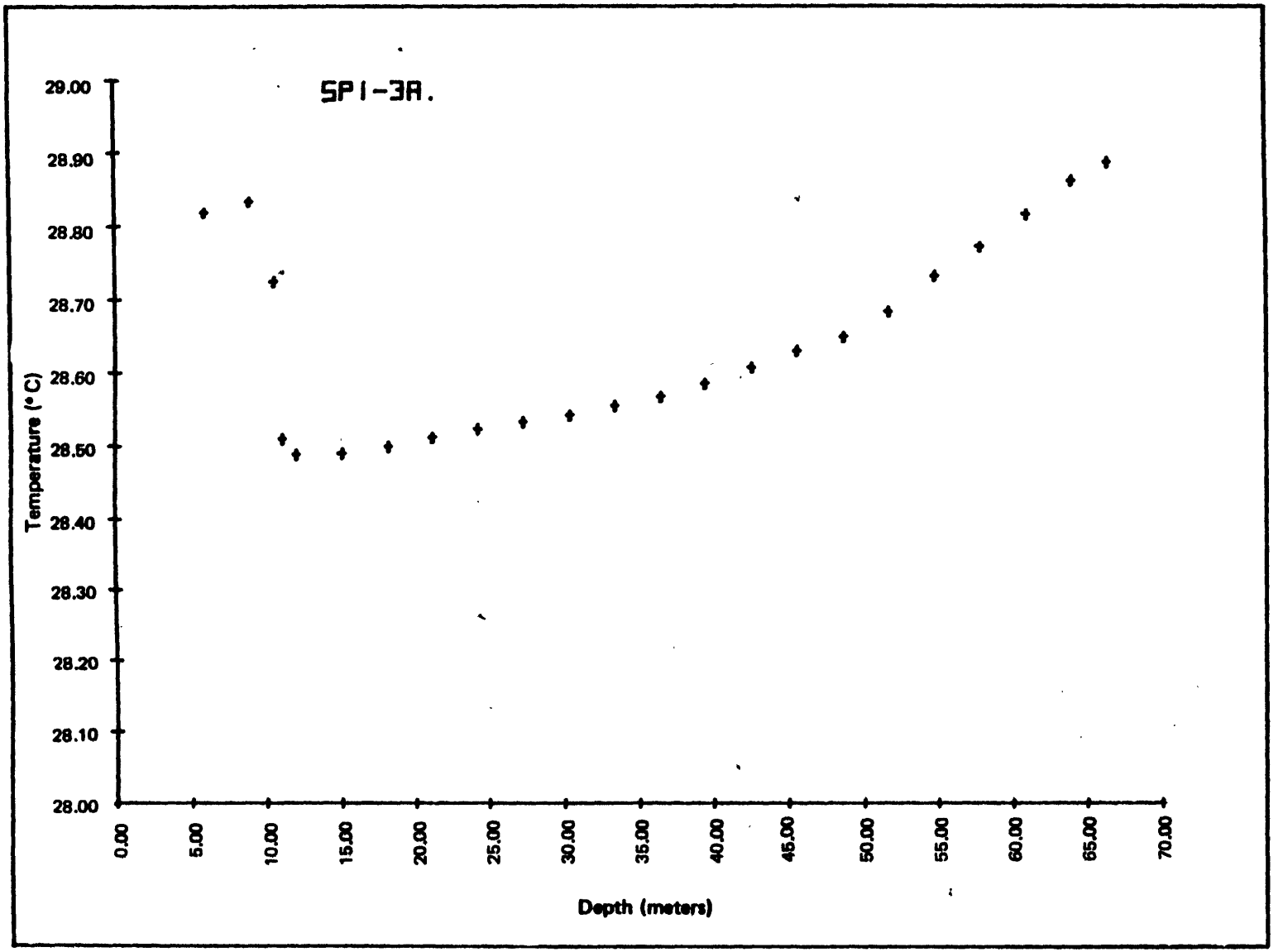

Figure 14.–Observed temperature versus depth profile for drill hole SP1-3, logged January 27, 1978.

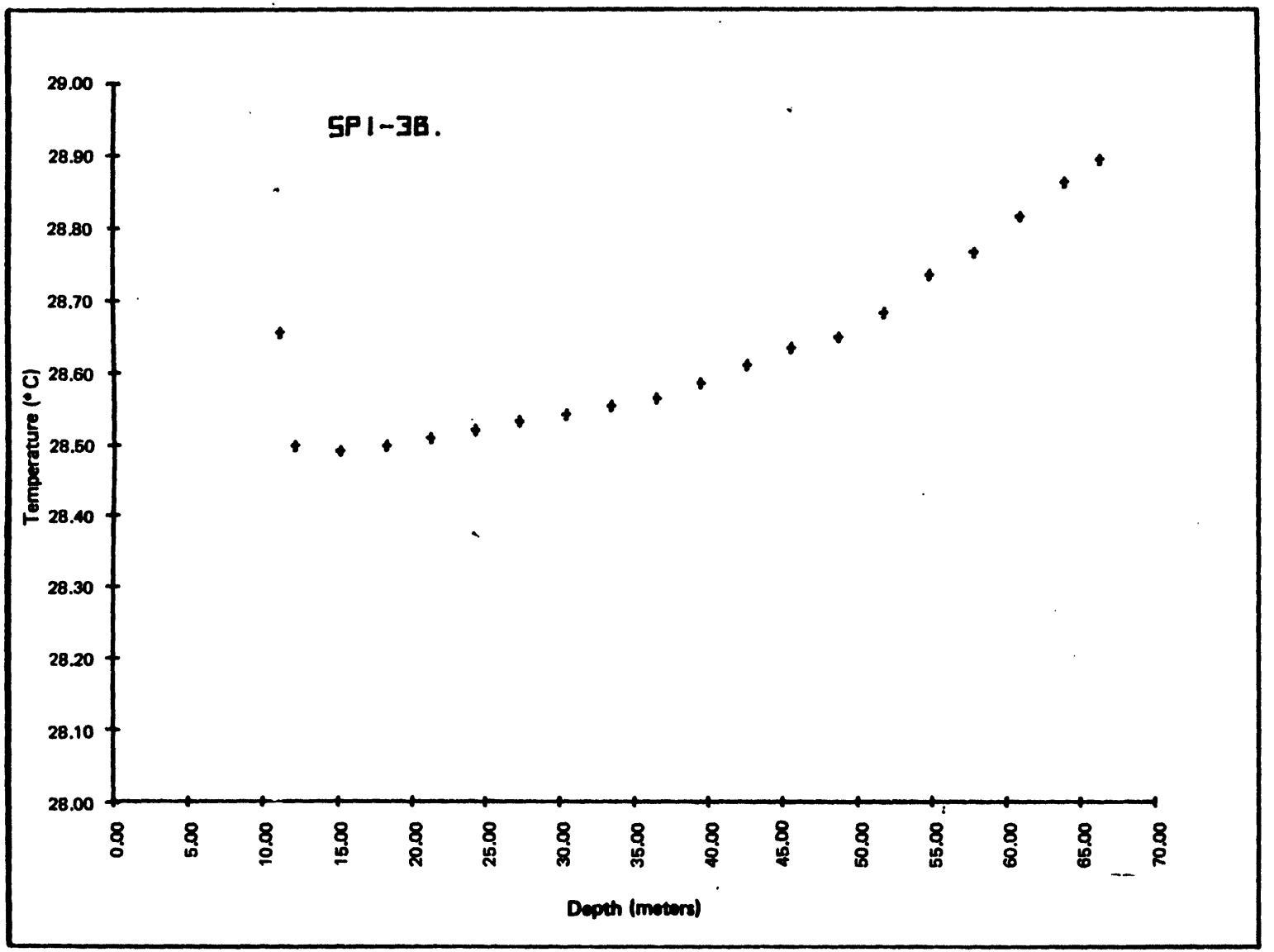

Figure 15.–Observed temperature versus depth profile for drill hole SP1-3, logged January 28, 1978.

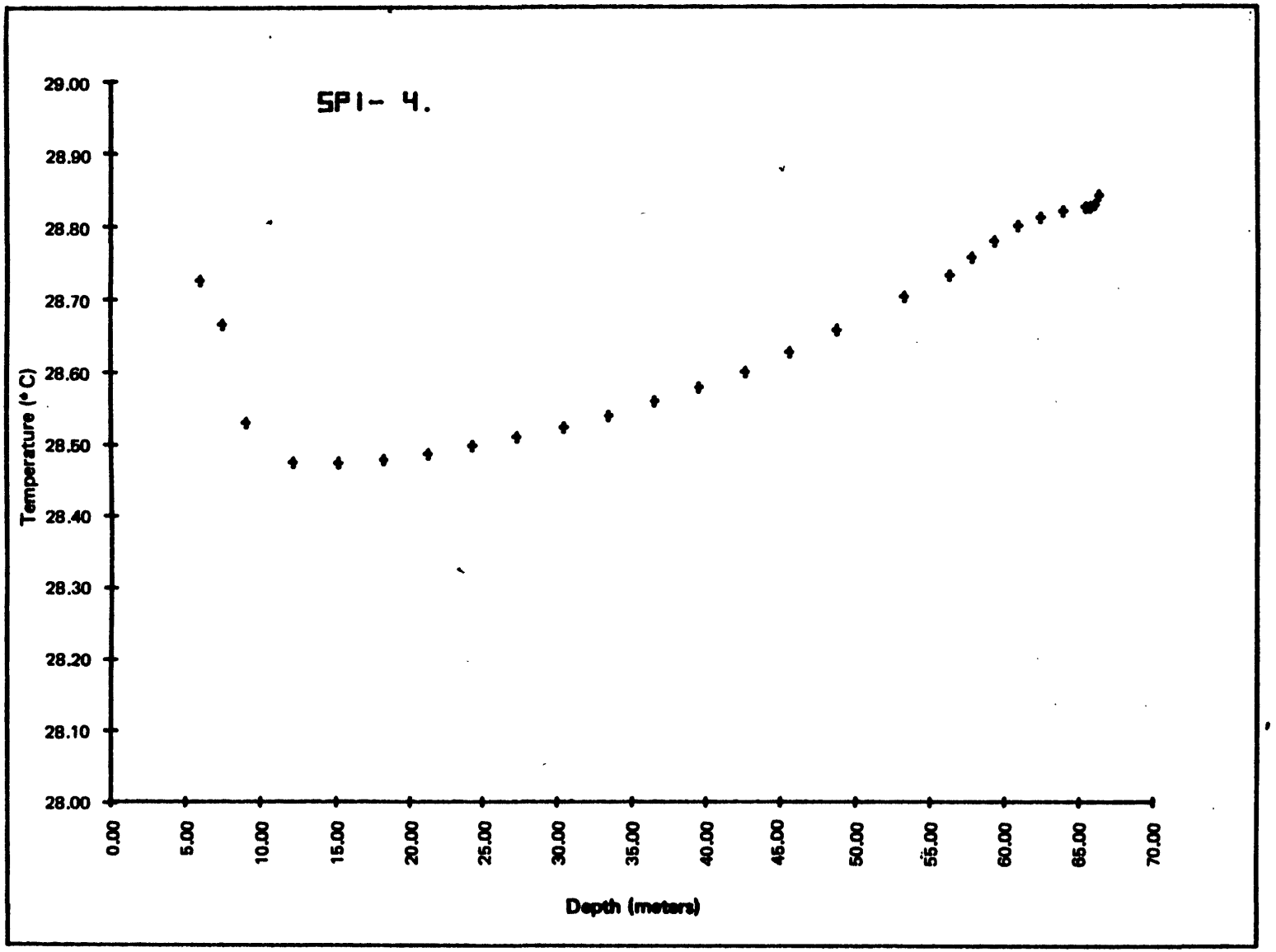

Figure 16.–Observed temperature versus depth profile for drill hole SP1-4.

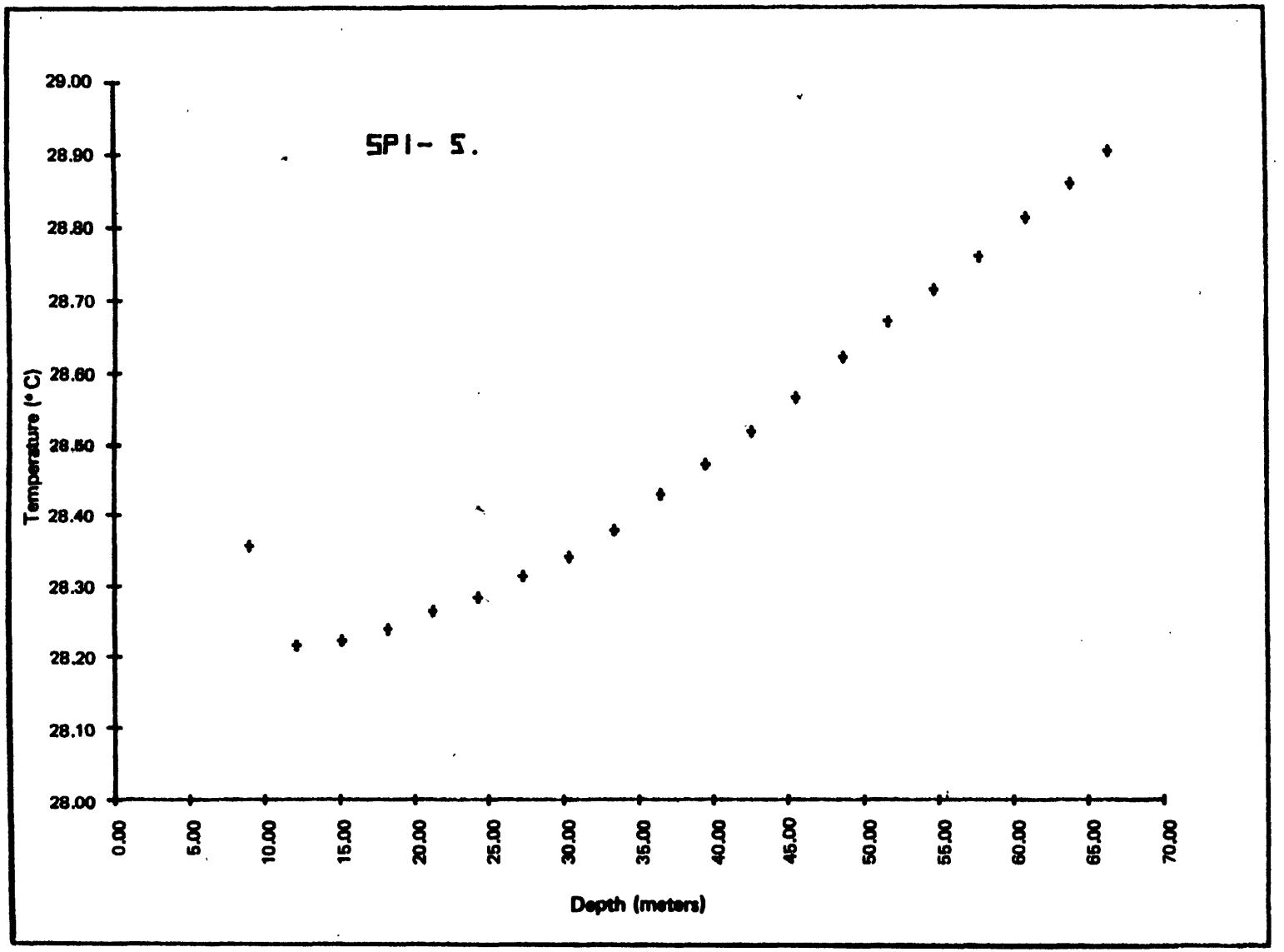

Figure 17.–Observed temperature versus depth profile for drill hole SP1-5.

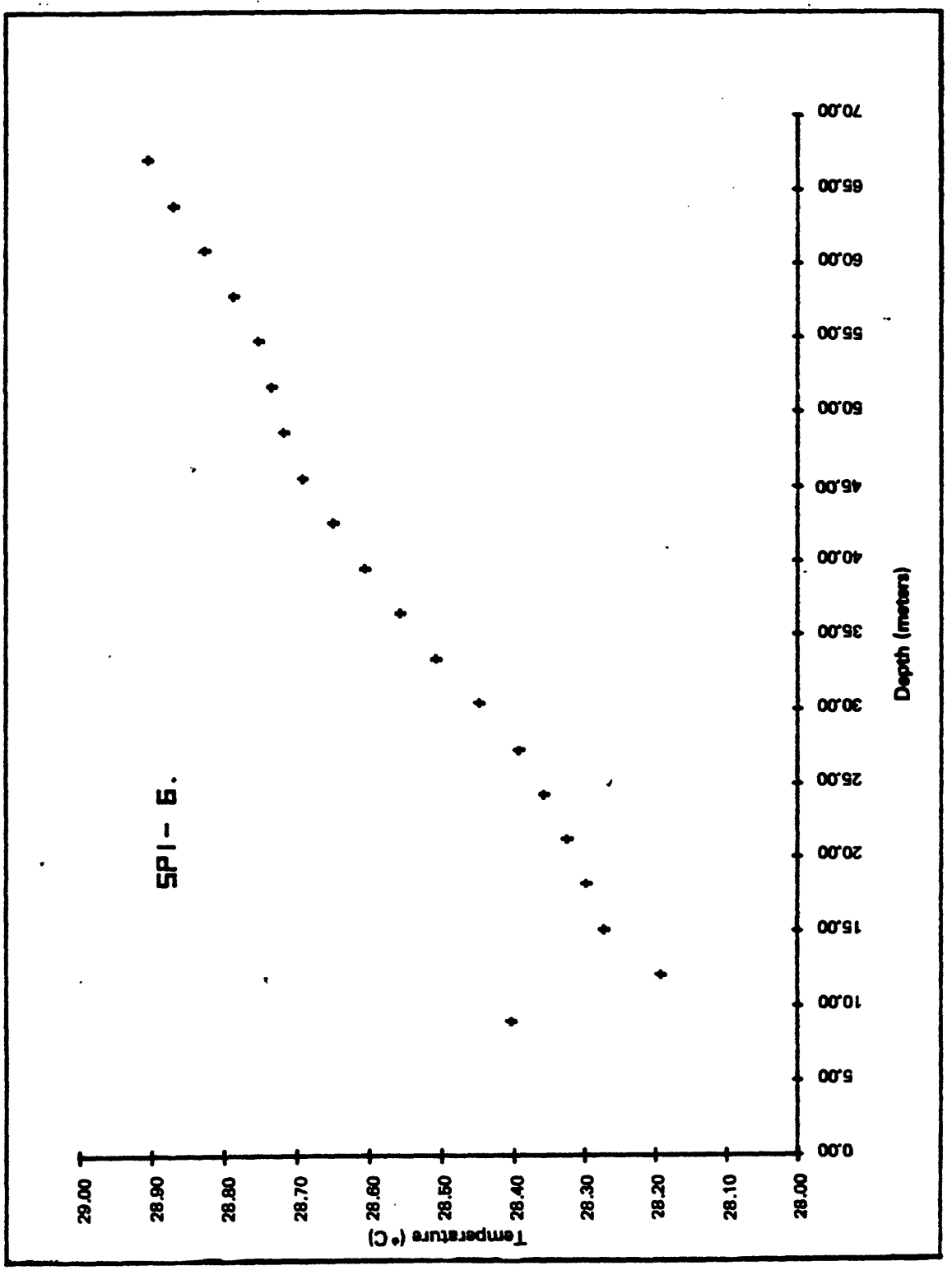

Figure 18.–Observed temperature versus depth profile for drill hole SP1-6.

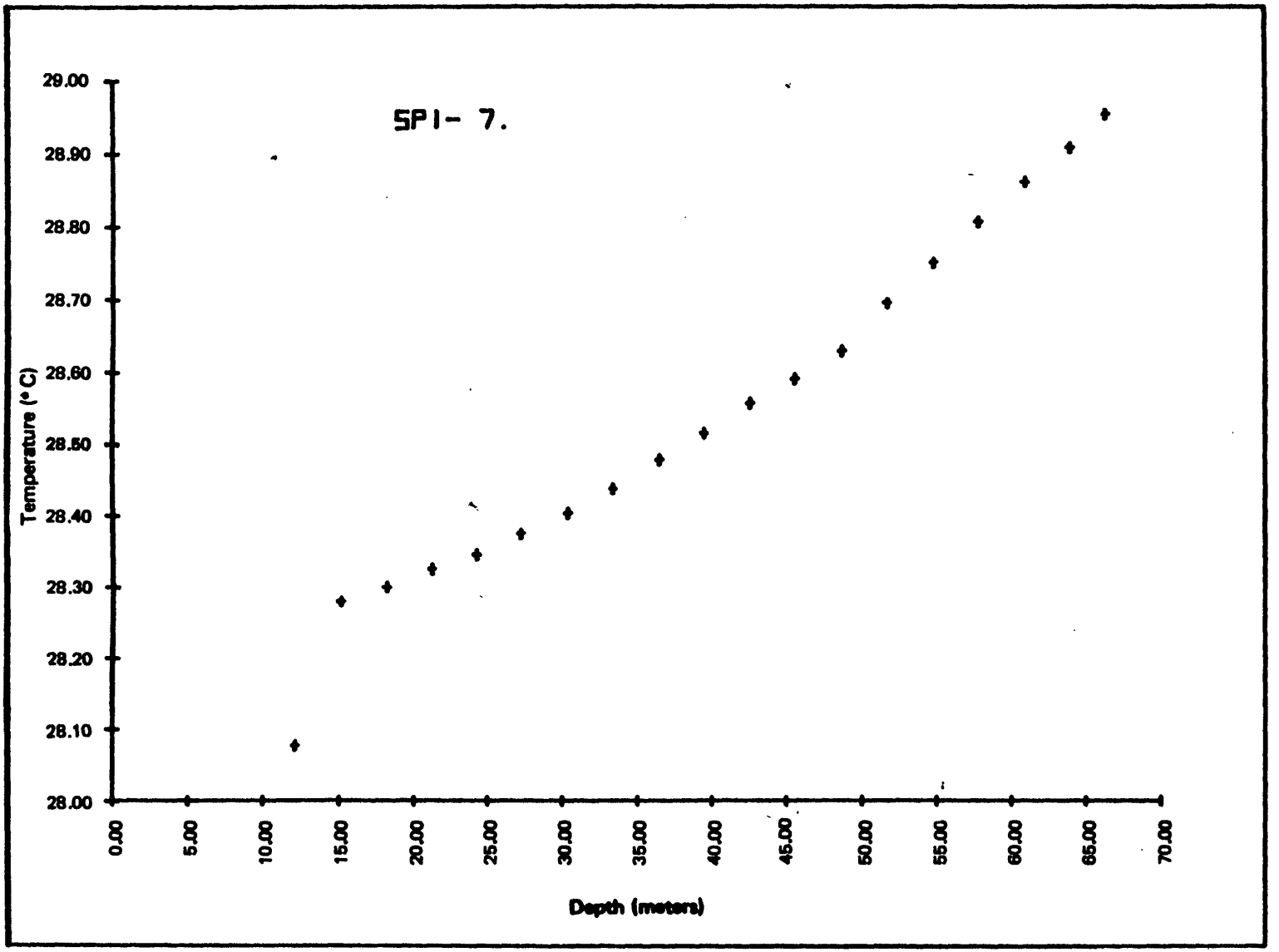

Figure 19.–Observed temperature versus depth profile for drill hole SP1-7.

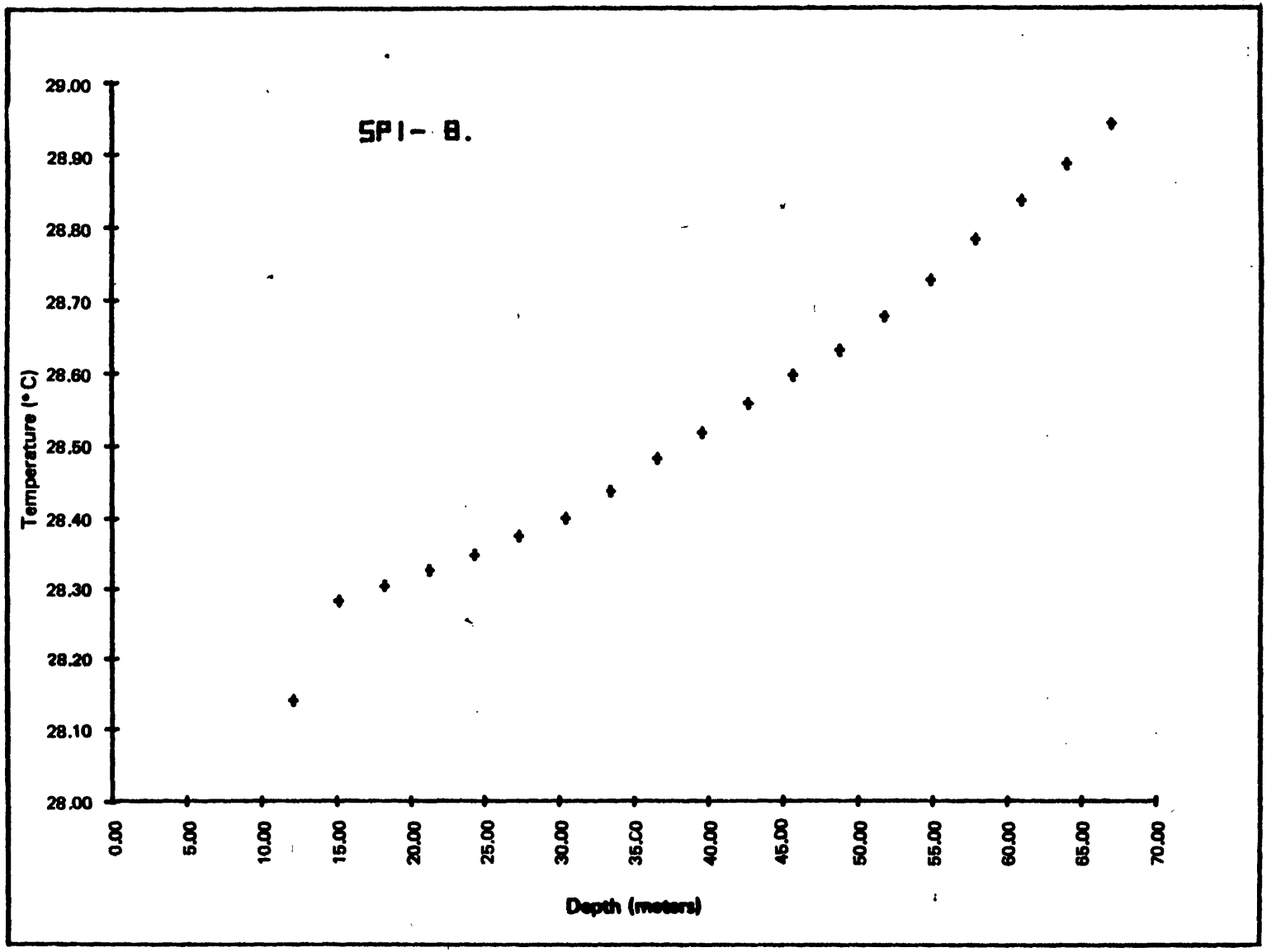

Figure 20.–Observed temperature versus depth profile for drill hole SP1-8.

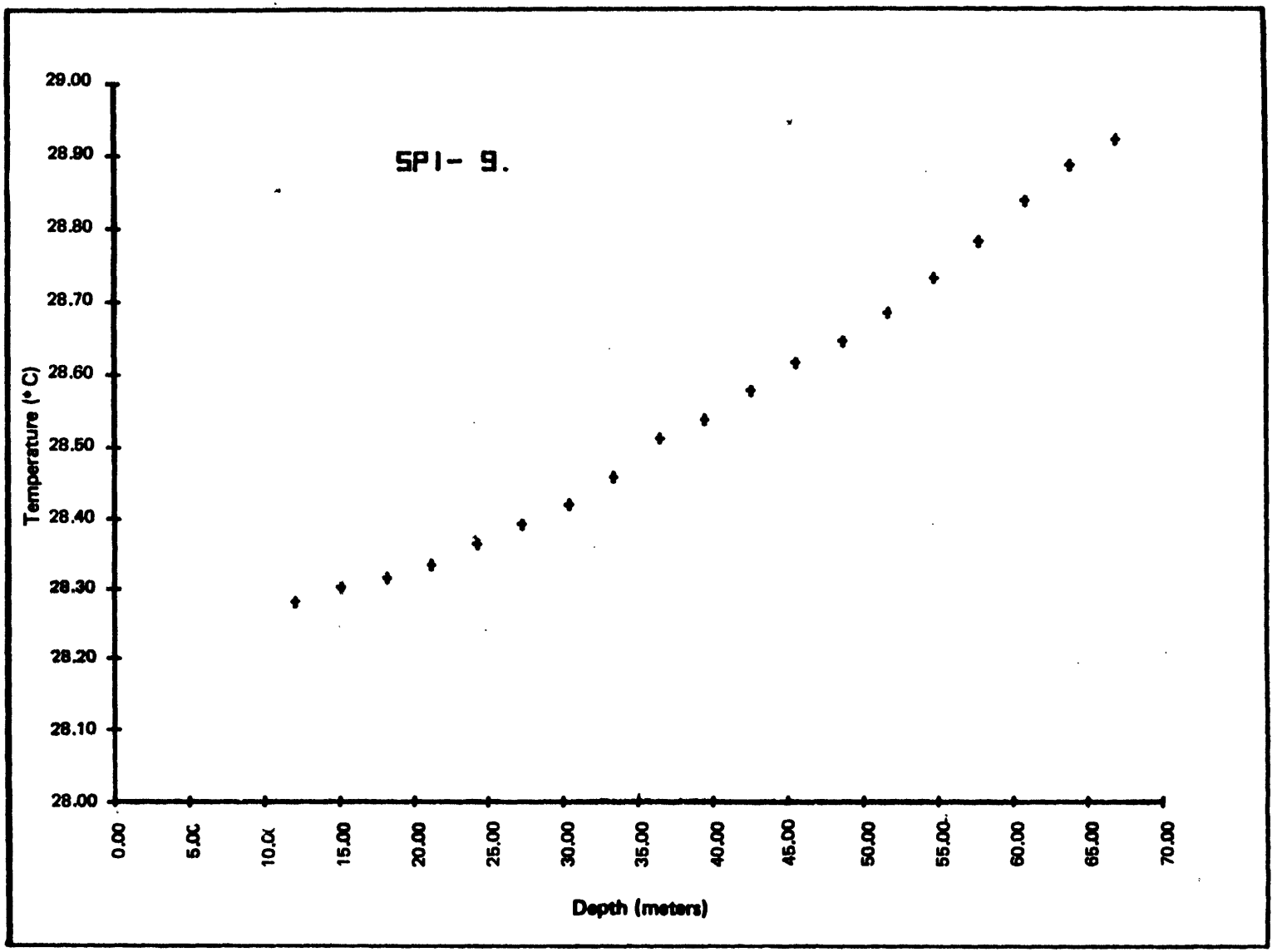

Figure 21.–Observed temperature versus depth profile for drill hole SP1-9.

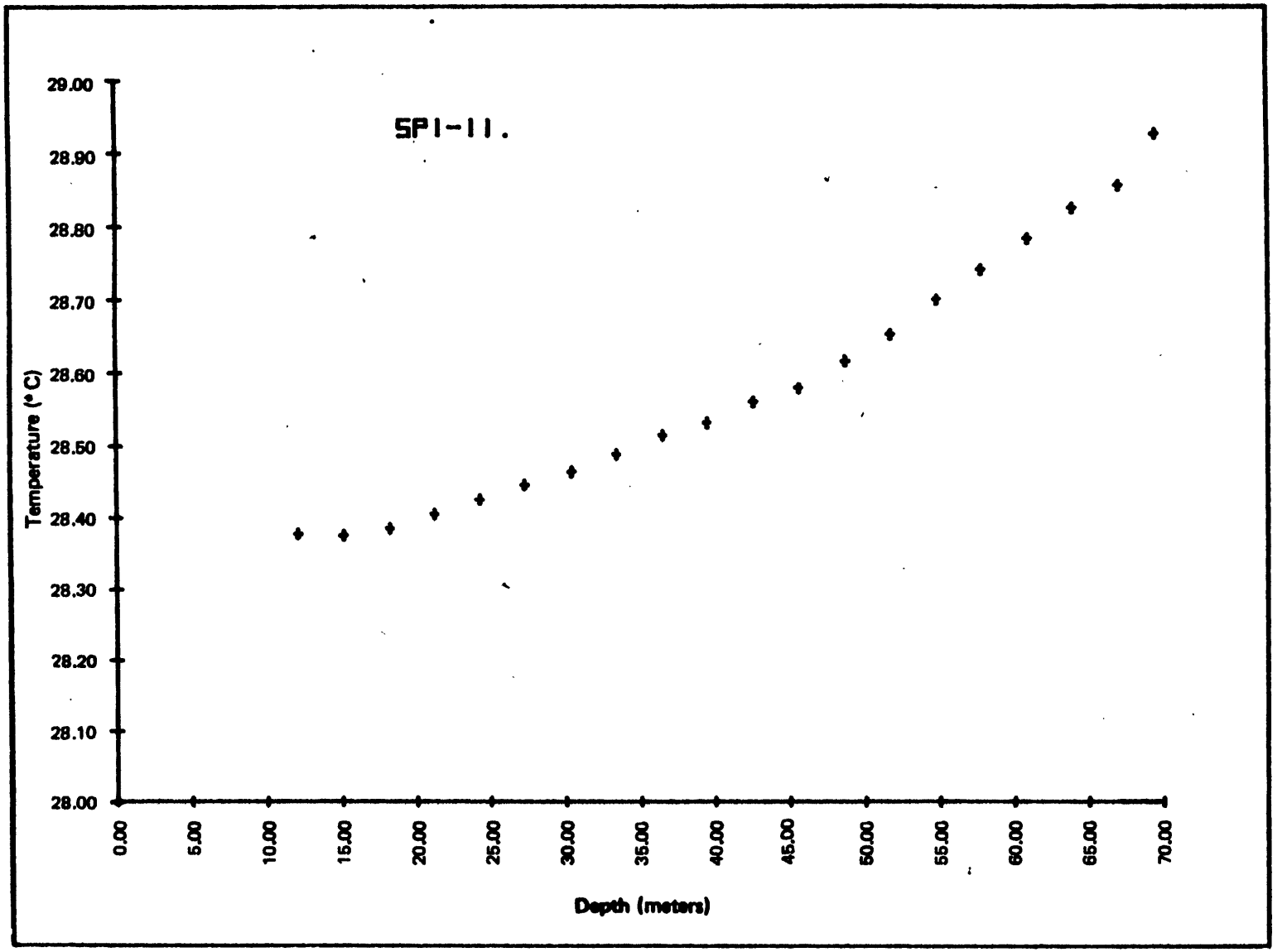

Figure 22.–Observed temperature versus depth profile for drill hole SP1-11.

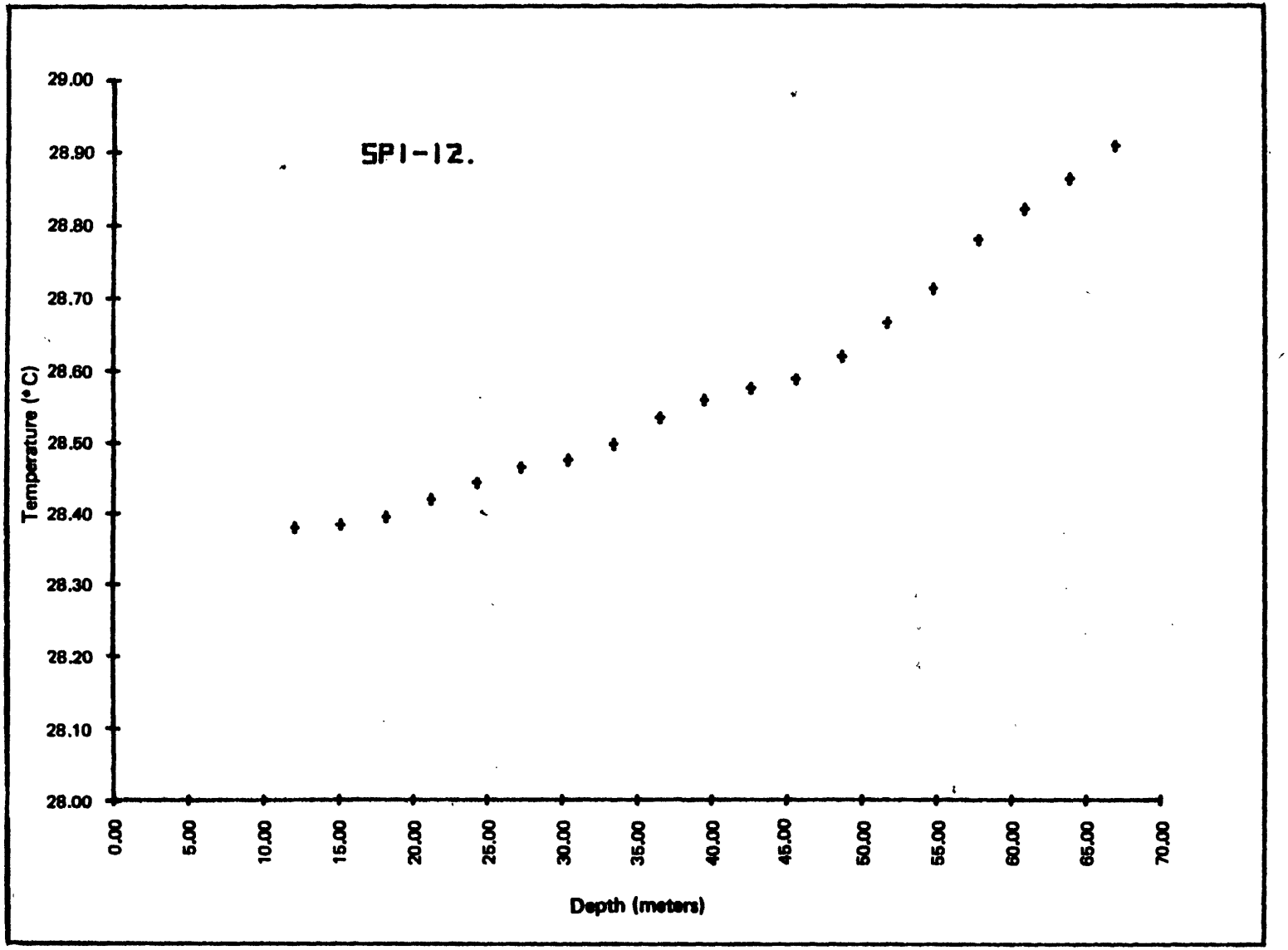

Figure 23.–Observed temperature versus depth profile for drill hole SP1-12.

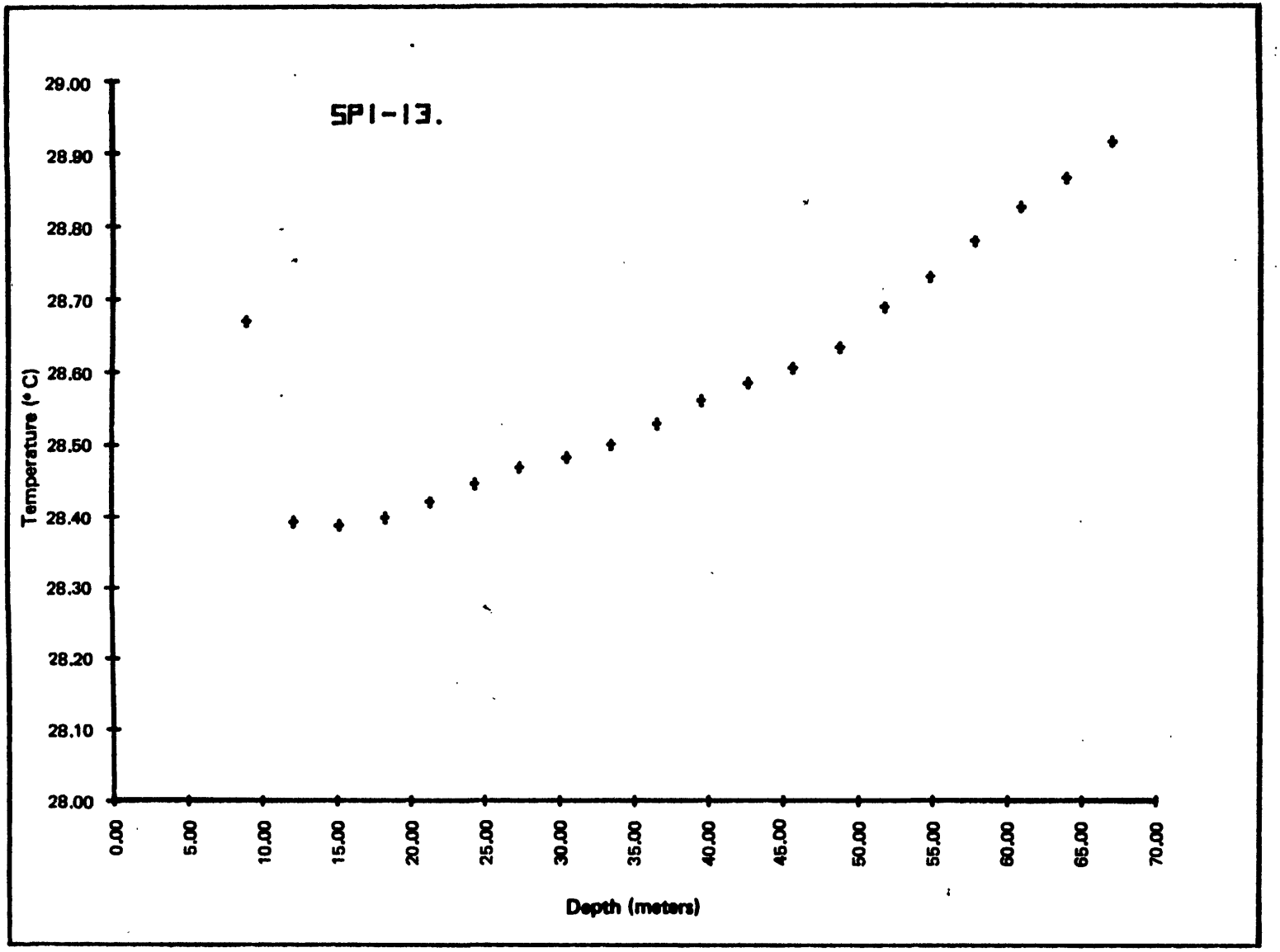

Figure 24.–Observed temperature versus depth profile for drill hole SP1-13.

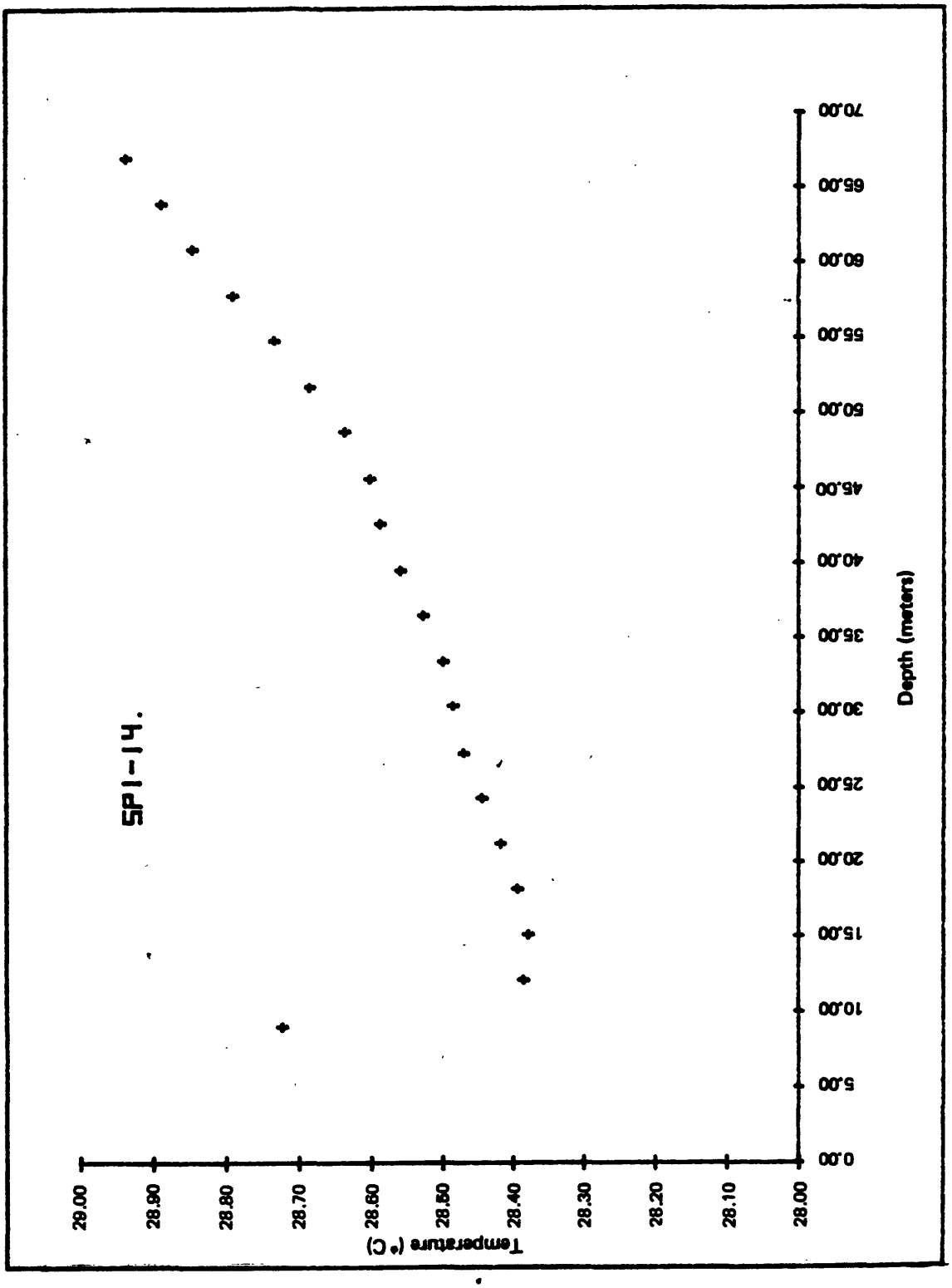

Figure 25.–Observed temperature versus depth profile for drill hole SP1-14.

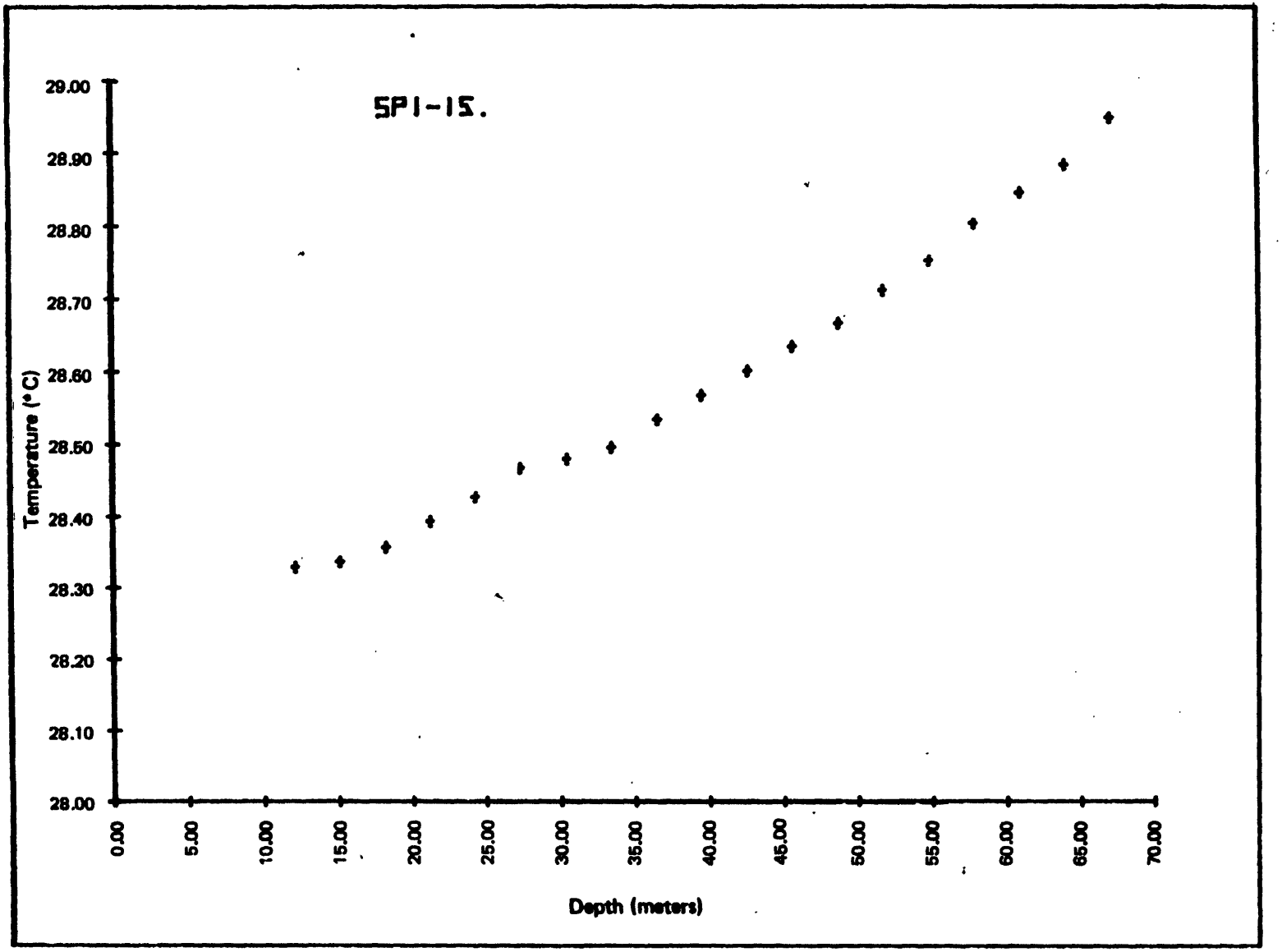

Figure 26.–Observed temperature versus depth profile for drill hole SP1-15.

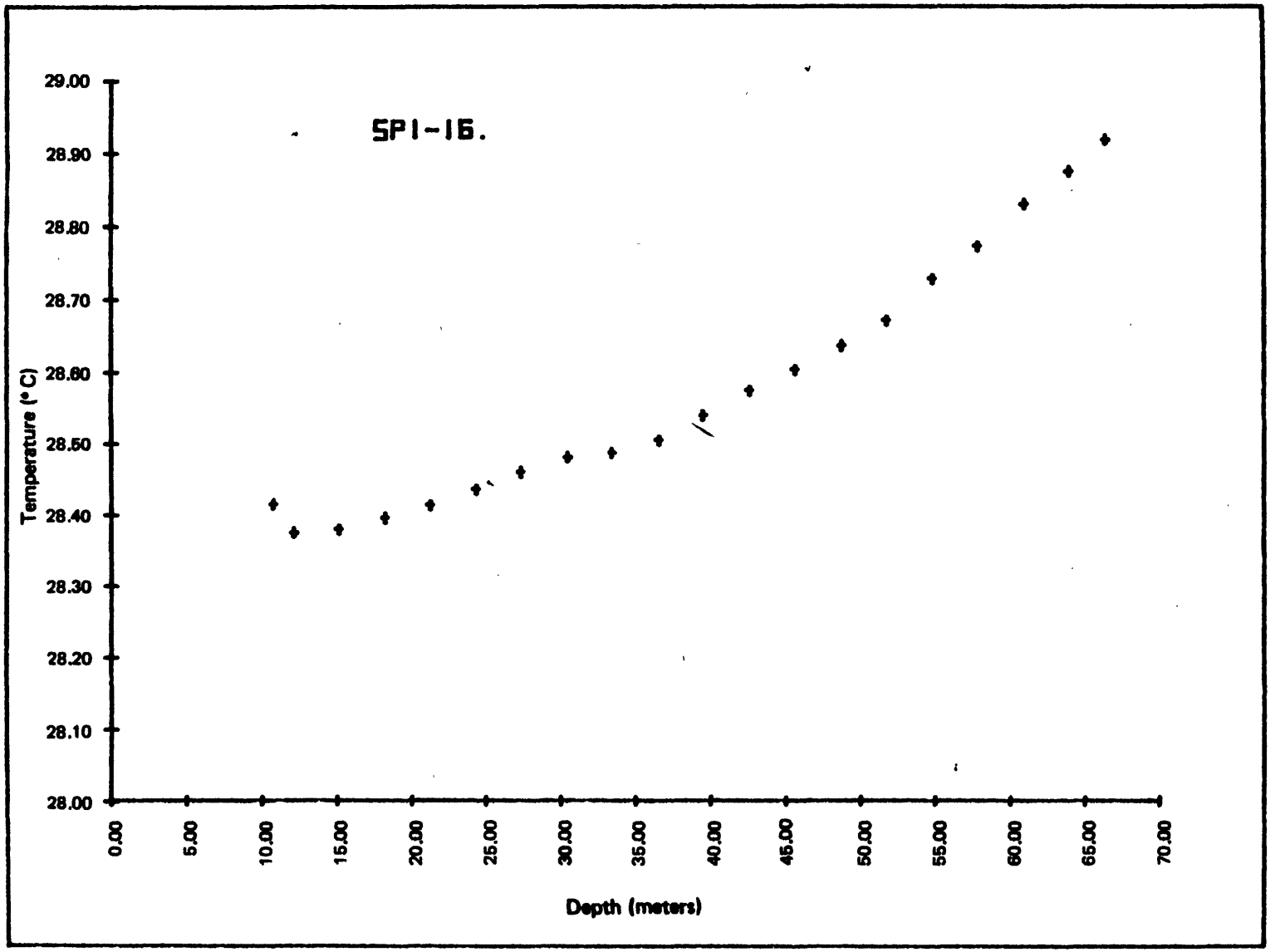

Figure 27.–Observed temperature versus depth profile for drill hole SP1-16.

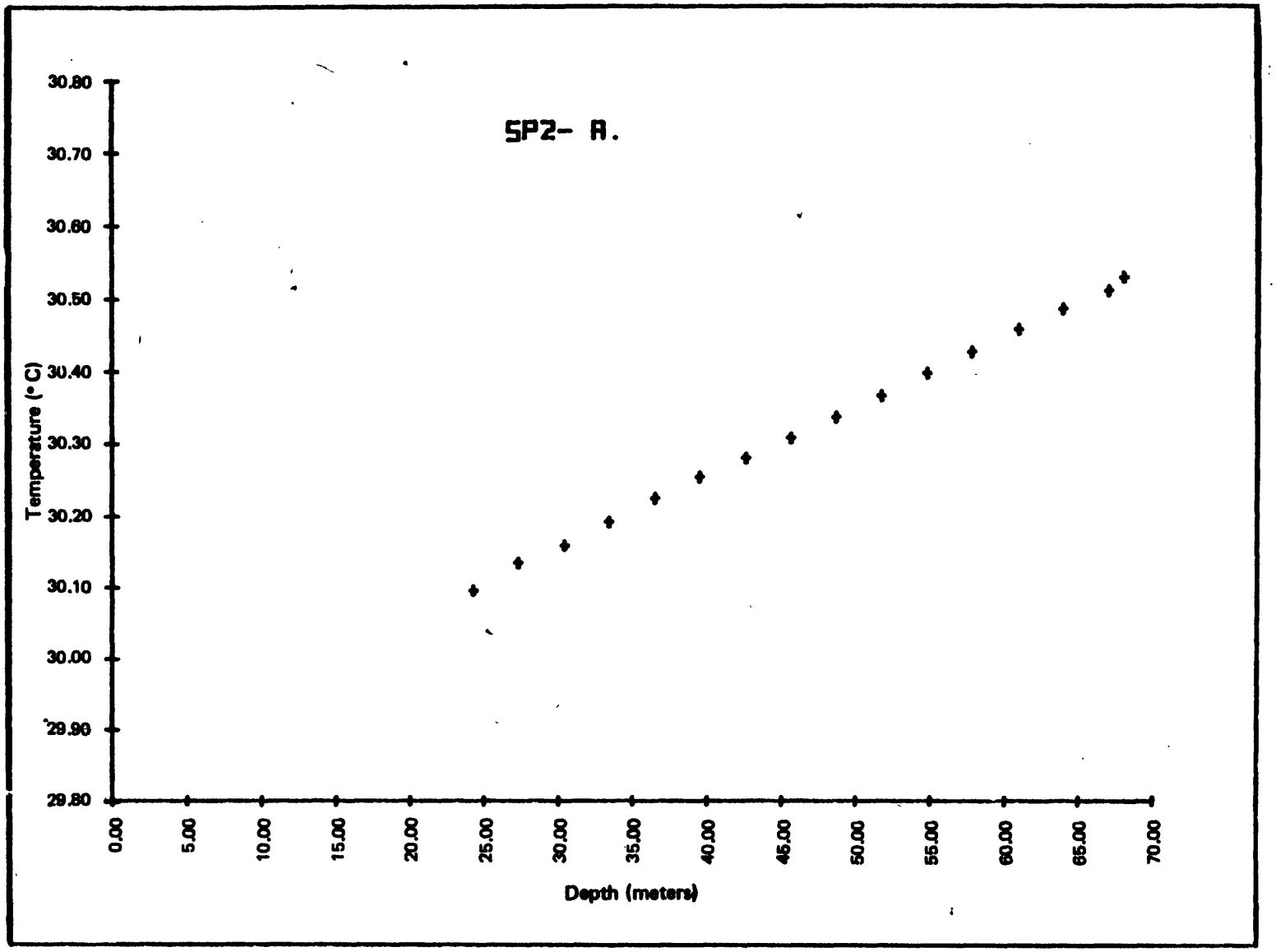

Figure 28.–Observed temperature versus depth profile for drill hole SP2-A.

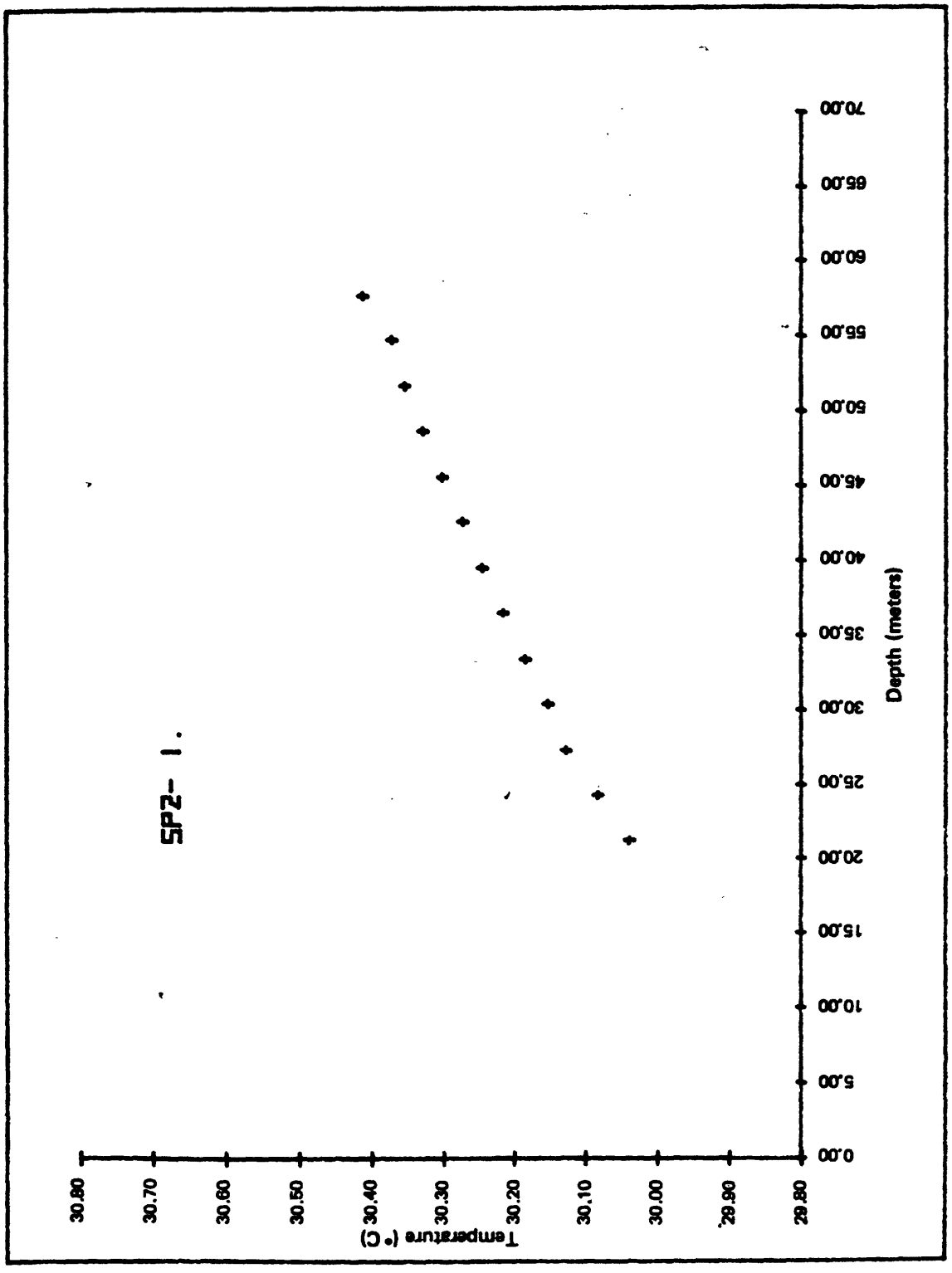

Figure 29.–Observed temperature versus depth profile for drill hole SP2-1.

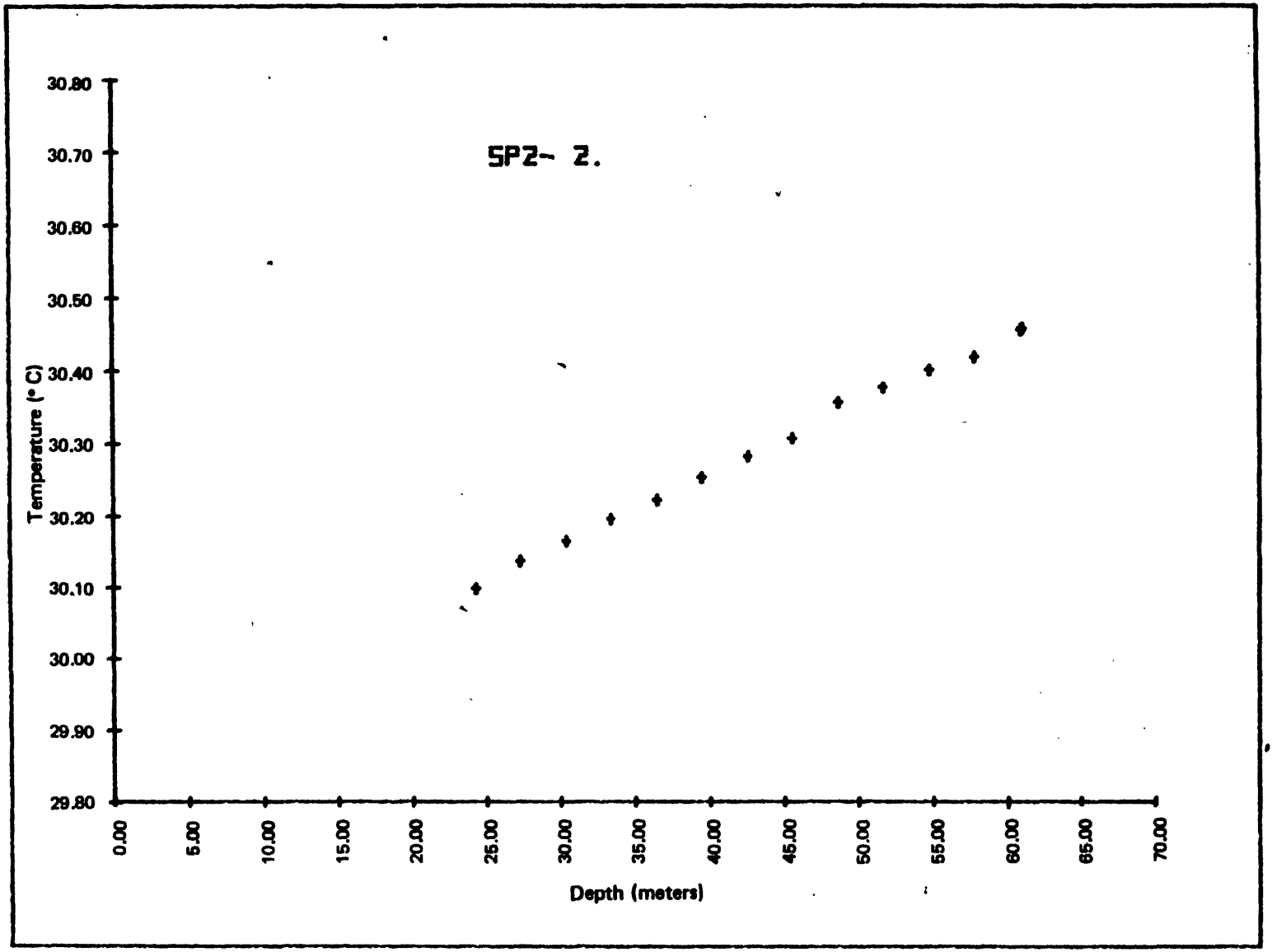

Figure 30.–Observed temperature versus depth profile for drill hole SP2-2.

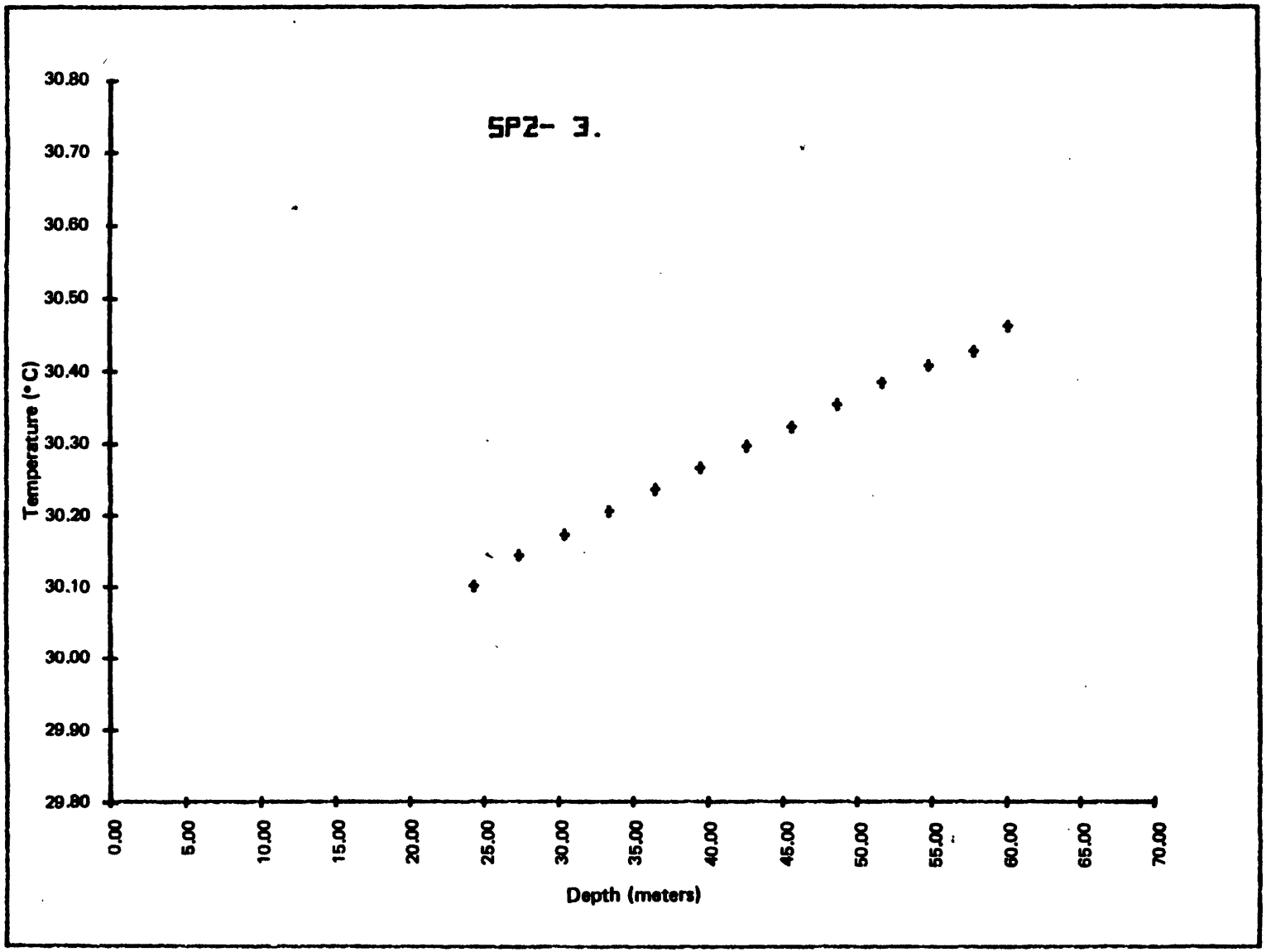

Figure 31.–Observed temperature versus depth profile for drill hole SP2-3.

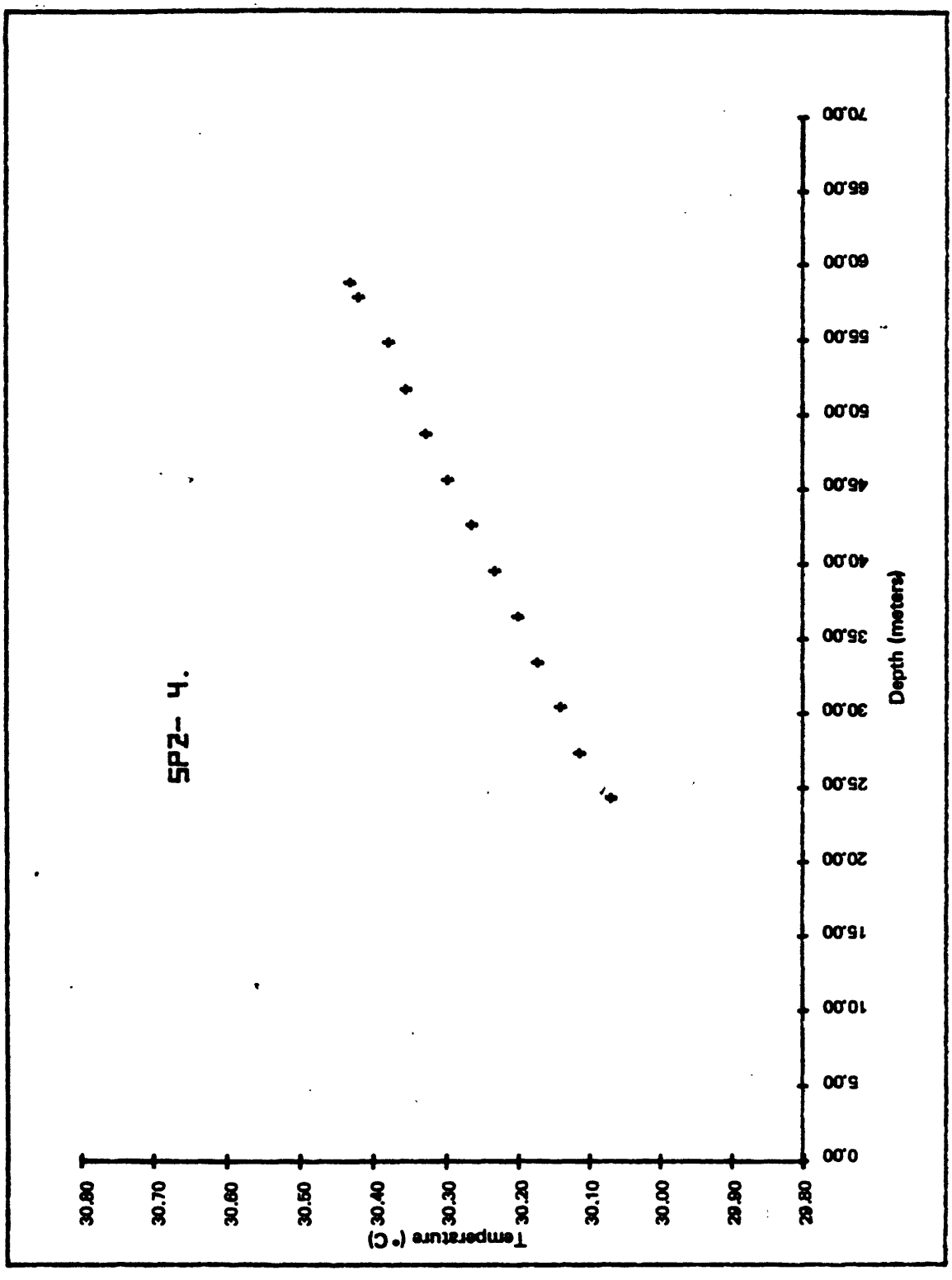

Figure 32.–Observed temperature versus depth profile for drill hole SP2-4.

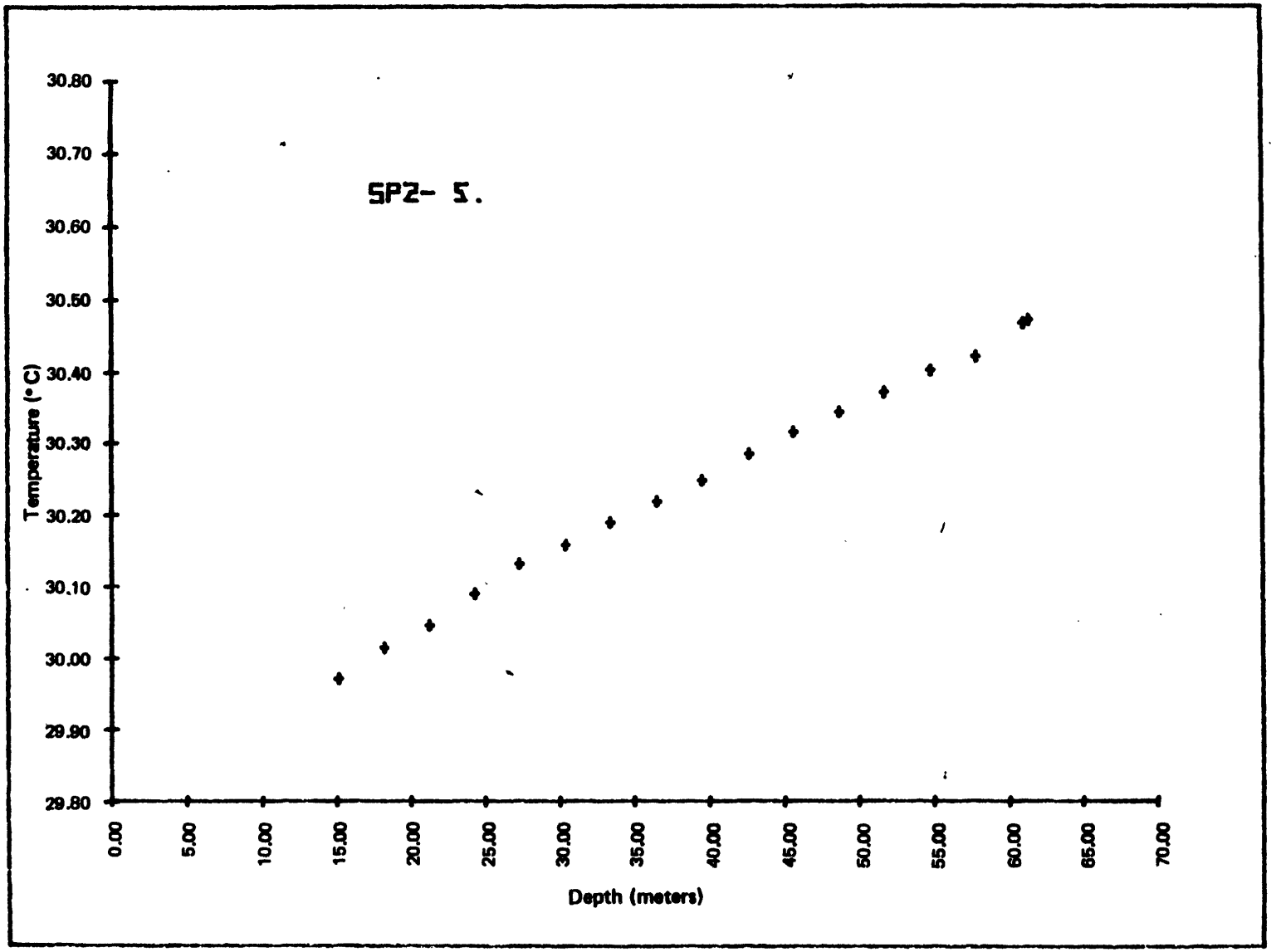

Figure 33.–Observed temperature versus depth profile for drill hole SP2-5.

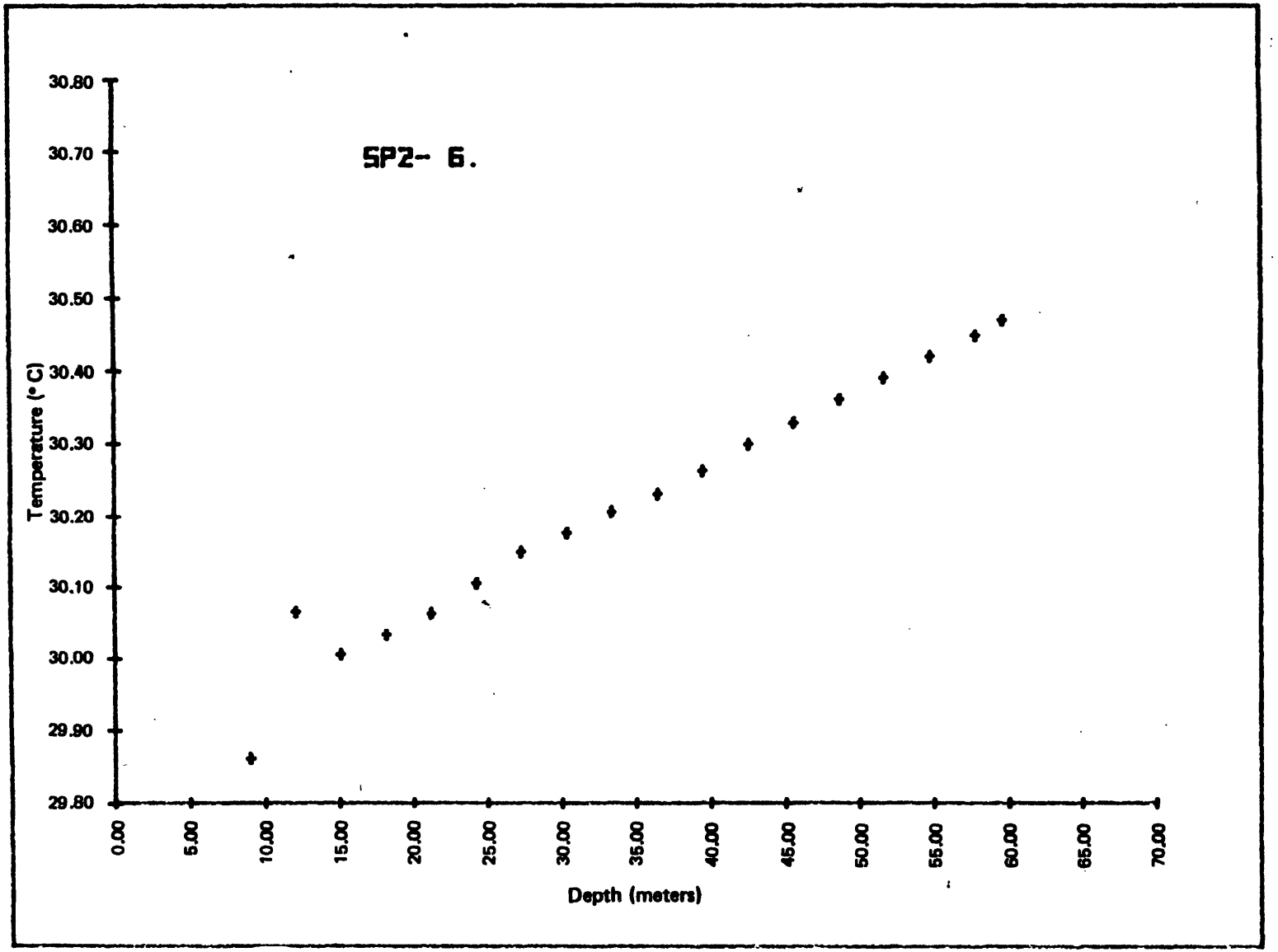

Figure 34.–Observed temperature versus depth profile for drill hole SP2-6.

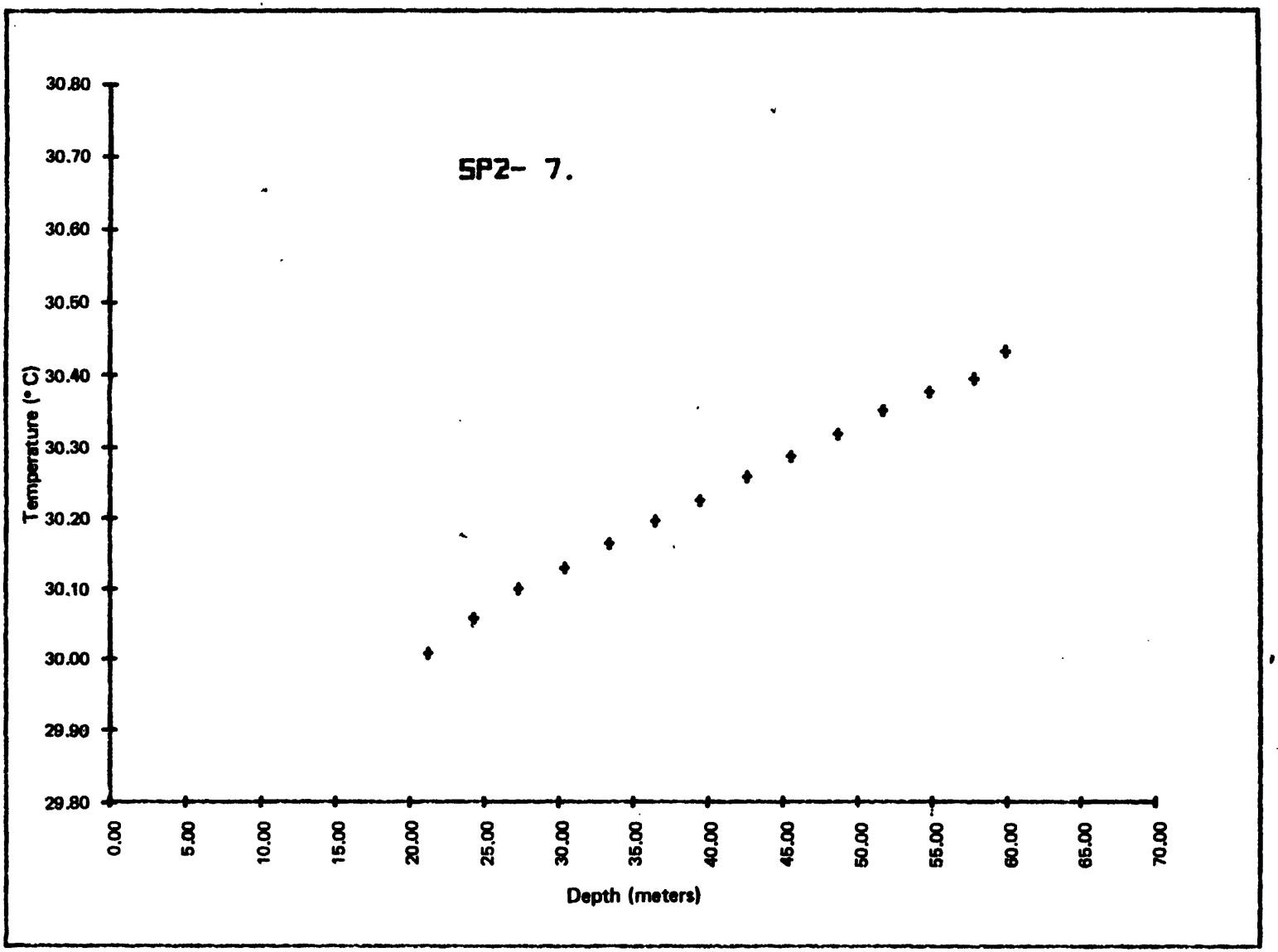

Figure 35.–Observed temperature versus depth profile for drill hole SP2-7.

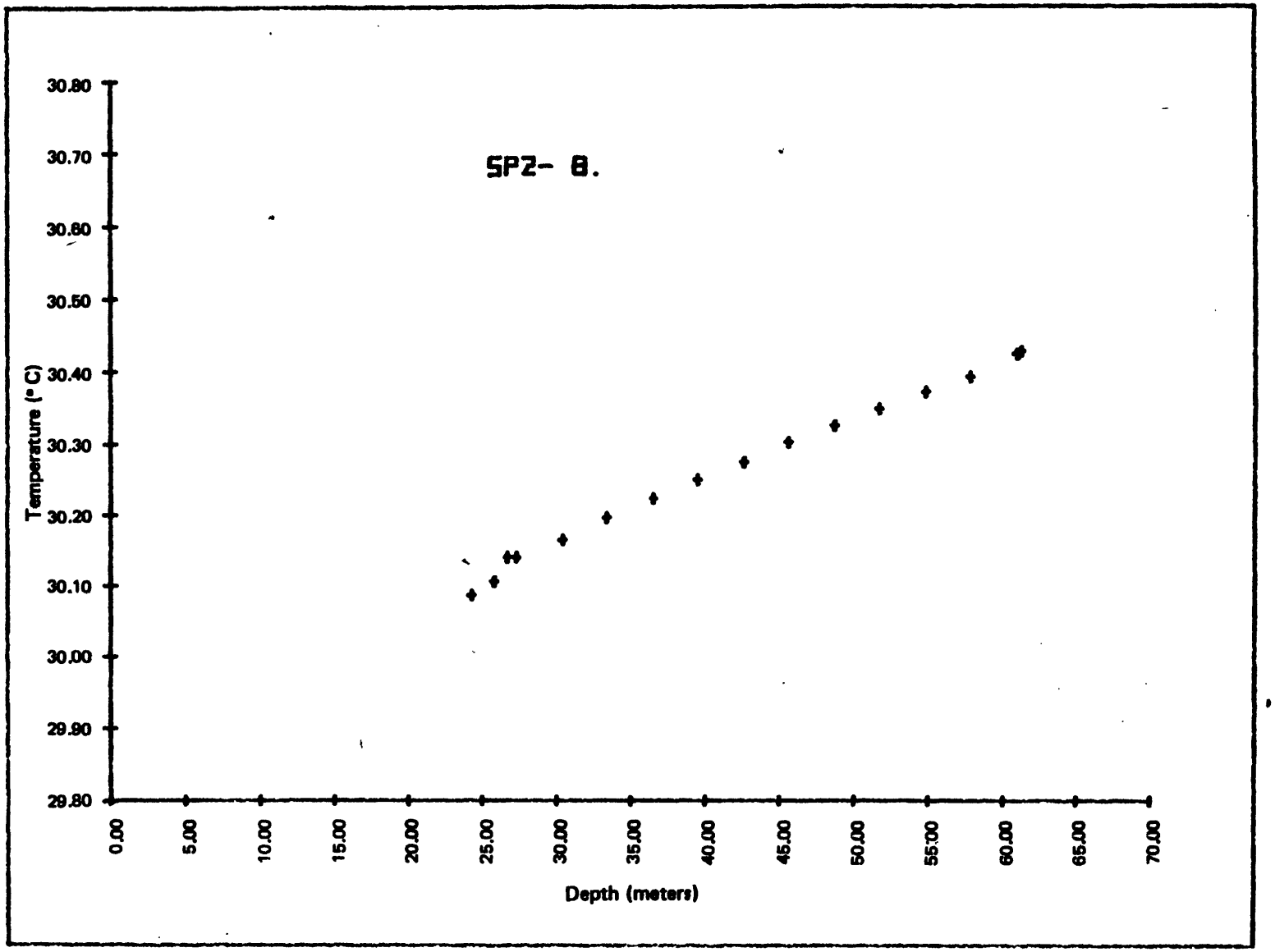

Figure 36.–Observed temperature versus depth profile for drill hole SP2-8.

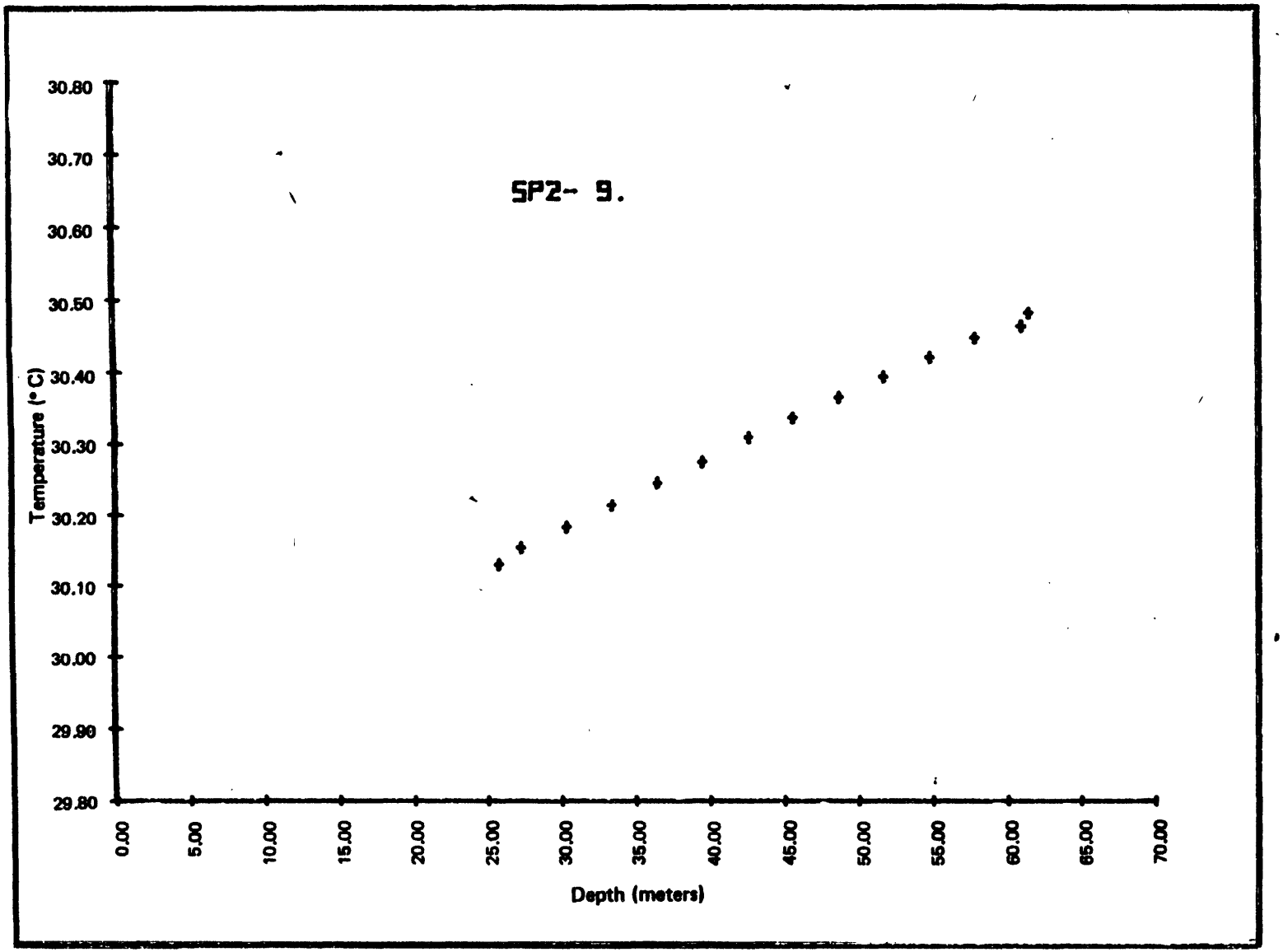

Figure 37.–Observed temperature versus depth profile for drill hole SP2-9.

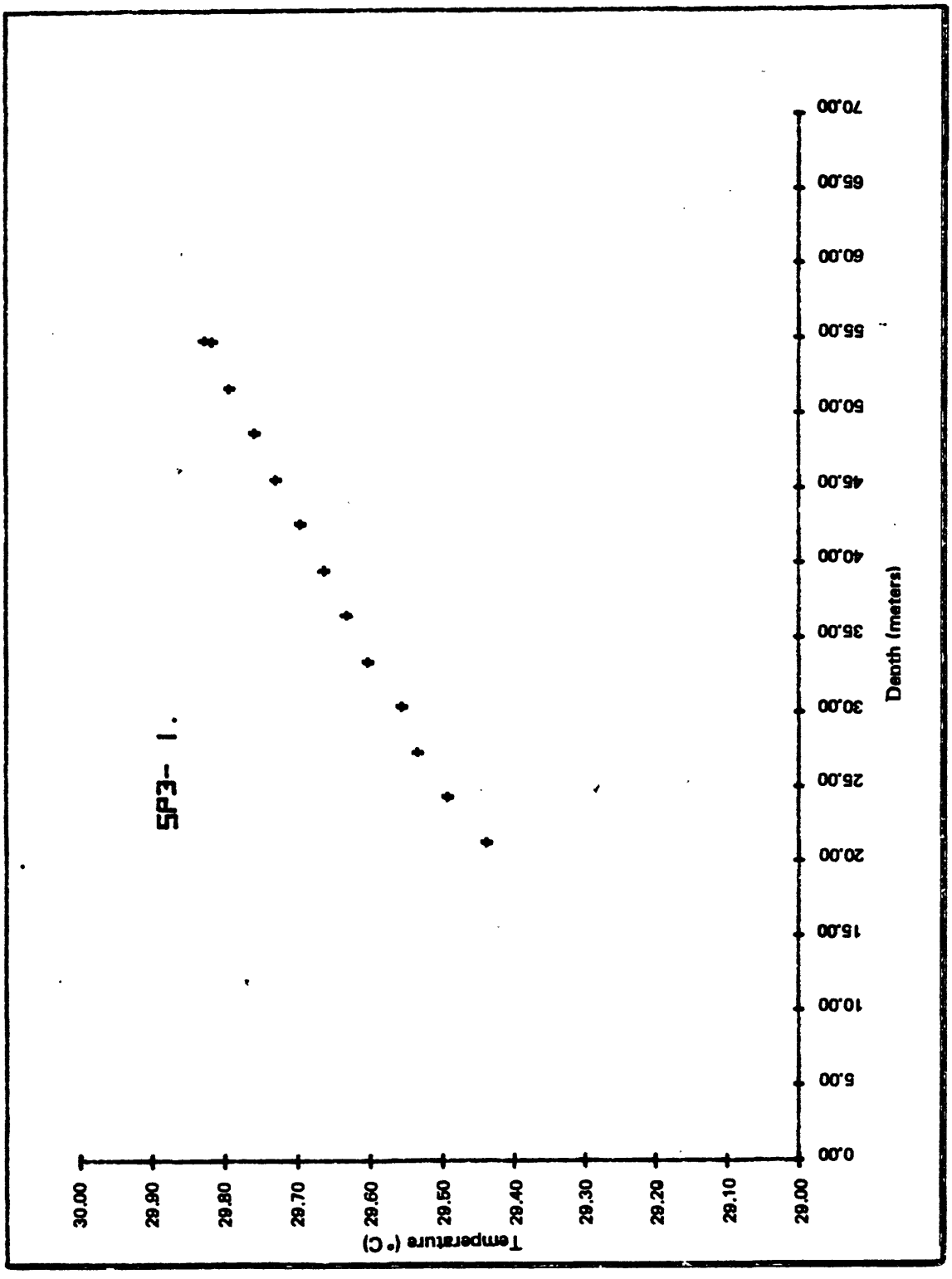

Figure 38.–Observed temperature versus depth profile for drill hole SP3-1.

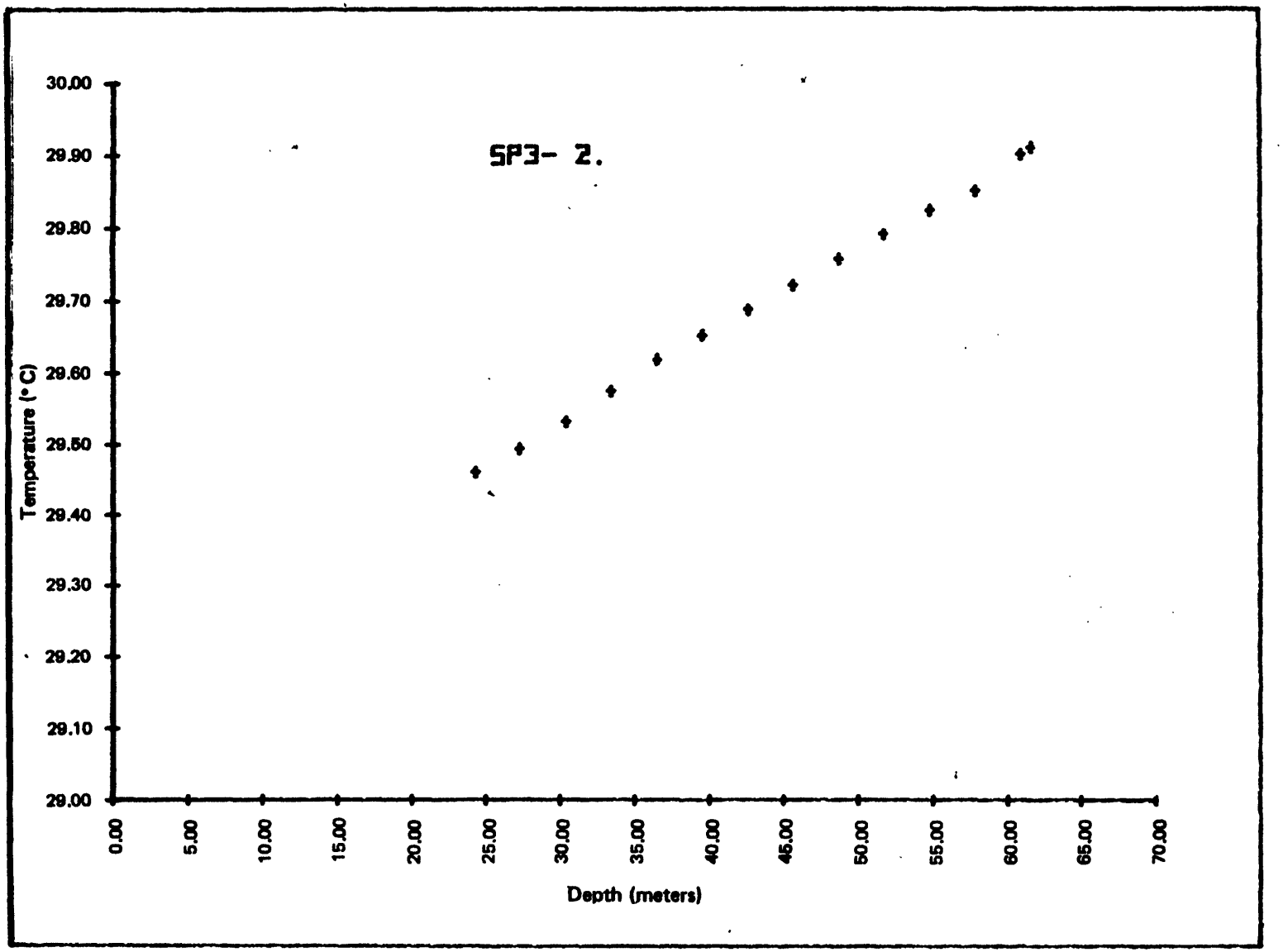

Figure 39.–Observed temperature versus depth profile for drill hole SP3-2.

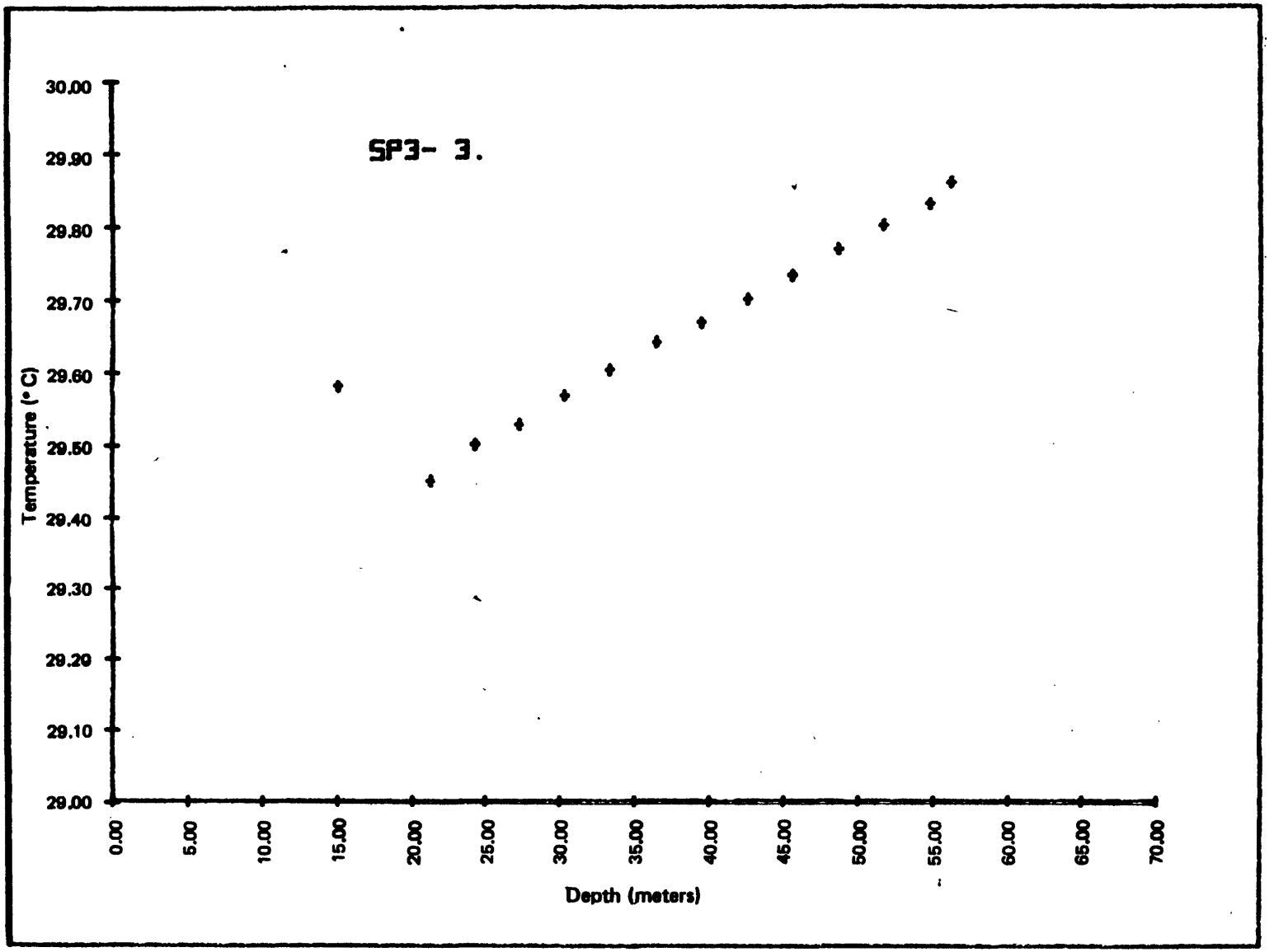

Figure 40.–Observed temperature versus depth profile for drill hole SP3-3.

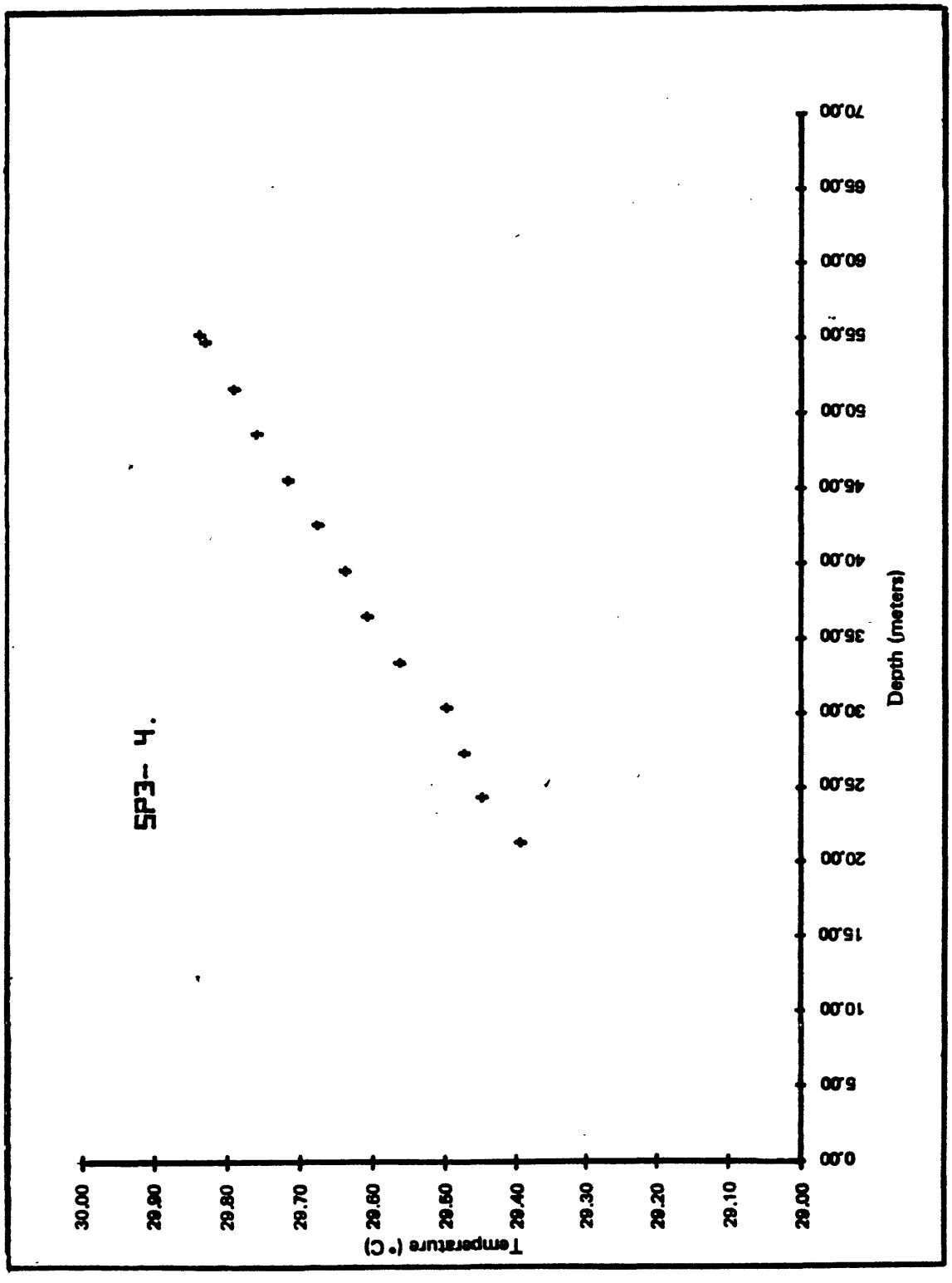

Figure 41.–Observed temperature versus depth profile for drill hole SP3-4.

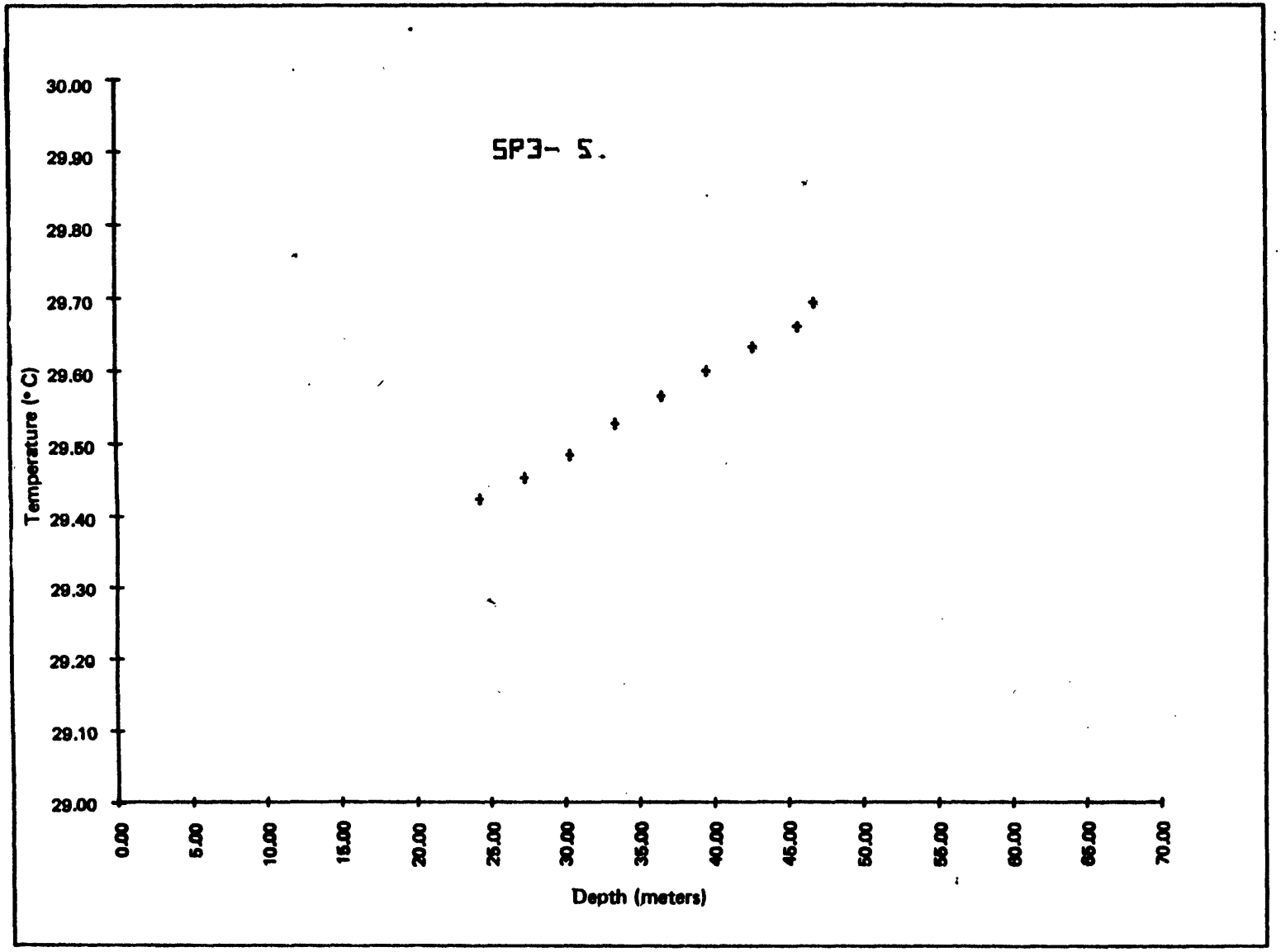

Figure 42.–Observed temperature versus depth profile for drill hole SP3-5.

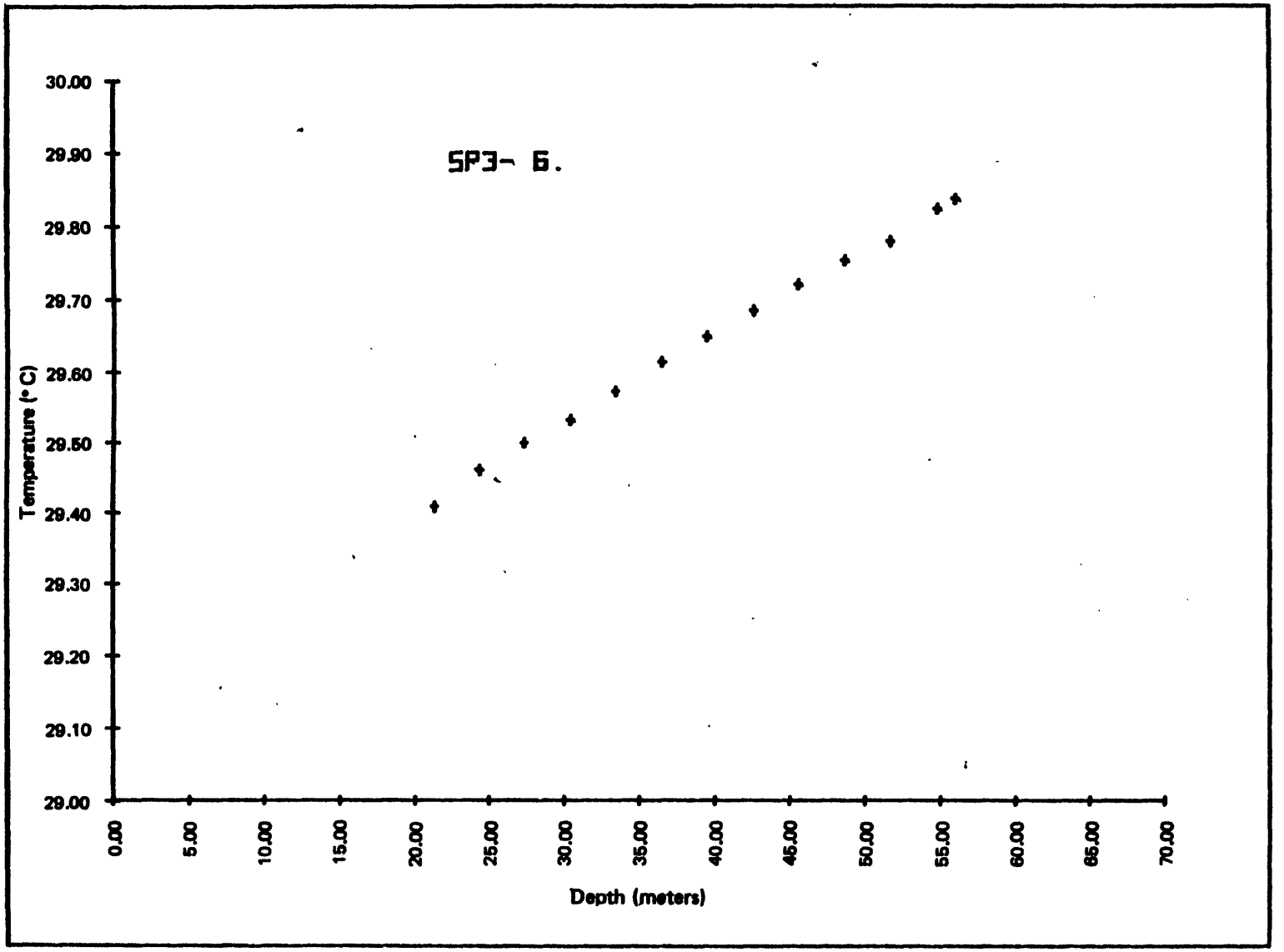

Figure 43.–Observed temperature versus depth profile for drill hole SP3-6.

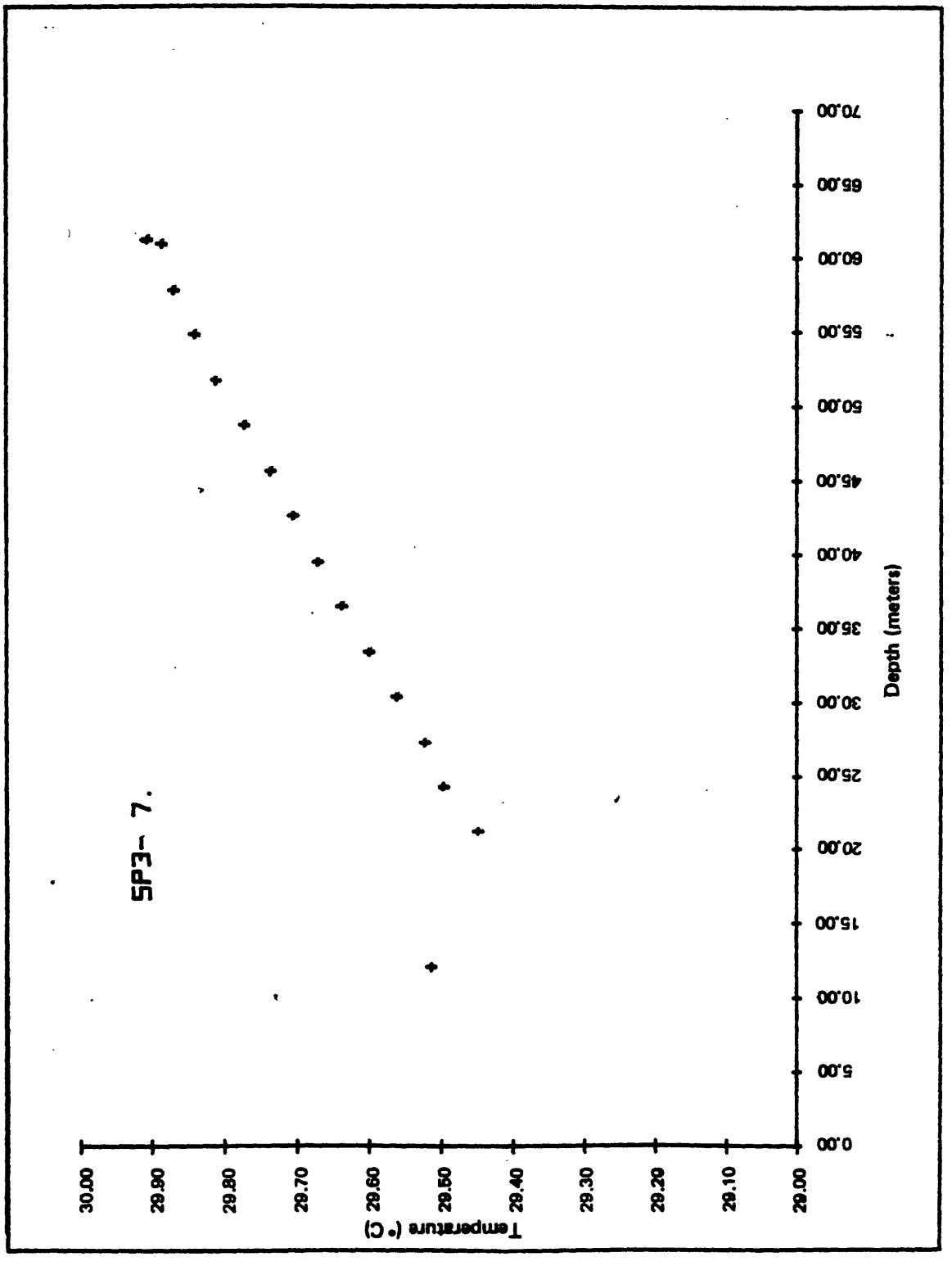

Figure 44.–Observed temperature versus depth profile for drill hole SP3-7.

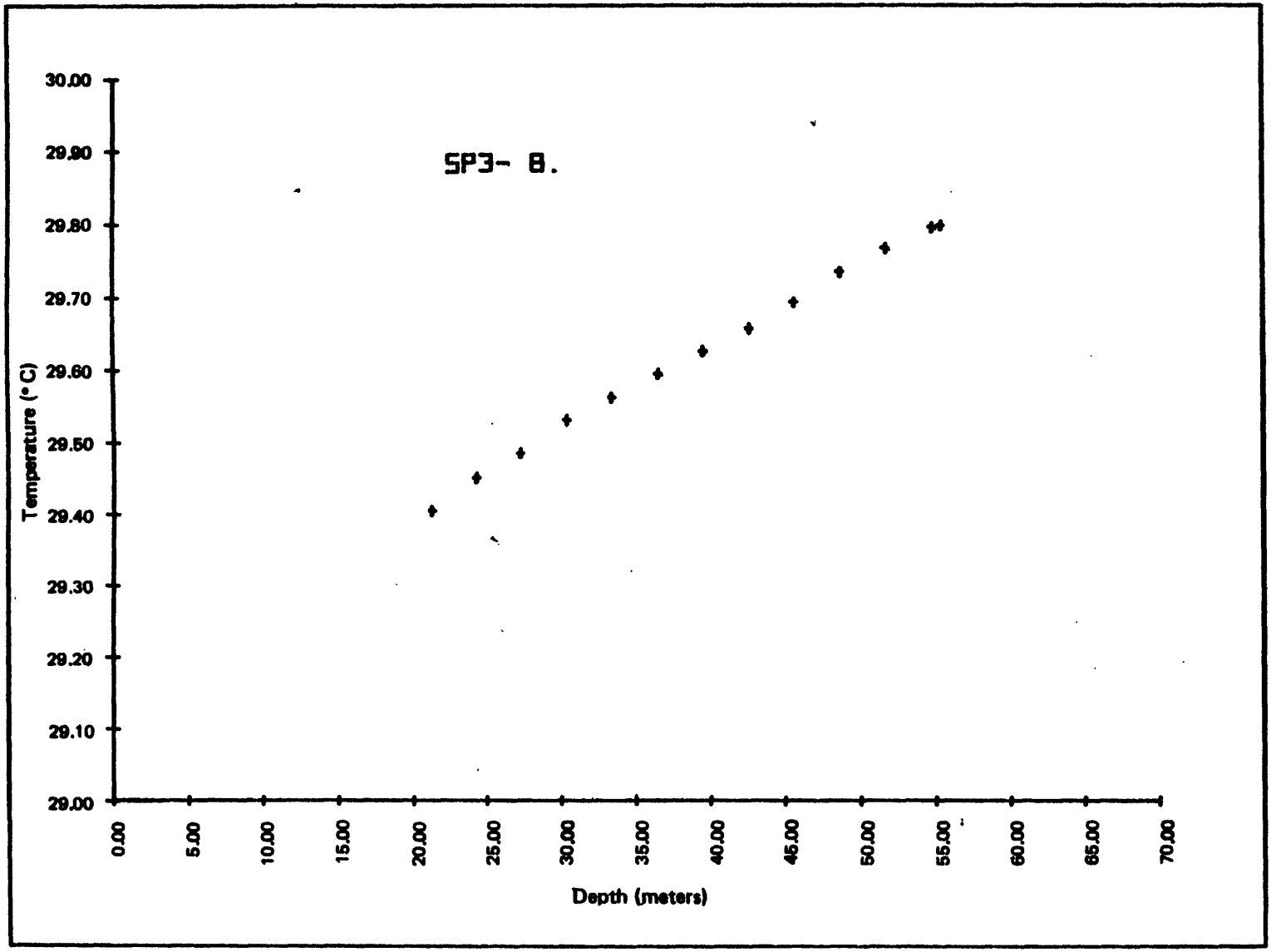

Figure 45.–Observed temperature versus depth profile for drill hole SP3-8.

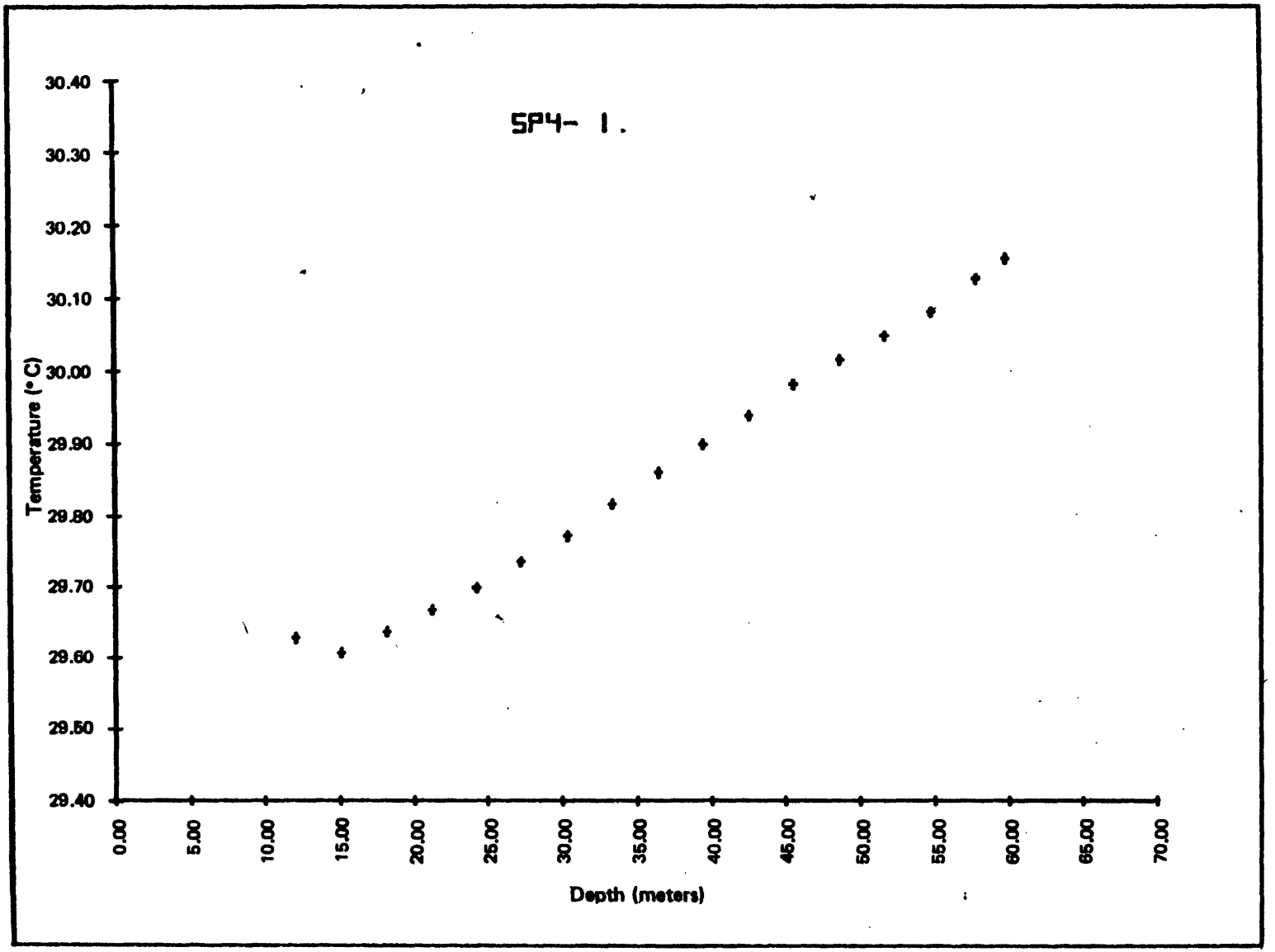

Figure 46.–Observed temperature versus depth profile for drill hole SP4-1.

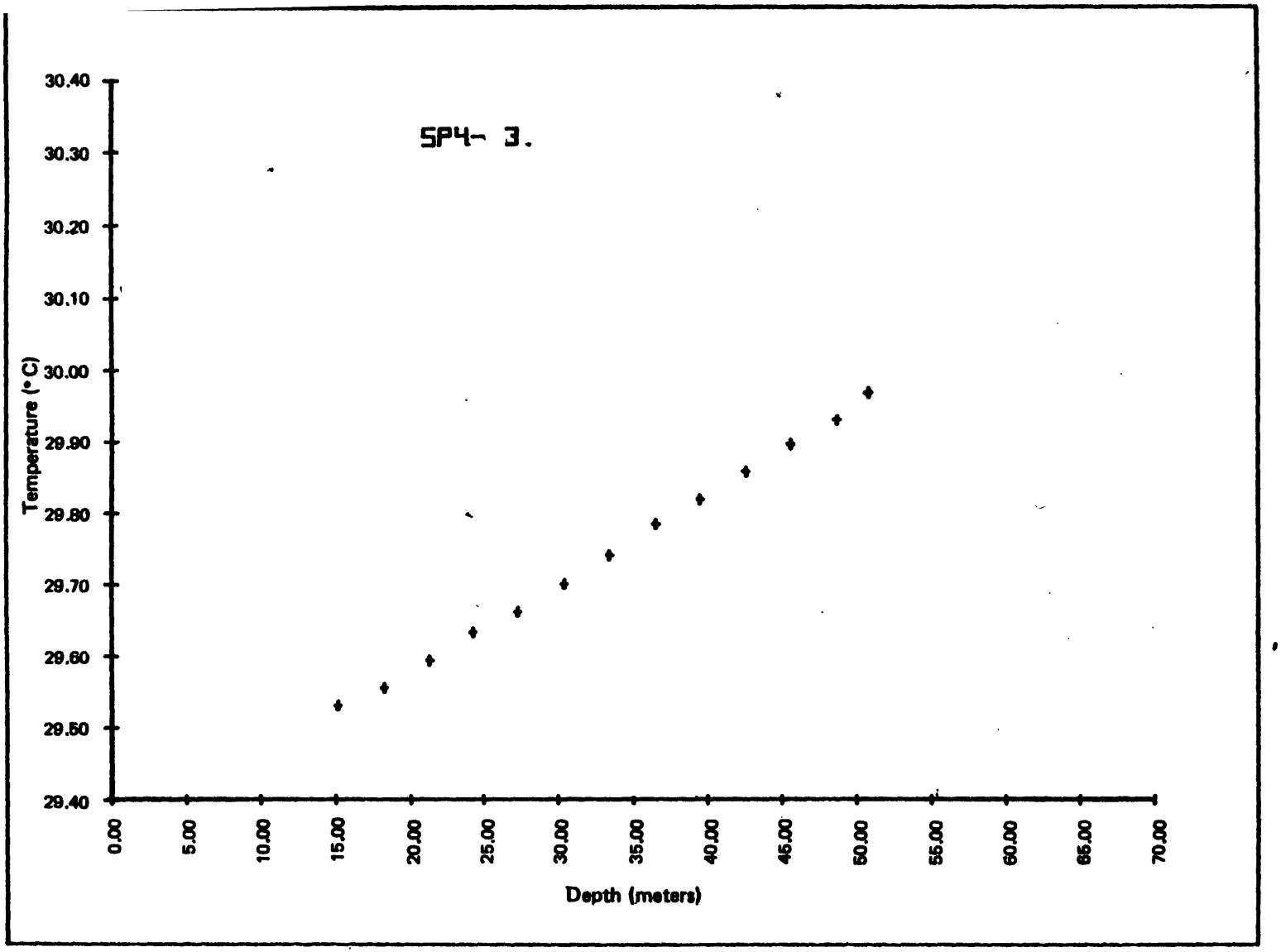

Figure 47.–Observed temperature versus depth profile for drill hole SP4-3.

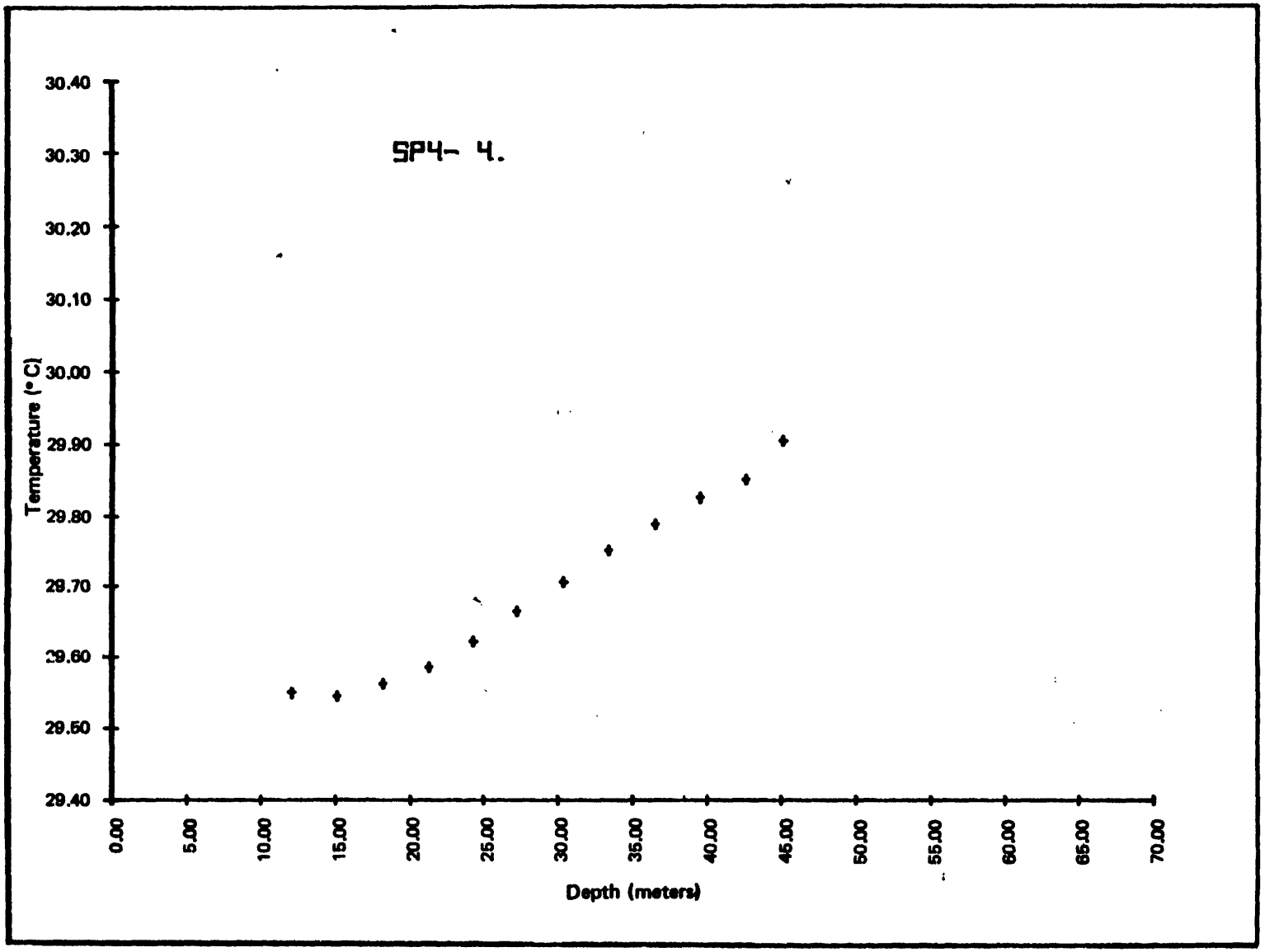

Figure 48.–Observed temperature versus depth profile for drill hole SP4-4.

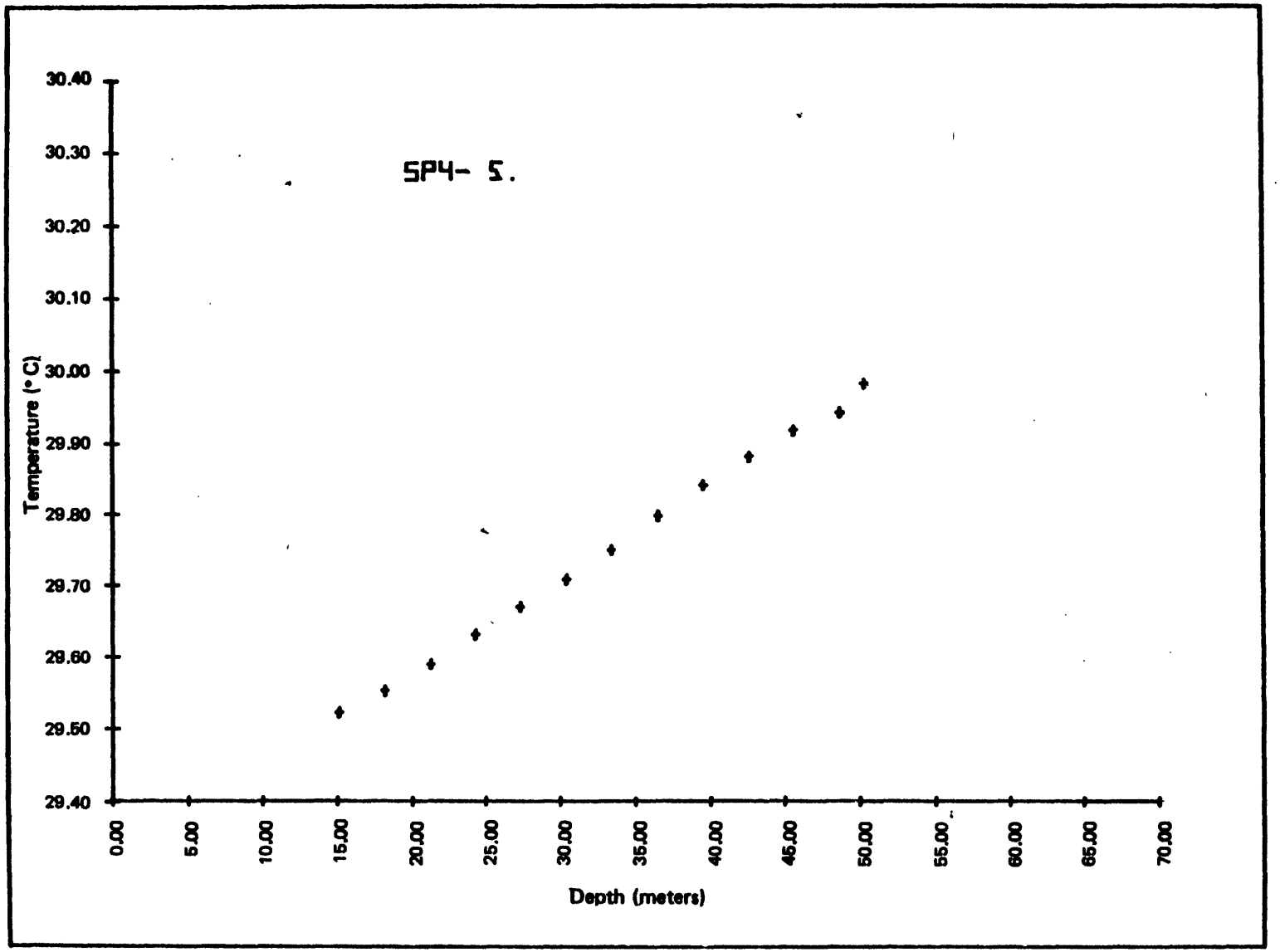

Figure 49.–Observed temperature versus depth profile for drill hole SP4-5.

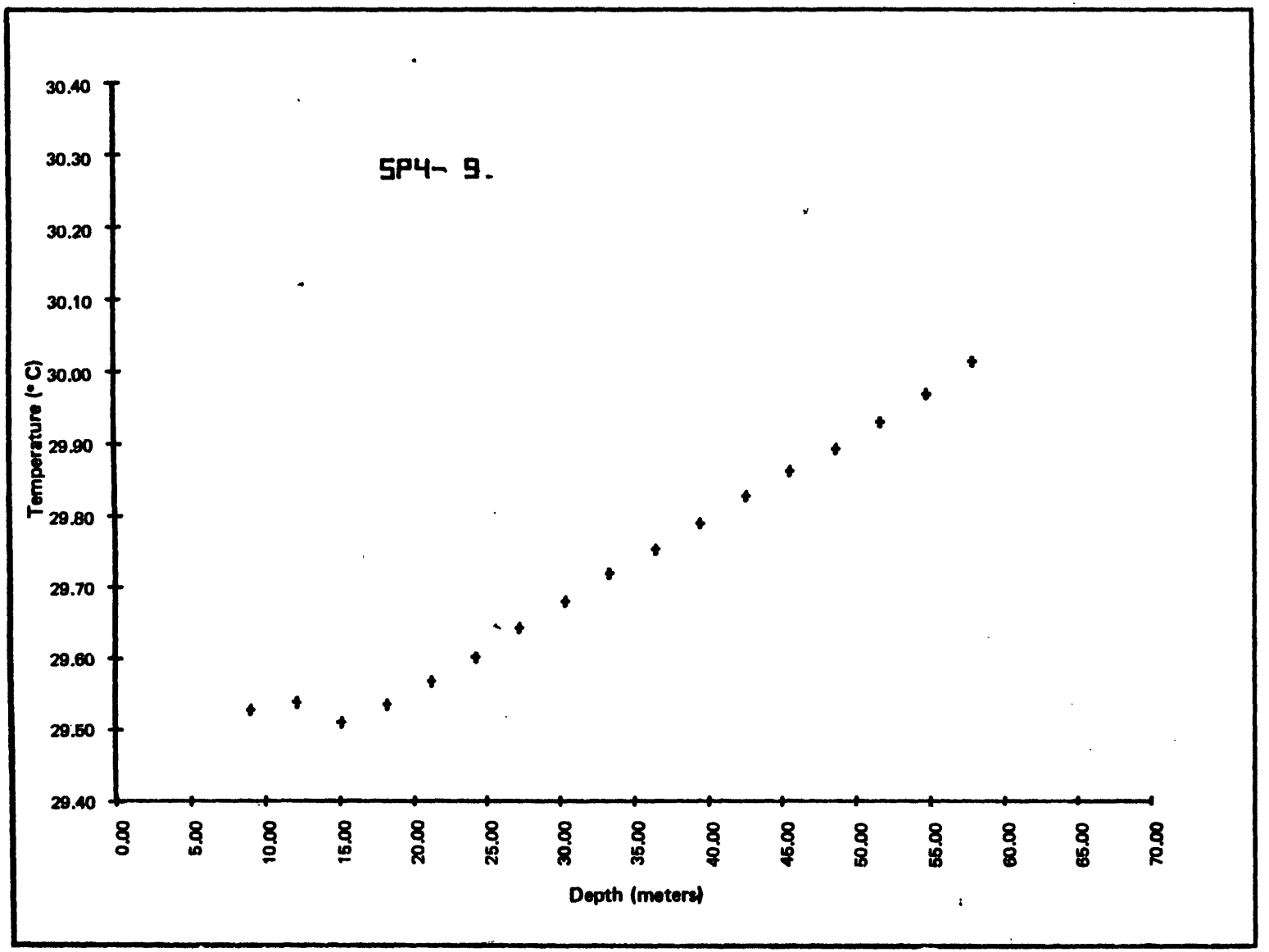

Figure 50.–Observed temperature versus depth profile for drill hole SP4-9.

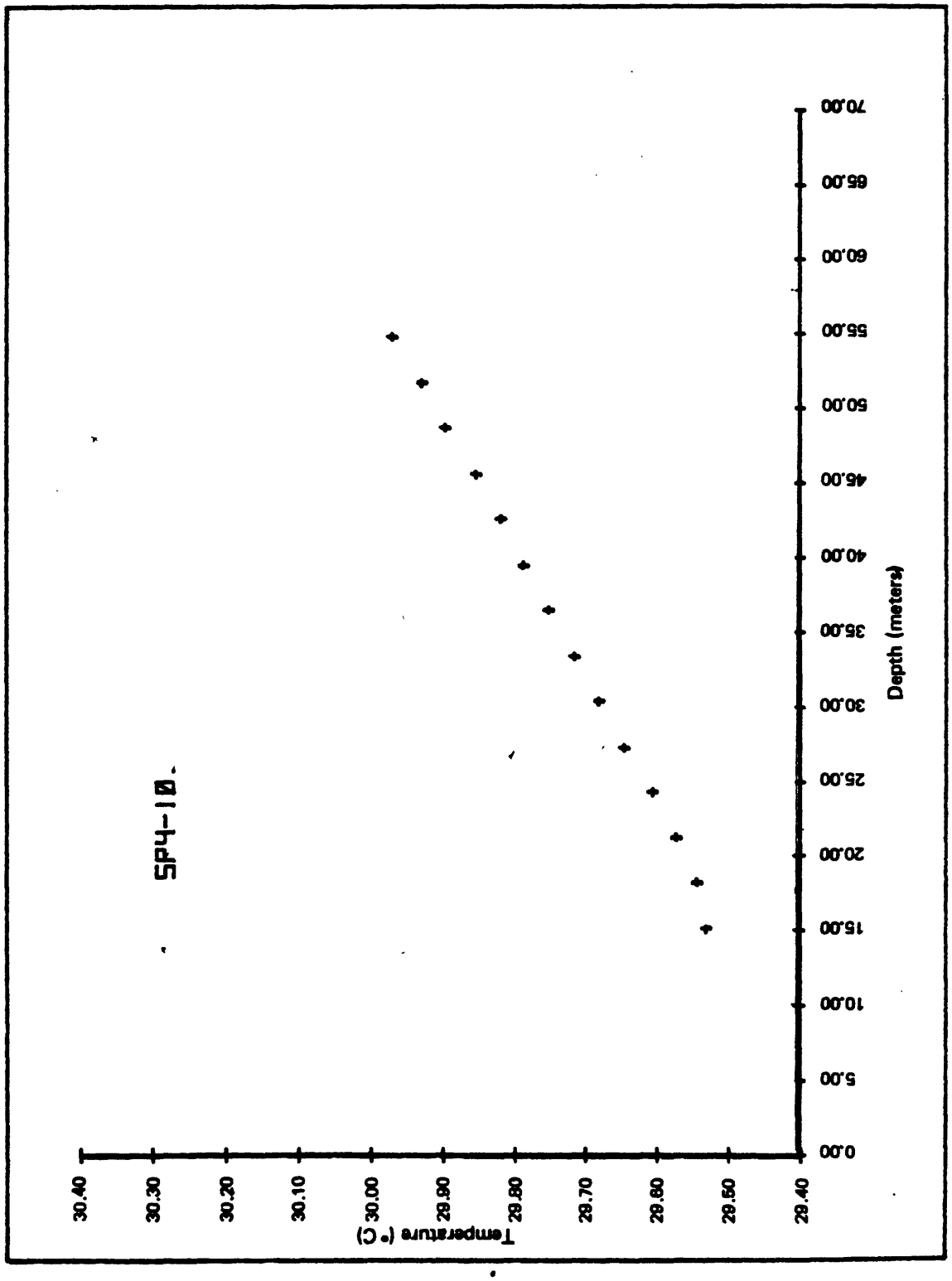

Figure 51.–Observed temperature versus depth profile for drill hole SP4-10.

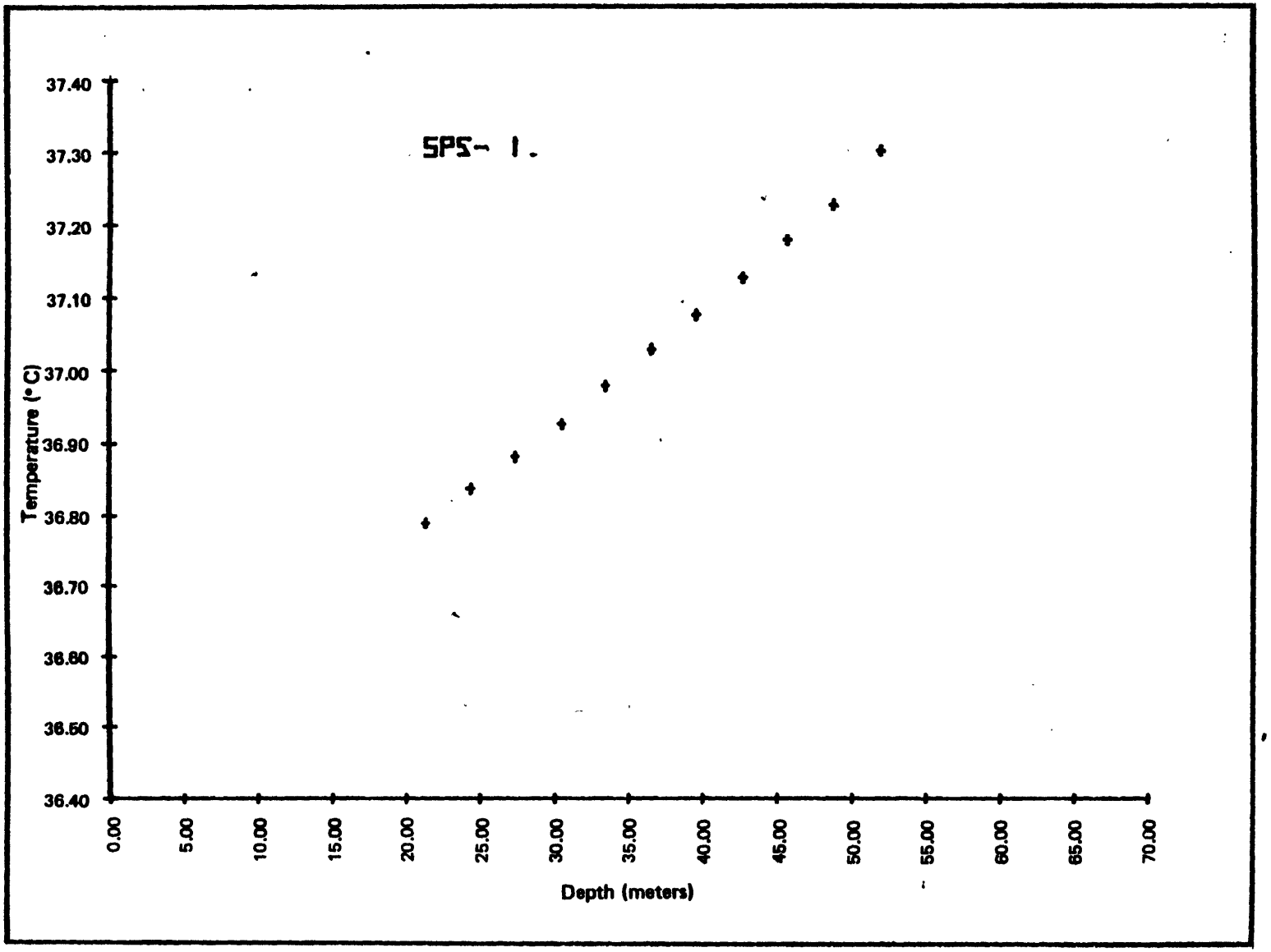

Figure 52.–Observed temperature versus depth profile for drill hole SP5-1.

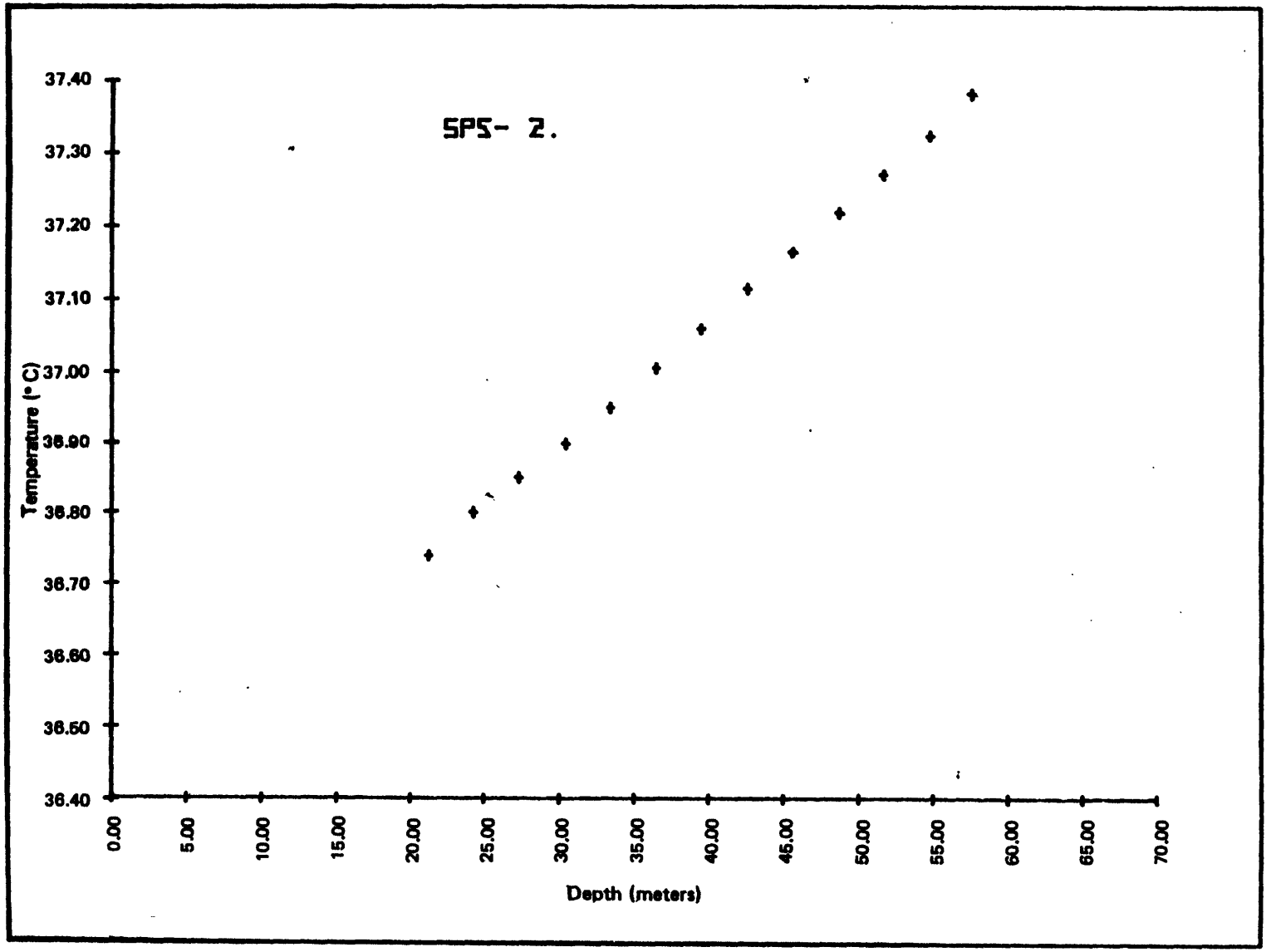

Figure 53.–Observed temperature versus depth profile for drill hole SP5-2.

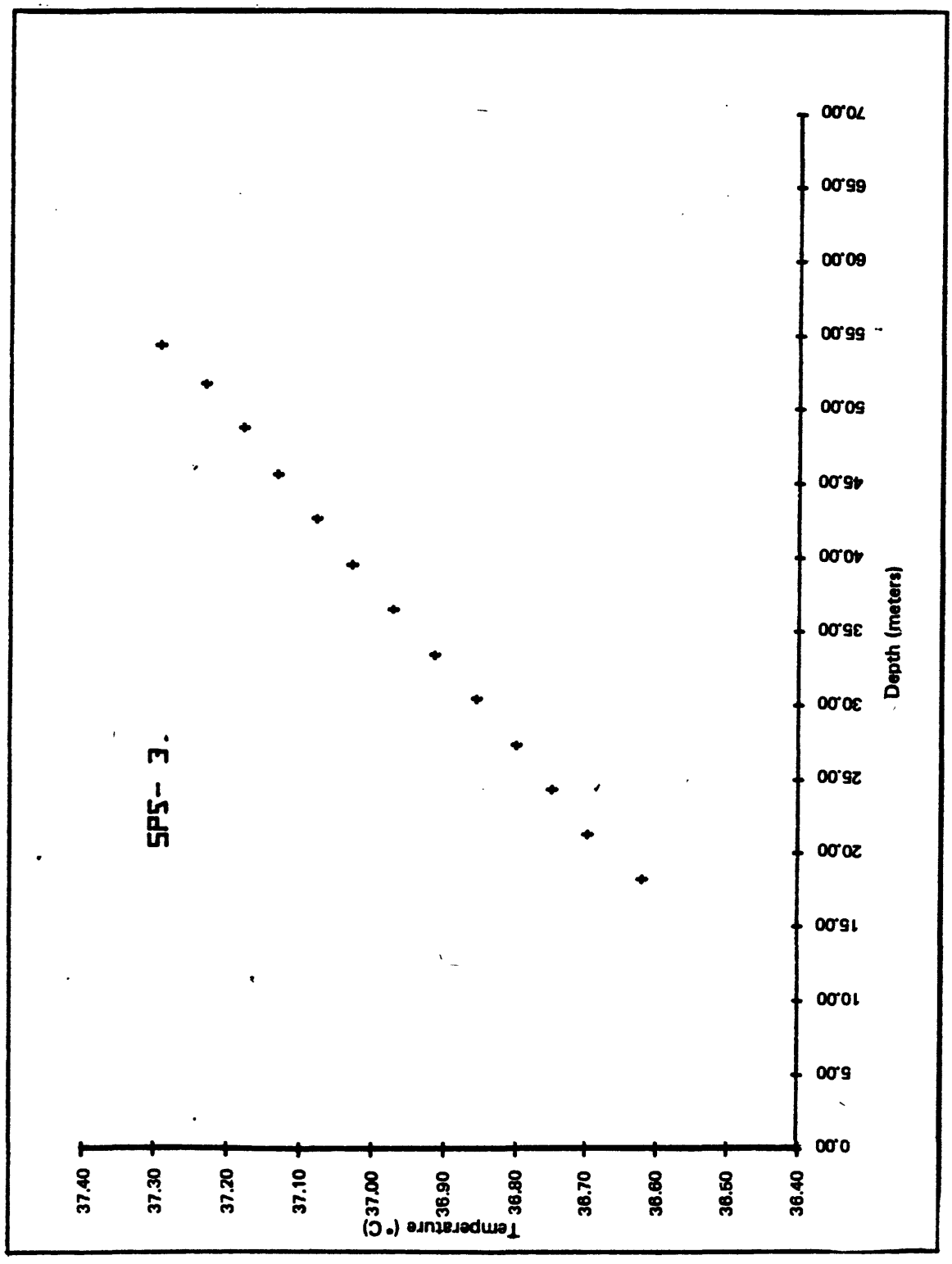

Figure 54.–Observed temperature versus depth profile for drill hole SP5-3.

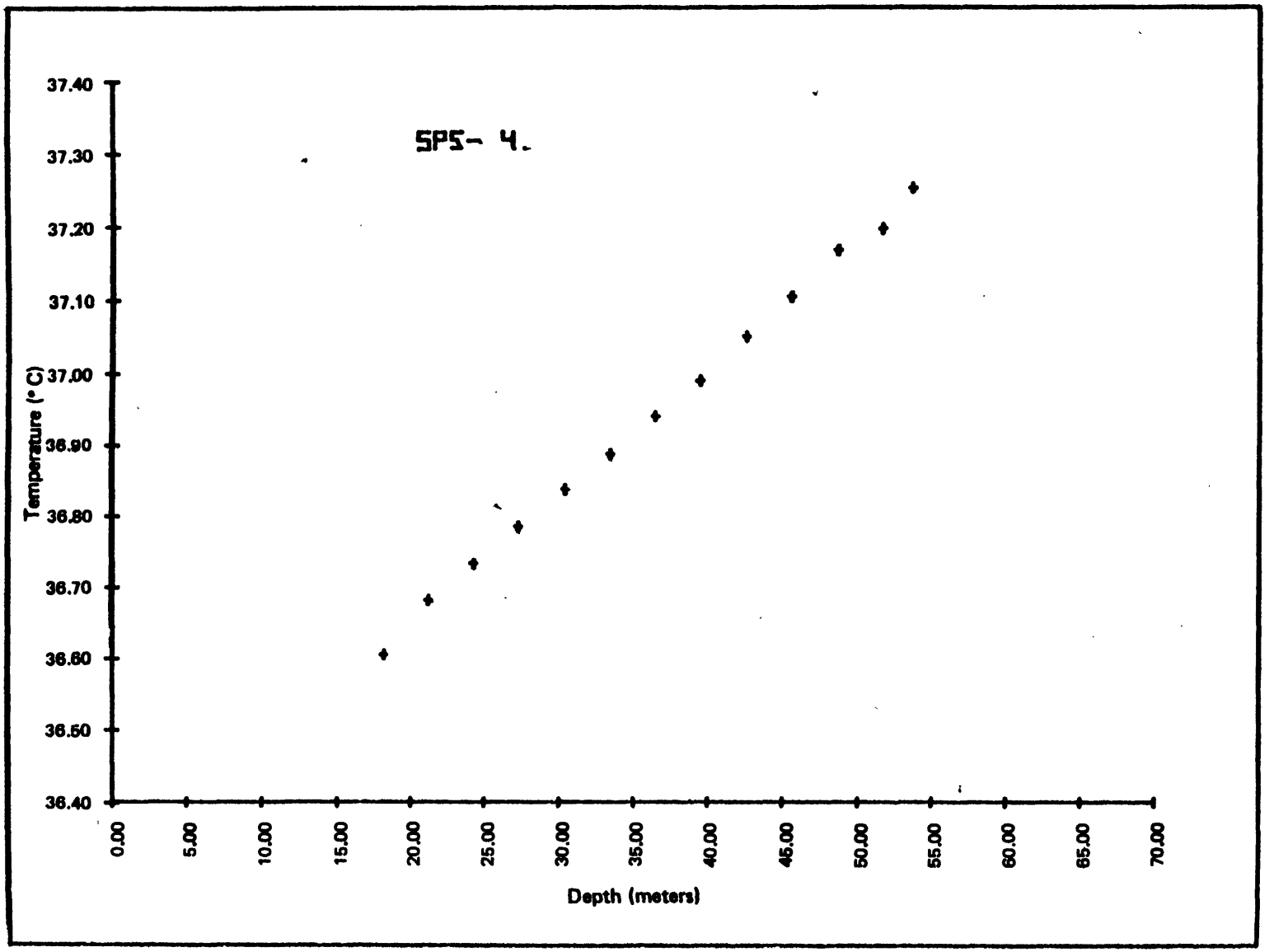

Figure 55.–Observed temperature versus depth profile for drill hole SP5-4.

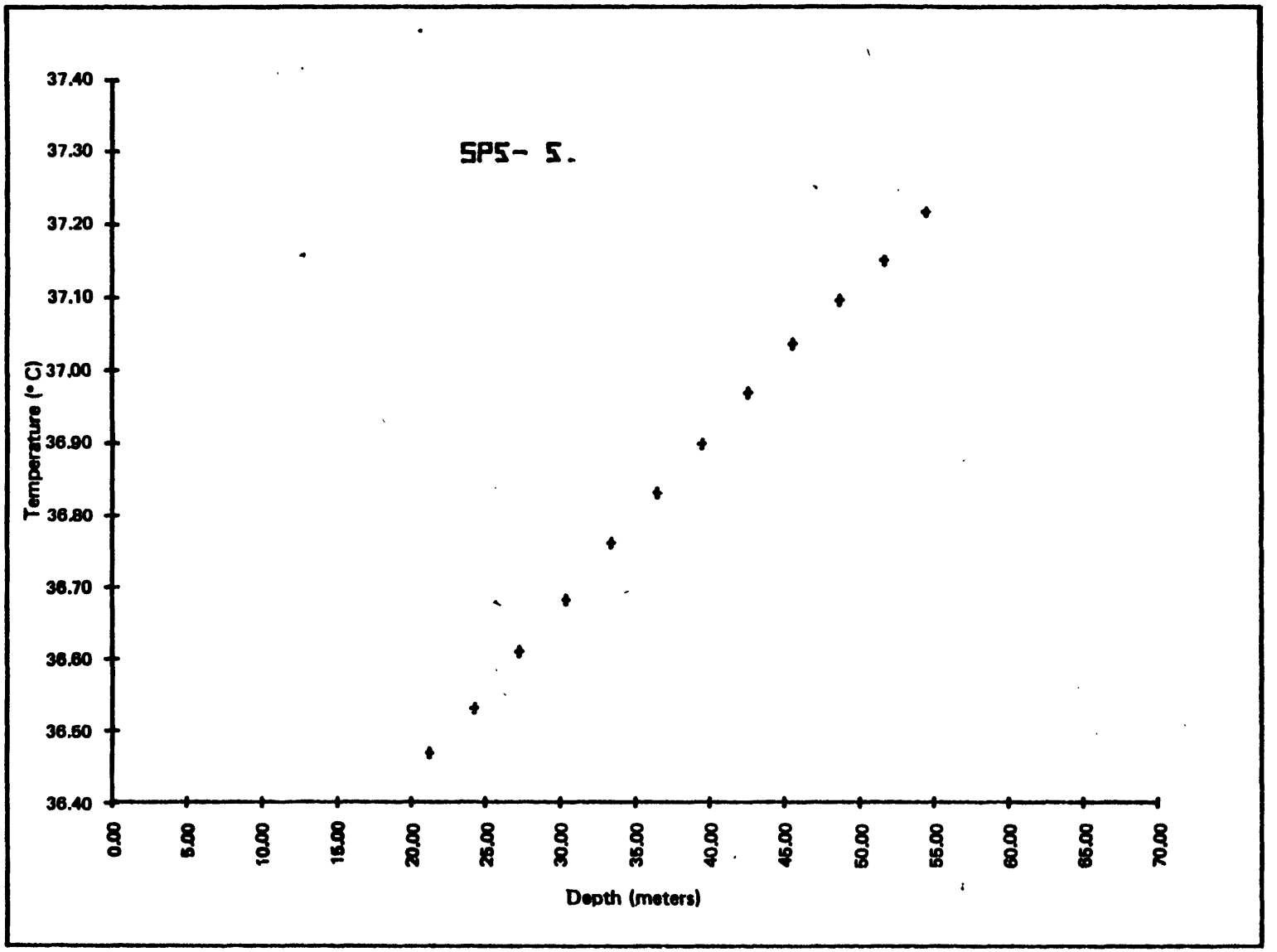

Figure 56.–Observed temperature versus depth profile for drill hole SP5-5.

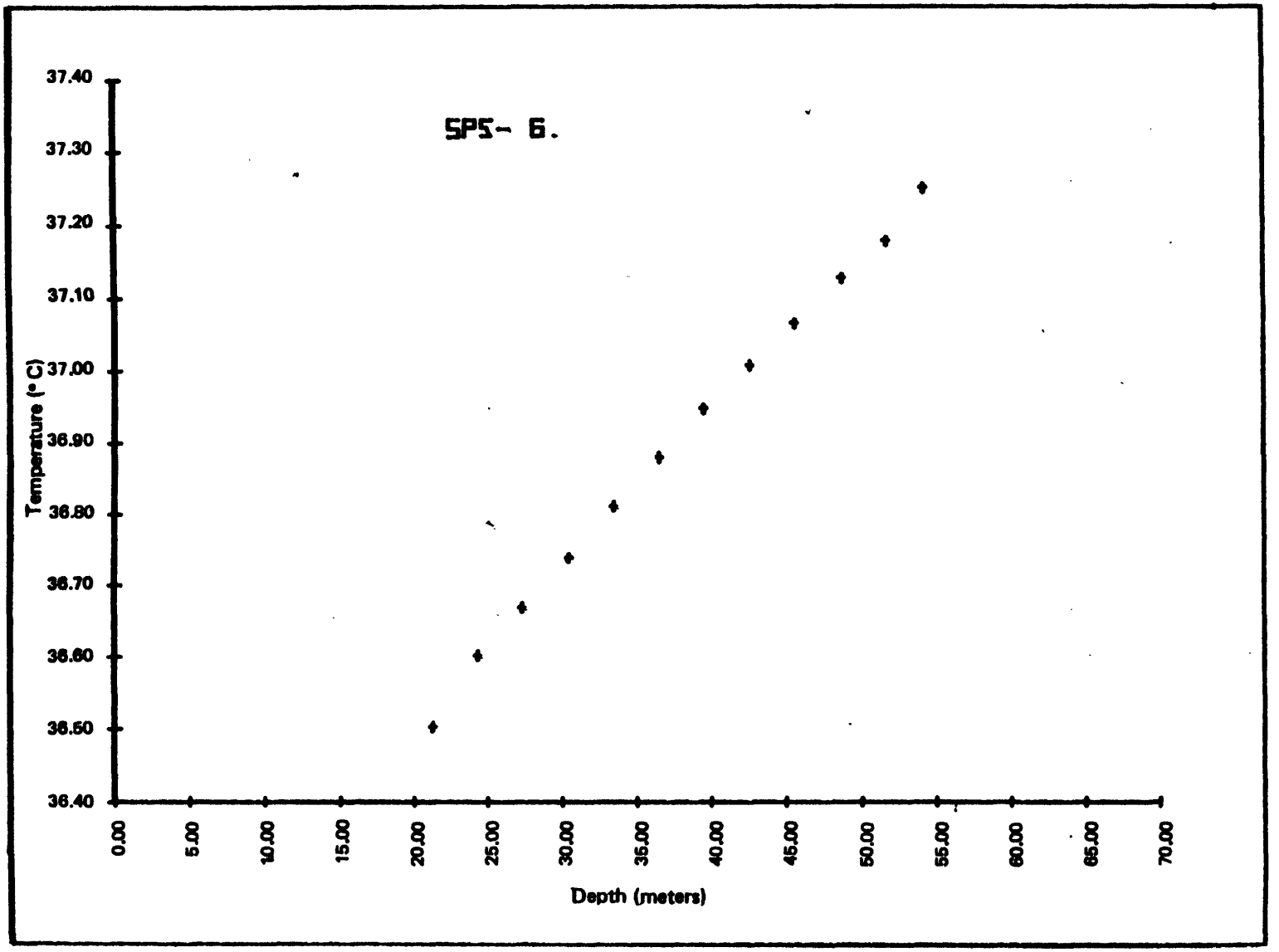

Figure 57.–Observed temperature versus depth profile for drill hole SP5-6.

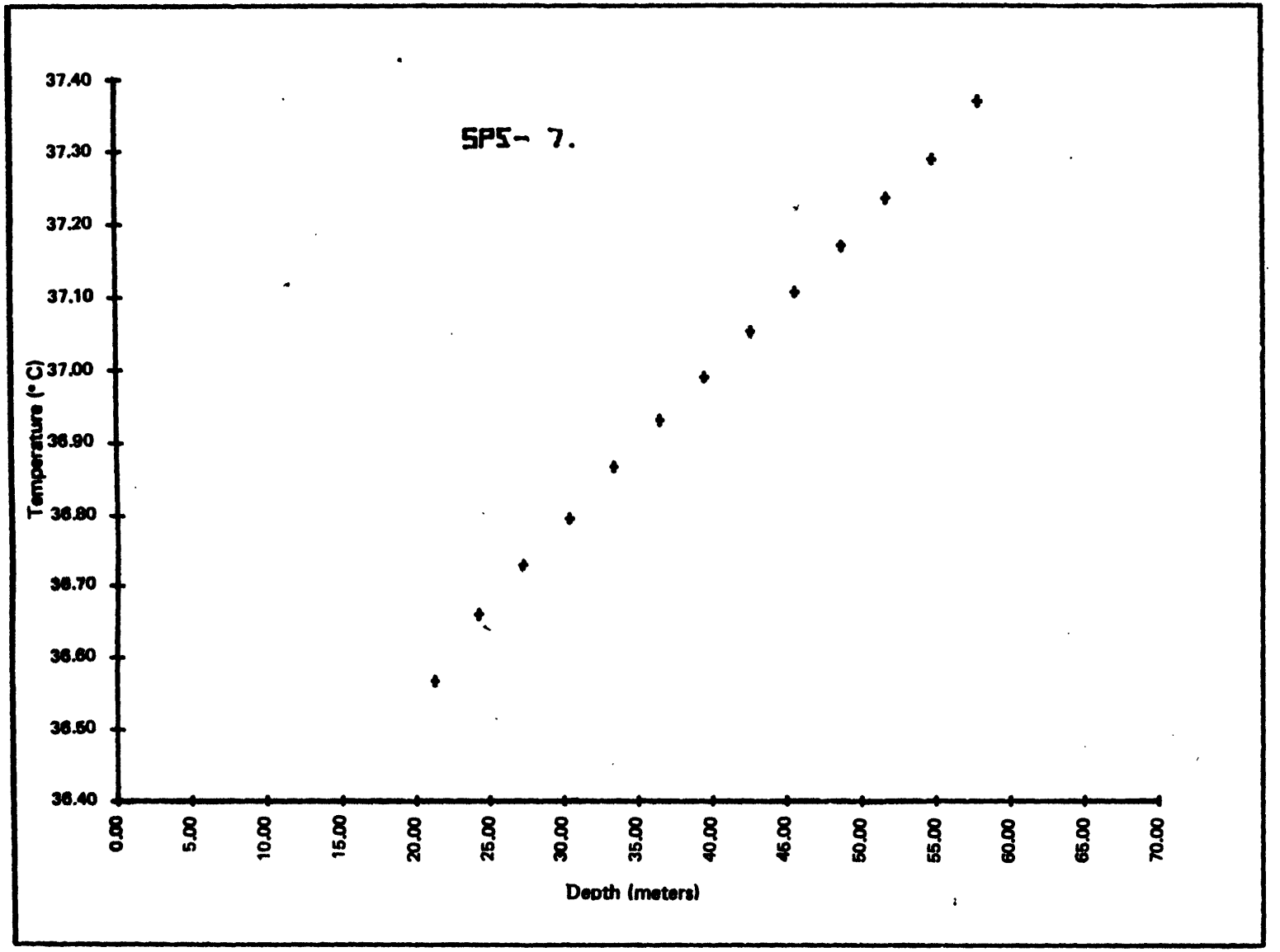

Figure 58.–Observed temperature versus depth profile for drill hole SP5-7.

An initial attempt to gain insight into conditions at the shot points consisted of constructing contour maps of the thermal gradients for the hole patterns as shown in figure 59. It should be noted that only shot point 1 shows strongly nonlinear behavior of the temperature-depth profiles; in this case, the fits of the 45- to 70-m-depth interval were used for contouring because they are most consistent among all the logs. Analysis of these maps suggests that the lithologic changes at shot points 2 and 3, with their consequent conductivity variations and three-dimensional heat flow, could adequately account for the variations in geothermal gradient. At shot point 3, for example, the meta-andesite xenolith, with a lower average conductivity than granite, should show higher observed thermal gradients than the granite, and this is the case. The same type of argument pertains to shot point 2.

At shot point 1, however, no significant lithologic variations are observed in the drill chips or electrical logs, and one immediately suspects ground-water movement. The same applies at shot point 5, where each row of holes gives a consistent but different thermal gradient. The fault zone is probably the agent responsible here, whereas at shot point 1 some sort of aquifer in the sedimentary sequence is the most likely possibility. In an effort to test the ground-water movement hypothesis, the treatment of Mansure and Reiter (1979) was attempted. In this method thermal gradients calculated for each measurement interval are plotted against temperature. In zones of ground-water motion, a line of nonzero slope should be obtained. The resulting plots are shown in figures 9 and 60-63 for shot point 1 and in figures 64 and 65 for shot point 5. For shot point 1, the results are ambiguous because there are "noisy zones" of approximately zero slope with immediate shifts to another level. At shot point 5 there is a definite nonzero slope, which is negative for holes SP5-1, SP5-2, and SP5-4, indicating downward flow (Mansure and Reiter, 1979), and positive for SP5-5, SP5-6, and SP5-7, indicating upward flow. The "noise" is normal in layered rocks of these types and reflects small variations in conductivity (Conaway, 1977; Conaway and Beck, 1977), but it makes interpretation difficult. For shot point 1, we interpret these curves, together with the correlation with the SP logs (see above), to indicate water flow above a depth of approximately 45 m, and we conclude that the only reliable gradients are those below this depth. This results in 14.74 ± 1.89°C/km as our best estimate of the geothermal gradient at shot point 1.

At shot point 5, the plot has no zero-slope segments, and although water flow is suggested, the estimate of the correct geothermal gradient is not. In figure 66, we have plotted all the temperature-depth profiles together. Those curves for holes interpreted to have downward flow are concave downward, while those in which upward flow is indicated are concave upward. These curves converge with depth on an asymptote, which we take as the best estimate from these data of the thermal gradient at shot point 5. The accepted geothermal gradient value for shot point 5 is 18.28 ± 2.0°C/km. At shot point 3, the accepted values are 13.04 ± 0.5°C/km for the meta-andesite and 11.64 ± 0.71°C/km for the granite. At shot point 2, our best thermal-gradient estimates are 10.28 ± 0.15°C/km for the schist and 8.22 ± 0.5°C/km for the granitoid.

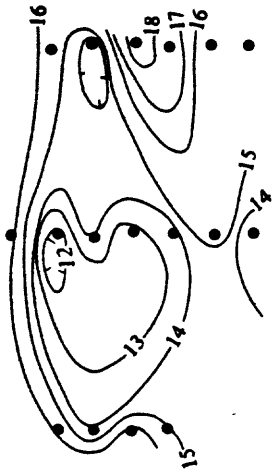

SHOT POINT 1

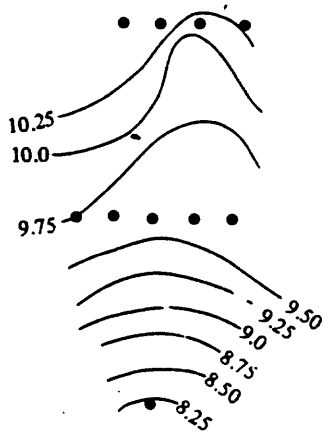

SHOT POINT 2

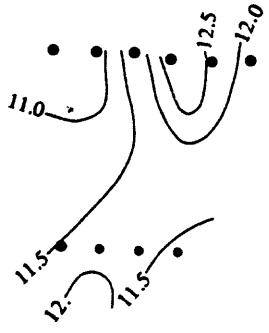

SHOT POINT 3

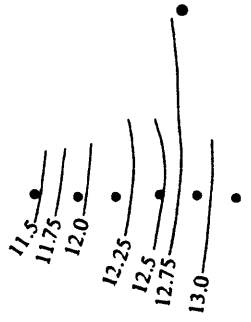

SHOT POINT 4

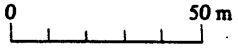

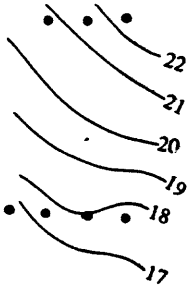

SHOT POINT 5

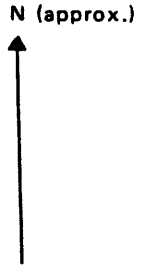

Figure 59.–Contour maps of thermal gradients determined by least-squares fits for the drill holes (solid dots) at shot points 1 to 5. At shot point 1, gradients from depths greater than 45 m have been used.

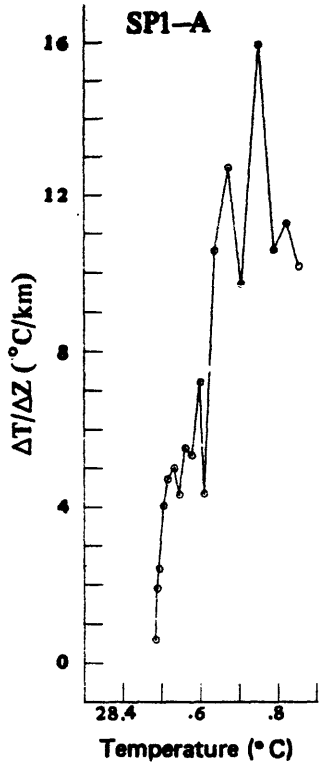

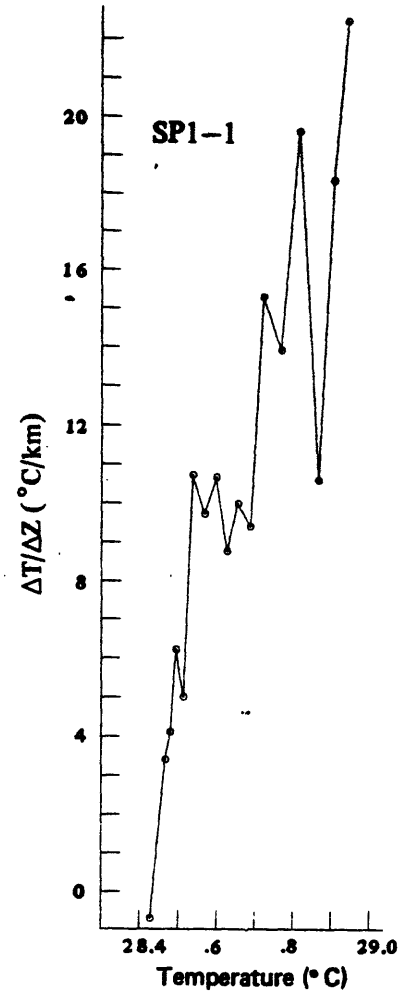

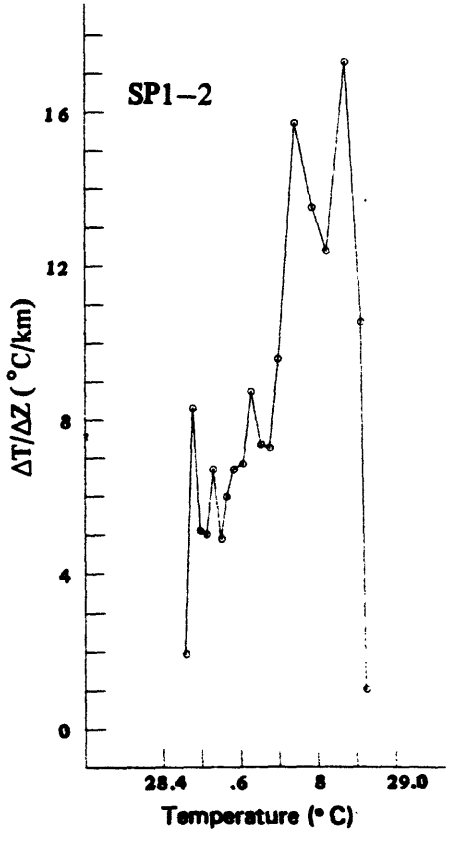

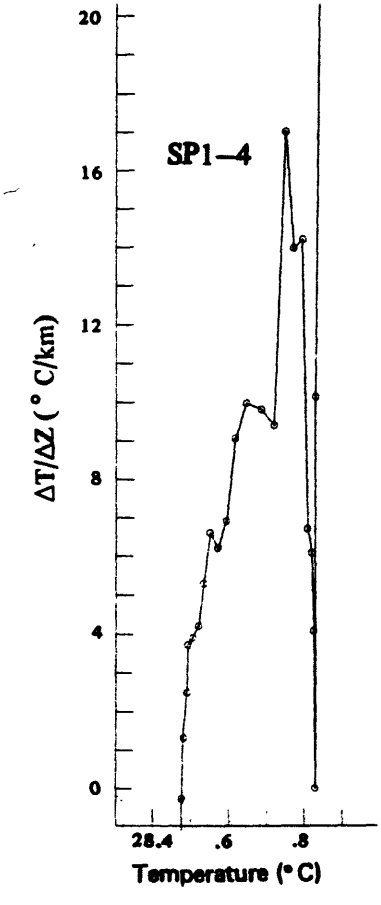

Figure 60.–Plots of observed thermal gradient versus temperature, drill holes SP1-A, -1, -2, and -4.

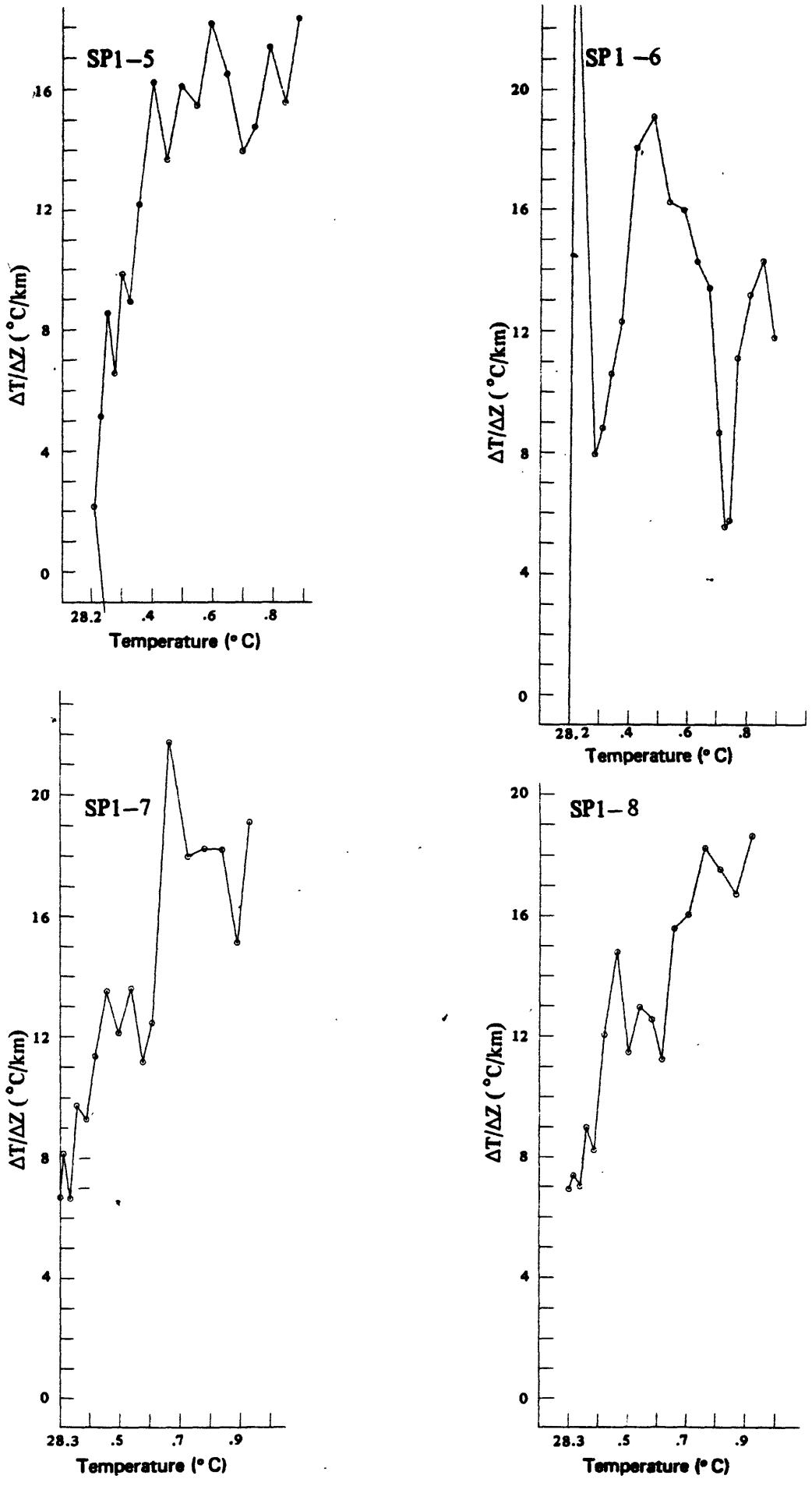

Figure 61.–Plots of observed thermal gradient versus temperature, drill holes SP1-5, -6, -7, and -8.

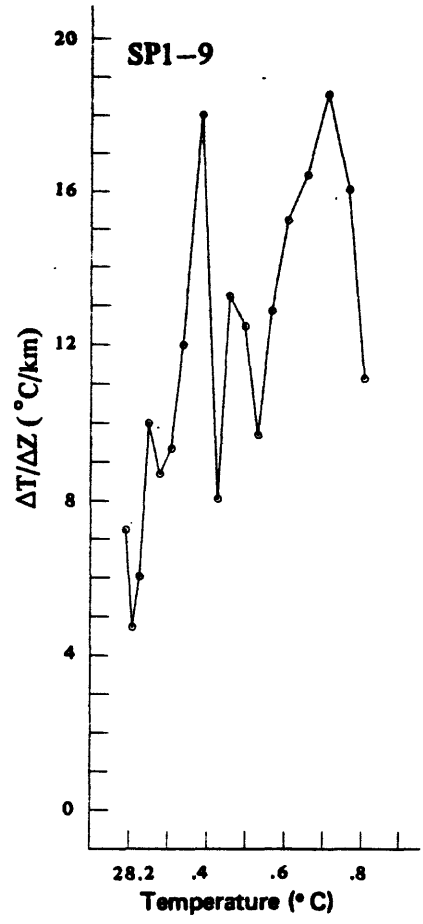

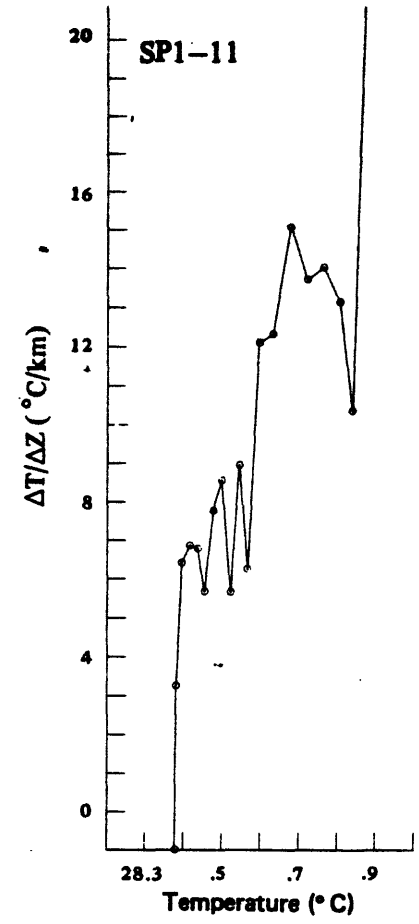

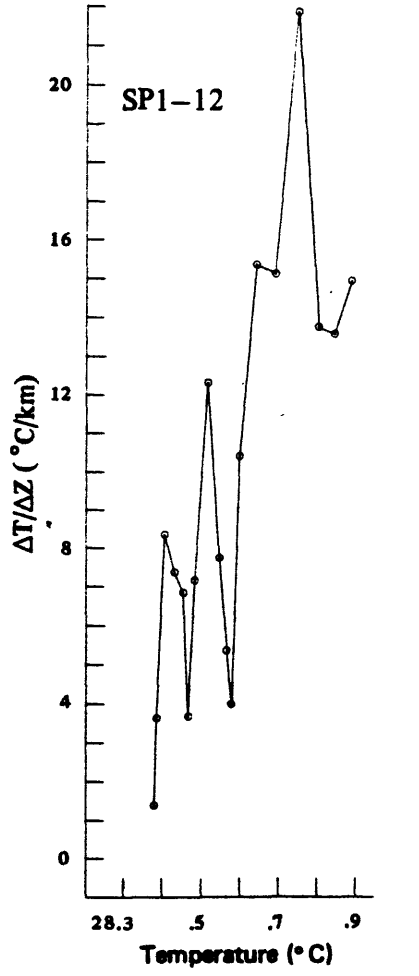

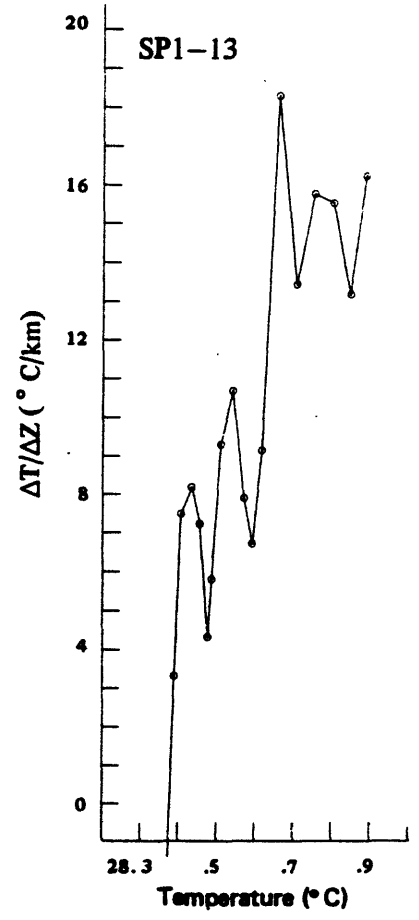

Figure 62.–Plots of observed thermal gradient versus temperature, drill holes SP1-9, -11, -12, and -13.

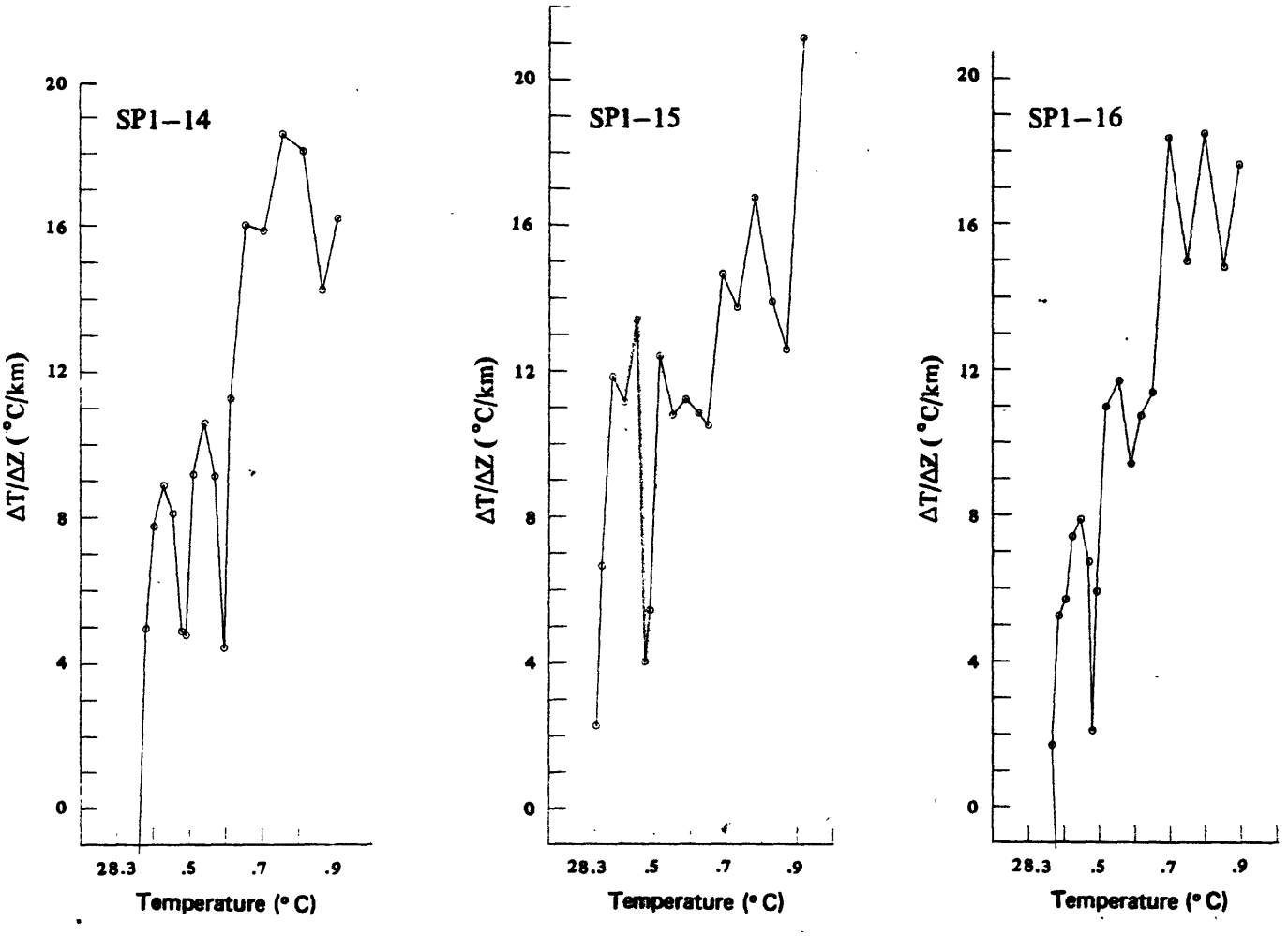

Figure 63.–Plots of observed thermal gradient versus temperature, drill holes SP1-14, -15, and -16.

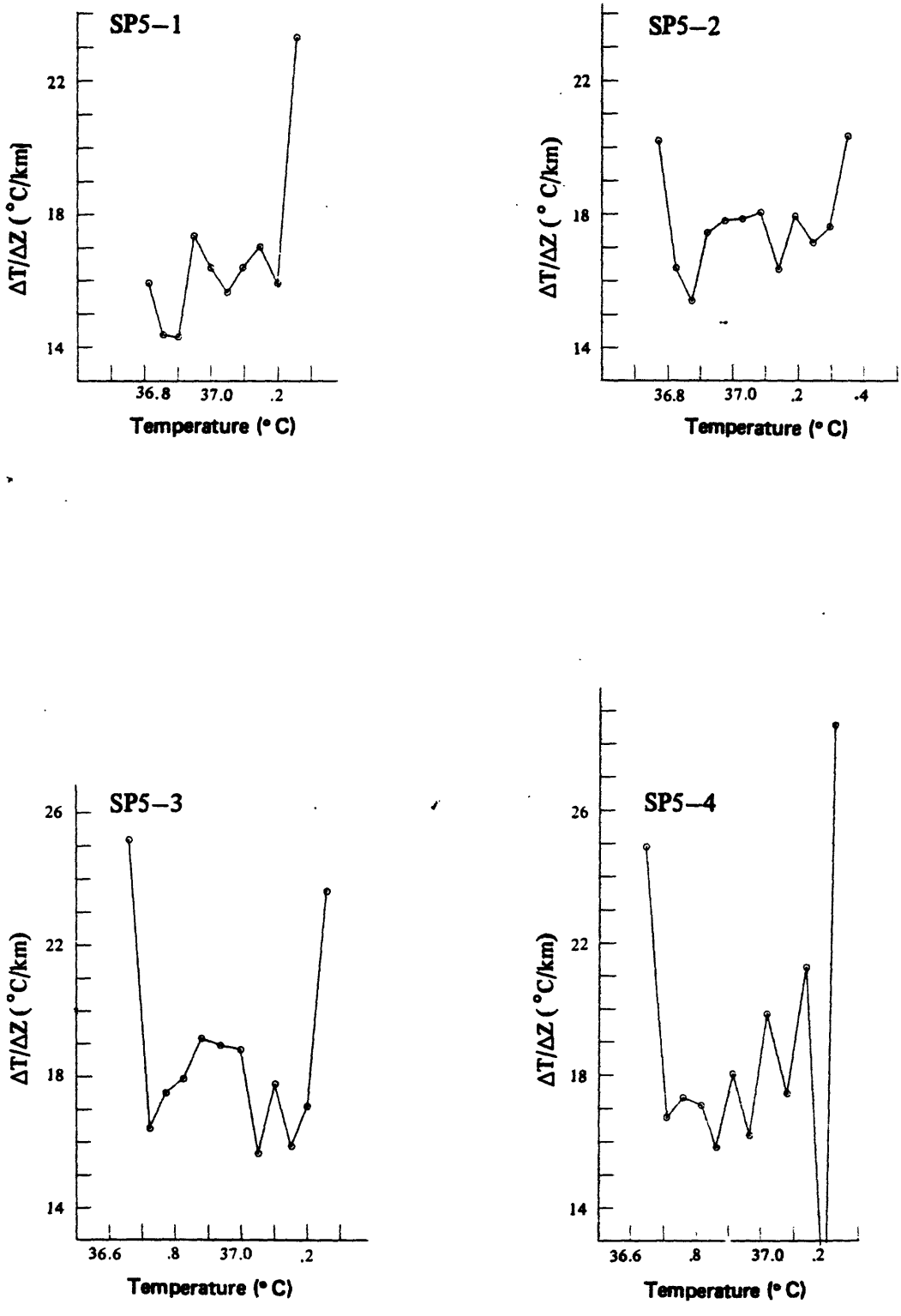

Figure 64.–Plots of observed thermal gradient versus temperature, drill holes SP5-1, -2, -3, and -4.

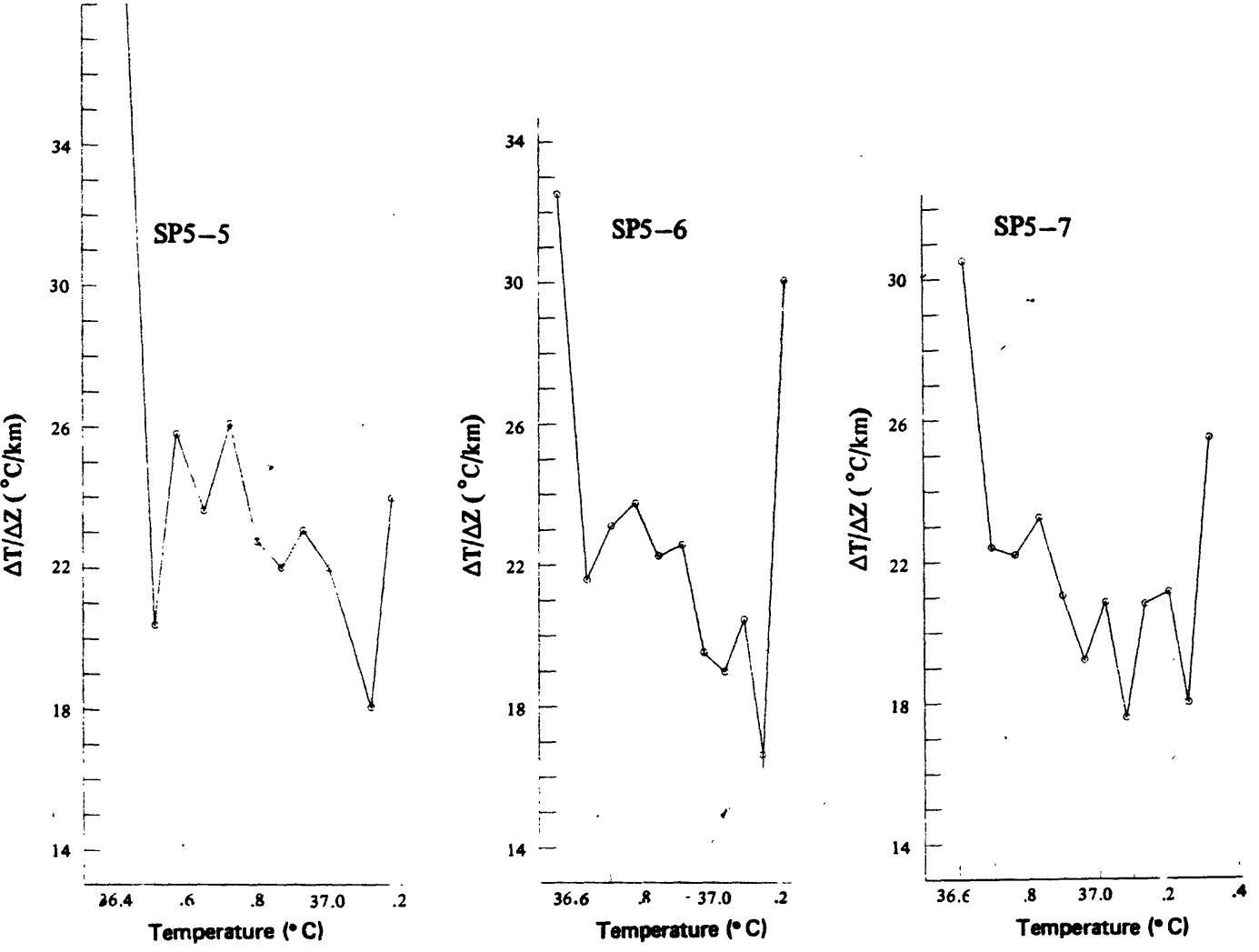

Figure 65.–Plots of observed thermal gradient versus temperature, drill holes SP5-5, -6, and -7.

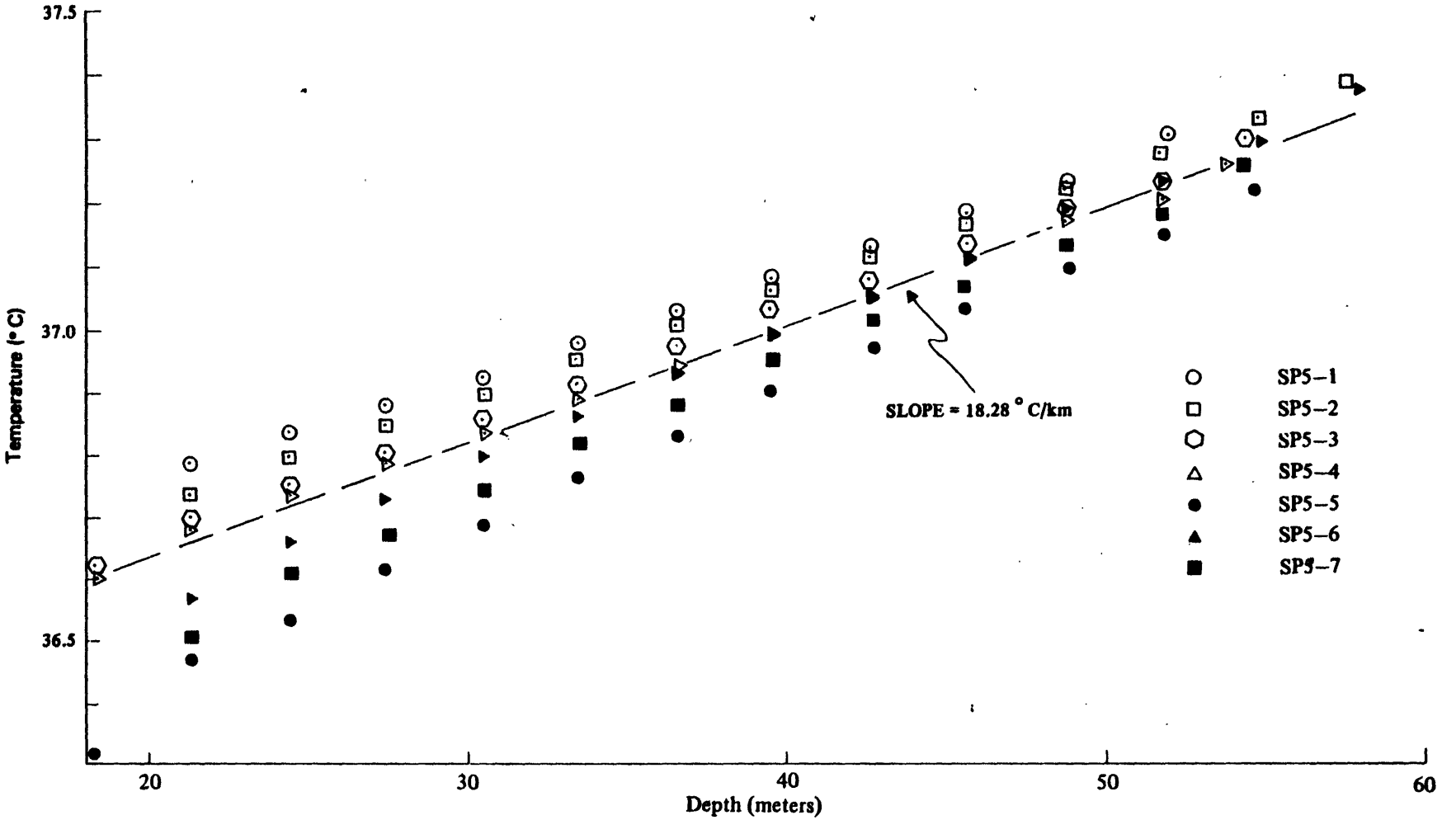

Figure 66.–Plot of temperature versus depth for the logs of drill holes at shot point 5, which shows convergence with increasing depth on the dashed line.

Shot point 5 is the only locality where the topographic effect is likely to be substantial. We have estimated this effect by approximating the valley of Wadi Itwad (fig. 8) by two 30° slopes, which bottom 15 m below the top of the holes and are displaced 65 m from the holes. Using the methods of Lachenbruch (1968), we find that the effect of the topography reduces the thermal gradient by 2 to 14 percent. For the gradients observed near the bottom of the hole, that is, the asymptotic values discussed above, this effect probably does not exceed 10 percent, within the estimated uncertainty of the gradient. If a 10 percent correction is applied, the geothermal gradient at shot point 5 is estimated to be 19.80±2.0°C/km.

THERMAL-CONDUCTIVITY AND HEAT-FLOW ESTIMATES

Thermal-conductivity estimates

Instrumentation for the measurement of thermal conductivity was not readily available for this work. Representative samples were sent for thermal-conductivity determinations to the USGS, Menlo Park, California, in March 1979, but the results have not yet been received. Thermal conductivities have been estimated from the modal mineral compositions of the rocks by several methods. This procedure ordinarily yields the thermal conductivity of the rock to within ±10 percent (Birch and Clark, 1940; Horai and Baldridge, 1972; Sibbitt and others, 1979). Estimates of thermal conductivity for the rocks of table 1 were computed using the thermal conductivity data of Horai (1971) for the individual mineral phases and the modal mineral compositions given in table 1.

Estimates were computed from the serial and parallel combinations of Birch and Clark (1940), the geometric-mean combination of Woodside and Messmer (1961), the Hashin-Shtrikman variational-bounds technique (Horai and Baldridge, 1972), and the continuous-phase formulation of Sibbitt and others (1979). The results of these estimates are presented in table 3, which shows that the variational-bounds technique and the continuous-phase formulation give results that generally are in excellent agreement and that are bracketed on the low side by the results of the serial and geometric-mean formulations and on the high side by the results of the parallel formulation. The values accepted were selected after comparison of published measured values (Clark, 1966; Sass and others, 1971a; Horai and Baldridge, 1972; Sibbitt and others, 1979, Smith and others, 1979) with the calculated ones. At shot point 1, the average value of thermal conductivity for shales for 17 sets of data, 6.28±0.72 $mcal\text{-}cm^{-1}\text{-}s^{-1}\text{-}°C^{-1}$ (Clark, 1966), was used.

The computed value of 12.90 $mcal\text{-}cm^{-1}\text{-}s^{-1}\text{-}°C^{-1}$ for the phyllite of shot point 5 corresponds to an isotropic conductivity. However, rocks such as phyllite are known to have highly anisotropic thermal conductivity (for example, Clark, 1966, p. 462), ranging from 4 to 6 $mcal\text{-}cm^{-1}\text{-}s^{-1}\text{-}°C^{-1}$ perpendicular to the foliation to about 14 $mcal\text{-}cm^{-1}\text{-}s^{-1}\text{-}°C^{-1}$ parallel with it. Fortunately, apparatus

Table 3. —*Thermal-conductivity estimates for specimens of table 1 computed from modal mineral proportions and individual mineral-conductivity data*

[See text for explanation. Conductivities are in units of mcal $cm^{-1}s^{-1}°K^{-1}$. Acpt value is the accepted value. Plag = plagioclase, qtz = quartz, kspar = potassium feldspar, chl = chlorite, hornbl = hornblende. -, indicates value not calculated]

Rock type	Specimen number	Serial	Parallel	Geometric	Variational k_μ	Variational k_ℓ	Variational k	Continuous phase[1/] k_{cp}	Continuous phase[1/] k_{cp}	Continuous phase[1/] k_{cp}	Acpt value	Ranges[2/]
Greenschist	SP2-1B	7.049	9.043	7.856	8.505	7.889	8.197	8.190 (plag+qtz)	-	-	8.19	4.1-8.9
Greenschist	SP2-1E	6.724	8.051	7.239	7.682	7.313	7.498	7.316 (plag+kspar)	7.425 (plag+qtz)	-	7.40	
Metatonalite	SP2-3	8.880	11.563	10.162	10.939	10.144	10.541	10.784 (qtz+plag)	10.93 (qtz)	-	10.65[3/]	6.2-9.0
Metagranite	SP2-5	9.934	11.975	10.965	11.523	10.999	11.261	11.436 (qtz+kspar)	-	-	11.35[3/]	(fresh)
Greenstone	SP3-4567	5.962	6.386	6.157	6.277	6.192	6.234	6.229 (hornbl)	-	-	6.23	4.1-6.6
Granite (alkali)	SP3-12	7.255	10.039	8.395	9.288	8.383	8.836	8.883 (kspar+qtz)	8.508 (kspar)	-	8.85	
Granite	SP3-12A	7.170	9.364	8.041	8.750	8.131	8.441	8.403 (qtz+kspar)	8.131 (kspar)	-	8.40	6.2-9.0
Granite	SP3-13	7.314	10.454	8.635	9.637	8.625	9.131	9.270 (qtz+kspar)	9.637 (qtz)	8.767 (kspar)	9.20	
Metadiorite	SP4-4	5.568	5.807	5.683	5.755	5.710	5.733	5.710 (plag)	5.730 (hornbl)	-	5.73	
Gneissic granite	SP4-6B	7.112	10.050	8.314	9.265	8.312	8.789	8.887 (qtz+kspar)	-	-	8.80	
Gneissic granite	SP4-8A	7.077	10.050	8.297	9.262	8.299	8.780	8.881 (qtz+kspar)	-	-	8.80	6.2-9.0
Gneissic granite	SP4-8B	6.617	9.218	7.631	8.501	7.653	8.077	8.131 (qtz+kspar)	-	-	8.10	
Phyllite	SP5-8	11.338	13.260	12.385	12.866	12.394	12.630	12.866 (qtz)	12.792 (qtz+chl)	12.730 (chl)	12.70	
Phyllite	SP5-14	11.846	13.645	12.838	13.275	12.835	13.055	13.210 (qtz+chl)	13.275 (qtz)	13.149 (chl)	13.10	6.5-14.0[4/]

1/ Estimates using various minerals (indicated in parentheses) as the continuous phase.
2/ Ranges of measured values given by Clark, 1966, p. 461-462.
3/ Chlorite alteration.
4/ Perpendicular and parallel to foliation.

for thermal-conductivity measurements became available in the late stages of this study, and a set of measurements of conductivity perpendicular to foliation (4.5 ± 0.9 mcal-cm^{-1}-s^{-1}-°C^{-1}) was obtained before instrument failure. A Showa Denko K. K. Shotherm QTM^{R}-D2 Quick Thermal Conductivity Meter was used. If the conductivity calculated from the modal mineral analyses is assumed to be a lower bound on the conductivity parallel with the foliation, the effective conductivity in the direction of the drill holes (vertical) relative to the 35° northeast- dipping foliation can be calculated. The formula given by Jaeger (1965, p. 20) was used and yields 10.10 ± 2.0 mcal-cm^{-1}-s^{-1}-°C^{-1} for the thermal conductivity at shot point 5.

Heat-flow estimates

The geothermal gradients and thermal-conductivity estimates, together with their uncertainties, and the resulting heat-flow values are summarized in table 4. For the final values at shot point 2, where two lithologies are represented, we have used the average value; the heat-flow values from the schist and granitoid are in agreement within their uncertainties, which are about 10 percent. At shot point 3, we have ignored the heat-flow values from the meta-andesite xenolith on the grounds that a three-dimensional heat-flow calculation is necessary here to adequately account for the geologic situation. We accept the value of 1.00 ± 0.12 HFU for the granite as our estimate of the heat flow at shot point 3. In figure 67, the accepted heat-flow values at each shot point have been plotted as a function of perpendicular distance from the Red Sea deep-water axis in the Farasan Islands area. The axial-trough and shelf values are taken from Girdler and Evans (1977).

The most striking feature of figure 67 is the trimodal distribution of heat-flow values. In the Red Sea, the heat-flow regimes seem to correlate with the known periods of active spreading. The axial trough, where crust has been created during the last 5 million years (Girdler and Styles, 1974; Hall and others, 1977), has the highest heat flow, about 4.5 HFU. The shelf areas, representing the Miocene phase of spreading (Girdler and Styles, 1974; Hall and others, 1977), have a heat flow of about 3.0 HFU (see also Girdler and Evans, 1977). Based on these limited data, the Arabian Shield appears to have an average heat flow of about 1 HFU. Although this value for the Shield is substantially below the worldwide mean heat flow of 1.4 HFU (Chapman and Pollack, 1975), it is not significantly different from the means for other Precambrian shield areas (Pollack and Chapman, 1977, table 1). Evidently the first-order feature to be explained by any lithospheric model of the Arabian Plate-Red Sea system is the three characteristic levels of heat flow; this task is undertaken in a companion report (Gettings, 1982).

Although shot point 5 is in the rocks of the Shield, it is so close to the oceanic plate that for the time periods in question, the rocks of the area have been heated nearly to oceanic plate values. For the other points in the Shield, we conclude only that the heat flow at shot points 1 and 2 may be somewhat lower than that at 3 and 4; uncertainties in the data preclude any definite conclusions. For most reasonable models of

Table 4.--*Heat-flow estimates from drill holes at shot points 1, 2, 3, 4, and 5*

Shot point	Latitude (north)	Longitude (east)	Altitude (meters)	Depth (meters)	Thermal Conductivity (mcal $cm^{-1}s^{-1}{}^{\circ}K^{-1}$)	Geothermal gradient ($^{\circ}K\ km^{-1}$)	Heat flow (HFU)	Geologic unit
SP1	26°16'12"	45°35'57"	692	43-70	6.28±0.72	14.74±1.89	0.93±0.16	Sudair Shale
SP2	23°17'28"	44°40'55"	887	17-69	7.80±0.78	10.28±0.15	0.80±0.08	Greenschist
					11.00±1.10	8.22±0.50[1/]	0.90±0.11	Granite
							0.85±0.07	Average
SP3	21°56'44"	43°34'16"	946	21-62	6.23±0.62	13.04±0.50[1/]	0.81±0.09	Metabasalt
					8.63±0.86	11.64±0.71	1.00±0.12	Granite
							1.00±0.12	Accepted value[2/]
SP4	20°05'13"	42°39'04"	1144	9-58	5.73±0.57	-	-	Metadiorite
					8.57±0.86	12.43±0.64	1.07±0.12	Granite
SP5	17°46'36"	42°20'47"	179	21-58	10.10±2.00	18.28,19.80[3/]±2.00	2.00±0.44	Phyllite

1/ Assumed value for uncertainty.
2/ Three-dimensional heat flow assumed to account for low value in metabasalt (see text).
3/ Value of 19.80 is terrain-corrected value (see text).

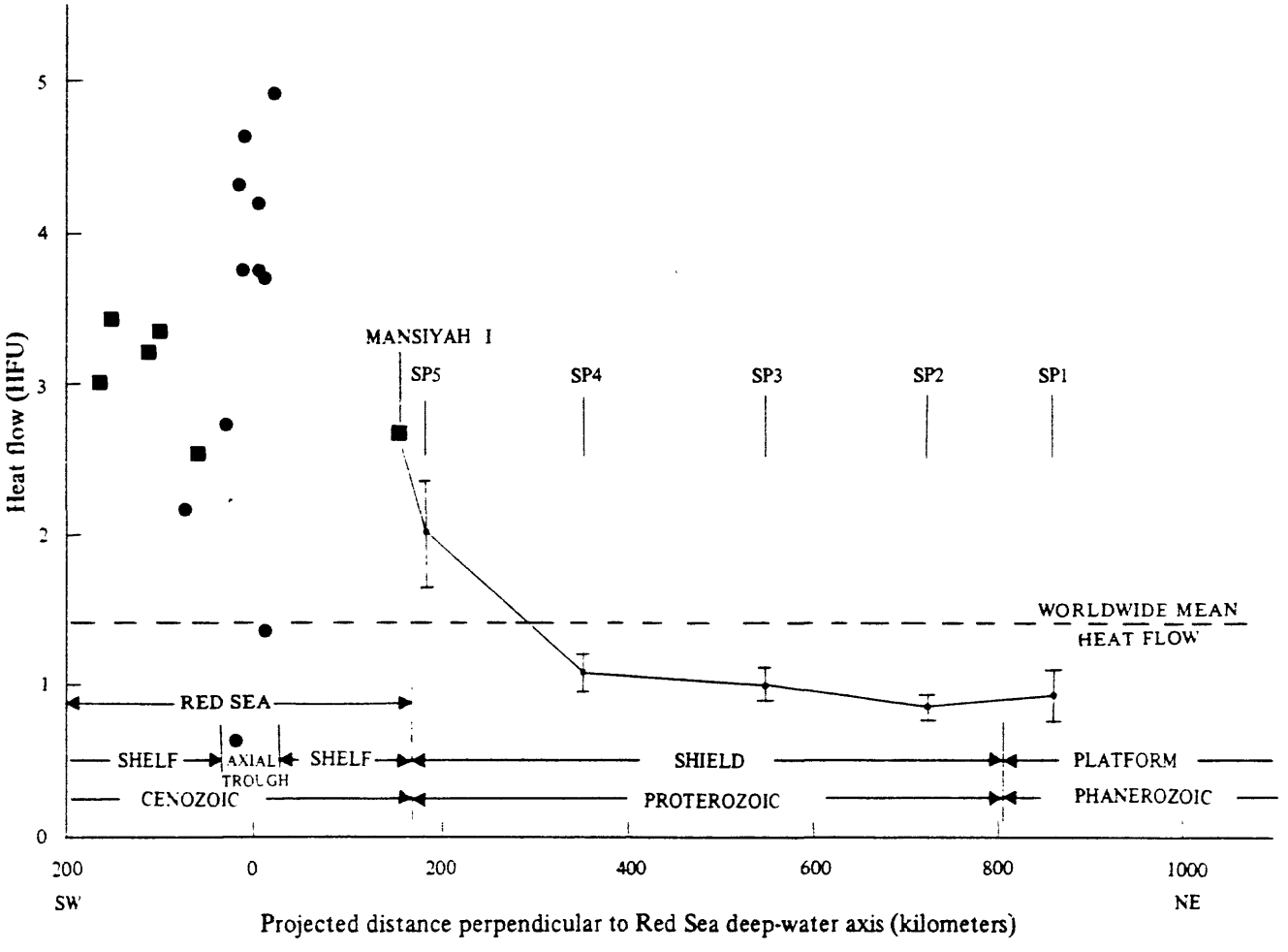

Figure 67.–Plot of heat flow as a function of distance from the axis of deep water in Red Sea (fig. 1). Heat-flow data for points other than shot points 1-5 are from Girdler and Evans (1977). (One HFU is 1E-6 cal cm^{-2} s^{-1} or 4.1868E-2 Wm^{-2}). Points in the Red Sea shown by a square are observations on the shelf area; those shown by a circle are observations in water more than 1 km deep.

Red Sea rifting, which postulate that the process has been going on for approximately the last 30 million years, and for an estimated crustal thickness of 40 km for the Shield (Blank and others, 1979), the thermal time constant (Lachenbruch and Sass, 1977) is such that only shot point 4 could possibly be "feeling" the thermal pulse from Red Sea rifting.

HEAT-PRODUCTION MEASUREMENTS

For shot points 2, 3, and 4, estimates of heat generation from potassium, uranium, and thorium in granitic country rock were made using gamma-ray spectrometry techniques. Laboratory determinations were not available, but a simple lead shield was constructed that enabled reasonably accurate determinations to be made using a field instrument. A Geometrics GR410 differential gamma-ray spectrometer was used; it has a GPX-21 detector that has a 3" x 3" NaI crystal. Samples were crushed to pea size or less and sealed in polyethylene bags for 2 weeks before counting. Samples weighing approximately 500 g were used. Samples were counted for 150 minutes in five 30-minute intervals, and 30-minute background counts (no sample present) were made at the beginning, between sample counts, and after completing the measurements on each sample. Sample counts were done in the period September 18-22, 1979.

The Compton "stripping ratios" for the instrument used have been well established by experimental runs with uranium and thorium sources at several concentrations. However, because of a lack of well-known standards, absolute sensitivity constants are not well known. Thus, our results are relatively precise but absolute concentrations reported are subject to systematic error. The heat generated by given concentrations of potassium (K, percent), uranium (U, ppm), and thorium (T, ppm) is given by $A = 0.317\ \rho\ (0.27K + 0.73U + 0.20T)$, where ρ is the density (assumed to be 2.70 gm cm^{-3}) and A is the heat generation in HGU ($cal\text{-}cm^{-3}\text{-}s^{-1}$ x 1E-13) (Birch, 1954).

A systematic error in determination of the concentrations of potassium, uranium, or thorium used in this equation will have the same effect on a plot of heat flow versus heat generation as changing the scale (units) of the heat-generation axis. The estimates of the intercept and slope of a linear relation will be changed, but if a linear relation between heat flow and heat generation exists, the data will still fall on a straight line.

The results of the gamma-ray spectrometry measurements are given in table 5. Uncertainties have been calculated using a standard propagation of errors method (Bevington, 1969) for all known sources of error and are believed to be realistic except for the systematic error. Heat flow is plotted against heat generation in figure 68, and although three points are too few for any firm conclusions, the plot certainly suggests that no linear relationship exists between the two. Considering the very active tectonism of this entire region from at least Miocene time until the present, lack of such a relationship is not surprising. On the contrary, we would expect that, as in other areas of active

Table 5. --*Thorium, uranium, and potassium abundances and heat production of granite specimens from shot points 2, 3, and 4 determined by gamma-ray spectrometry.*
[See text for details. Thorium and uranium abundances in ppm; potassium in percent]

Locality	Element	Gamma-ray emission (counts min^{-1})	Abundance	Heat Generation (HGU)	Total heat generation (HGU)
SP2	Thorium	1.768±0.282	9.3±1.5	1.60±0.26	
	Uranium	0.628±0.381	0.9±0.5	0.54±0.33	
	Potassium	13.212±0.818	1.53±0.20	0.35±0.05	
					2.49±0.42
SP3	Thorium	1.964±0.284	10.4±1.5	1.77±0.27	
	Uranium	0.997±0.375	1.4±0.5	0.85±0.32	
	Potassium	35.523±0.882	3.76±0.44	0.87±0.11	
					3.49±0.43
SP4	Thorium	0.914±0.296	3.5±1.1	0.60±0.19	
	Uranium	1.778±0.410	1.8±0.4	1.09±0.26	
	Potassium	40.411±0.982	3.37±0.39	0.78±0.09	
					2.47±0.33

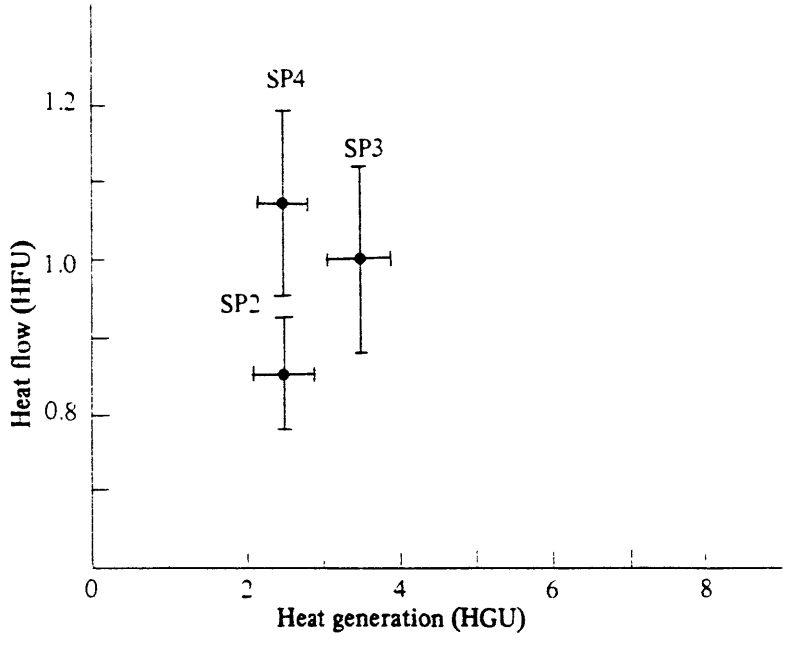

Figure 68.–Plot of heat flow versus heat generation for the three observations in granitic rocks of the Arabian Shield. Note the apparent lack of linear relation. (One HFU is 1E-6 cal $cm^{-2} s^{-1}$ or 4.1868E-2 Wm^{-2}; one HGU is 1E-13 cal s^{-1} cm^{-3} or 4.1868E-7 Wm^{-3}.)

lithospheric extension such as the Basin and Range province of the western United States (Lachenbruch and Sass, 1977), heat flow and heat production will be essentially uncorrelated.

SUMMARY

This study has established the first heat-flow observations on the Saudi Arabian Shield, and the five sites sample all the major tectonic elements of the Shield. To a first approximation, heat flow is constant across the Shield at about 1.0 HFU, except near the Tertiary rocks of the Red Sea rift, where heat flow has been increased by the emplacement of hot oceanic crust. Considerable insight into the age and tectonic processes of the Red Sea rift could be gained by a detailed heat-flow profile from the Tertiary crust of the rift inland toward shot point 4.

The present data suggest that no linear relationship exists between heat generation and heat flow for the plutonic rocks of the Arabian Shield. However, this conclusion is by no means established, and more measurements are essential to either confirm or reject it. Further, no conclusions regarding second-order structure in the heat-flow field of the Arabian Shield can be drawn until more observations are available.

Finally, as a function of distance from the axis of the Red Sea trough, the heat-flow profile consists essentially of three levels: about 4.5 HFU over the young oceanic crust (0 to 4.5 m.y. in age); about 3.0 HFU over the shelf (Miocene oceanic crust); and about 1.0 HFU in the Shield well away from the oceanic crust. A companion report (Gettings, 1982) deals with construction of a lithospheric model, which satisfies these relations as well as the constraints imposed by seismic refraction and gravity data.

REFERENCES CITED

Bevington, P. R., 1969, Data reduction and error analysis for the physical sciences: New York, McGraw-Hill, 336 p.

Birch, A. F., 1954, Heat from radioactivity, in Faul, Henry, ed., Nuclear geology: New York, John Wiley, p. 148-174.

Birch, A. F., and Clark, Harry, 1940, The thermal conductivity of rocks and its dependence upon temperature and composition: American Journal of Science, v. 238, p. 529-635; pt. 2, v. 238, p. 613-635.

Blank, H. R., Healy, J. H., Roller, John, Lamson, Ralph, Fisher, Fred, McClearn, Robert, and Allen, Steve, 1979, Seismic refraction profile, Kingdom of Saudi Arabia-field operations, instrumentation, and initial results: U.S. Geological Survey Open-File Report 79-1568, 49 p.

Brown, G. F., 1972, Tectonic map of the Arabian Peninsula: Saudi Arabia Directorate General of Mineral Resources Arabian Peninsula Map AP-2, scale 1:4,000,000.

Chapman, D. S., and Pollack, H. N., 1975, Global heat flow, a new look: Earth and Planetary Science Letters, v. 28, p. 23-32.

Clark, S. P., Jr., 1966, Handbook of physical constants: Geological Society of America Memoir 97, 587 p.

Coleman, R. G., Hadley, D. G., Fleck, R. G., Hedge, C. T., Donato, M. M., 1979, The Miocene Tihama Asir ophiolite and its bearing on the opening of the Red Sea, in Evolution and mineralization of the Arabian-Nubian Shield, v. 1: Oxford-New York, Pergamon, p. 173-185.

Conaway, J. G., 1977, Deconvolution of temperature gradient logs: Geophysics, v. 42, p. 823-837.

Conaway, J. G., and Beck, A. E., 1977, Fine-scale correlation between temperature gradient logs and lithology: Geophysics, v. 24, p. 1401-1410.

Fitch, F. H., 1978, Information lithostratigraphic lexicon for the Arabian Shield: Saudi Arabian Directorate General of Mineral Resources Technical Record TR-1978-1, 163 p.

Gettings, 1982, Heat-flow measurements at shot points along the 1978 Saudi Arabian seismic deep-refraction line, part 2: Discussion and interpretation: U.S. Geological Survey Open-File Report 82-794, 58 p. Open-File Report USGS-OF-02-40 (Interagency Report 444).

Girdler, R. W., 1970, A review of Red Sea heat flow: Philosophical Transactions of the Royal Society of London, v. 267, p. 191-204.

Girdler, R. W., and Evans, T. R., 1977, Red Sea heat flow: Geophysical Journal of the Royal Astronomical Society, v. 51, p. 245-251.

Girdler, R. W., and Styles, P., 1974, Two stage Red Sea floor spreading: Nature, v. 247, p. 7-11.

Hall, S. A., Andreasen, G. E., and Girdler, R. W., 1977, Total-intensity magnetic anomaly map of the Red Sea and adjacent coastal areas, a description and preliminary interpretation, in Red Sea Research 1970-1975: Saudi Arabian Directorate General of Mineral Resources Bulletin 22, p. F1-F15.

Horai, Ki-iti, 1971, Thermal conductivity of rock-forming minerals: Journal of Geophysical Research, v. 76, p. 1278-1308.

Horai, Ki-iti, and Baldridge, S., 1972, Thermal conductivity of nineteen igneous rocks, II: estimation of the thermal conductivity of rock from the mineral and chemical compositions: Physics of the Earth and Planetary Interiors, v. 5, p. 157-166.

International Union of Geological Sciences Subcommission on the Systematics of Igneous Rocks, 1973, Plutonic rocks, classification and nomenclature recommended by the IUGS Subcommission on the systematics of Igneous Rocks: Geotimes, v. 18, no. 10, p. 26-30.

Jaeger, J. C., 1965, Application of the theory of heat conduction to geothermal measurements, chapter 2, in Lee, W. H. J., ed., Terrestrial heat flow: American Geophysical Union, Geophysical Monograph 8, p. 7-23.

Lachenbruch, A. H., 1968, Rapid estimation of the topographic disturbance to superficial thermal gradients: Reviews of Geophysics, v. 6, p. 365-400.

Lachenbruch, A. H., and Sass, J. H., 1977, Heat flow in the United States and the thermal regime of the crust, in Heacock, J. G., ed., The Earth's crust: American Geophysical Union, Geophysical Monograph 20, p. 626-675.

Mansure, A. J., and Reiter, M., 1979, A vertical groundwater movement correction for heat flow: Journal of Geophysical Research, v. 84, p. 3490-3496.

Pollack, H. N., and Chapman, D. S., 1977, On the regional variation of heat flow, geotherms, and lithospheric thickness: Tectonophysics, v. 38, p. 279-296.

Powers, R. W., Ramirez, L. F., Redmond, C. D., and Elberg, E. L., Jr., 1966, Geology of the Arabian Peninsula--Sedimentary geology of Saudi Arabia: U.S. Geological Survey Professional Paper 560-D, 147 p.

Sass, J. H., Lachenbruch, A. H., and Munroe, R. J., 1971a, Thermal conductivity of rocks from measurements on fragments and its application to heat-flow determinations: Journal of Geophysical Research, v. 76, p. 3391-3401.

Sass, J. H., Lachenbruch, A. H., Munroe, R. J., Green, J. W., and Moses, T. H., 1971b, Heat flow in the western United States: Journal of Geophysical Research, v. 76, p. 6376-6413.

Schmidt, D. L., Hadley, D. G., and Stoeser, D. B., 1979, Late Proterozoic crustal history of the Arabian Shield, southern Najd province, Kingdom of Saudi Arabia, in Evolution and mineralization of the Arabian-Nubian Shield, v. 2: Oxford-New York, Pergamon, p. 41-58.

Sibbitt, W. L., Dodson, J. G., and Tester, J. W., 1979, Thermal conductivity of crystalline rocks associated with energy extraction from dry hot rock geothermal systems: Journal of Geophysical Research, v. 84, p. 1117-1124.

Smith, D. L., Nuckels, C. E., III, Jones, R. L., and Cook, G. A., 1979, Distribution of heat flow and radioactive heat generation in northern Mexico: Journal of Geophysical Research, v. 84, p. 2371-2379.

Vincent, G., 1968, Geology and mineral resources of the Halaban-Sabhah region (sheet 118, zone 2): Bureau de Recherches Geologiques et Minieres (Saudi Arabian Mission) Report 68-JED-1, 47 p.

Woodside, W., and Messmer, J. H., 1961, Thermal conductivity of porous media, I. unconsolidated sands: Journal of Applied Physics, v. 32, p. 1688-1699.

Appendix.--*Borehole depth and temperature measurement data at shot points along the seismic deep-refraction line*

SP1- A		SP1- 1		SP1- 2		SP1- 3		SP1-3A	
DEPTH M	TEMP. DEG.C	DEPTH M	TEMP. DEG.C	DEPTH M	TEMP. DEG.C	DEPTH M	TEMP. DEG.C	DEPTH M	TEMP. DEG.C
12.2	28.485	10.7	28.644	12.2	28.460	9.1	28.592	6.1	28.817
15.2	28.487	12.2	28.467	15.2	28.466	10.7	28.575	9.1	28.833
18.3	28.493	15.2	28.465	18.3	28.491	12.2	28.546	10.7	28.723
21.3	28.500	18.3	28.475	21.3	28.507	15.2	28.488	11.3	28.509
24.4	28.512	21.3	28.487	24.4	28.522	18.3	28.463	12.2	28.488
27.4	28.527	24.4	28.506	27.4	28.542	21.3	28.503	15.2	28.489
30.5	28.542	27.4	28.522	30.5	28.557	24.4	28.512	18.3	28.498
33.5	28.555	30.5	28.554	33.5	28.576	27.4	28.522	21.3	28.510
36.6	28.572	33.5	28.584	36.6	28.596	30.5	28.537	24.4	28.522
39.6	28.588	36.6	28.616	39.6	28.617	33.5	28.550	27.4	28.532
42.7	28.610	39.6	28.643	42.7	28.643	36.6	28.564	30.5	28.541
45.7	28.623	42.7	28.673	45.7	28.666	39.6	28.586	33.5	28.554
48.8	28.655	45.7	28.702	48.8	28.688	42.7	28.608	36.6	28.566
51.8	28.694	48.8	28.748	51.8	28.717	45.7	28.651	39.6	28.584
54.9	28.724	51.8	28.791	54.9	28.765	48.8	28.696	42.7	28.606
57.9	28.772	54.9	28.850	57.9	28.806	51.8	28.729	45.7	28.629
61.0	28.804	57.9	28.883	61.0	28.844	54.9	28.776	48.8	28.648
64.0	28.839	61.0	28.938	64.0	28.897	57.9	28.817	51.8	28.682
67.1	28.870	61.6	28.952	66.4	28.922	61.0	28.844	54.9	28.731
				67.1	28.923	64.0	28.879	57.9	28.771
						66.4	28.901	61.0	28.815
								64.0	28.861
								66.4	28.887

Appendix.–*Borehole depth and temperature measurement data at shot points along the seismic deep-refraction line* [continued]

SP1-3B		SP1- 4		SP1- 5		SP1- 6		SP1- 7	
DEPTH M	TEMP. DEG.C	DEPTH M	TEMP. DEG.C	DEPTH M	TEMP. DEG.C	DEPTH M	TEMP. DEG.C	DEPTH M	TEMP. DEG.C
11.2	28.655	6.1	28.725	9.1	28.356	9.1	28.404	12.2	28.077
12.2	28.498	7.6	28.665	12.2	28.215	12.2	28.192	15.2	28.279
15.2	28.491	9.1	28.530	15.2	28.221	15.2	28.272	18.3	28.299
18.3	28.498	12.2	28.475	18.3	28.237	18.3	28.297	21.3	28.324
21.3	28.509	15.2	28.474	21.3	28.263	21.3	28.324	24.4	28.344
24.4	28.520	18.3	28.478	24.4	28.283	24.4	28.356	27.4	28.373
27.4	28.532	21.3	28.486	27.4	28.313	27.4	28.393	30.5	28.402
30.5	28.541	24.4	28.497	30.5	28.340	30.5	28.448	33.5	28.436
33.5	28.553	27.4	28.509	33.5	28.377	33.5	28.507	36.6	28.477
36.6	28.563	30.5	28.522	36.6	28.427	36.6	28.556	39.6	28.514
39.6	28.584	33.5	28.538	39.6	28.469	39.6	28.605	42.7	28.556
42.7	28.609	36.6	28.558	42.7	28.518	42.7	28.649	45.7	28.590
45.7	28.632	39.6	28.577	45.7	28.565	45.7	28.690	48.8	28.628
48.8	28.648	42.7	28.598	48.8	28.620	48.8	28.716	51.8	28.694
51.8	28.681	45.7	28.626	51.8	28.670	51.8	28.733	54.9	28.749
54.9	28.733	48.8	28.656	54.9	28.713	54.9	28.751	57.9	28.805
57.9	28.764	53.3	28.701	57.9	28.758	57.9	28.785	61.0	28.860
61.0	28.813	56.4	28.730	61.0	28.811	61.0	28.825	64.0	28.907
64.0	28.861	57.9	28.755	64.0	28.358	64.0	28.868	66.4	28.952
66.4	28.892	59.4	28.777	66.5	28.903	67.1	28.904		
		61.0	28.798						
		62.5	28.809						
		64.0	28.818						
		65.5	28.824						
		65.8	28.824						
		66.1	28.827						
		66.4	28.840						

Appendix.–*Borehole depth and temperature measurement data at shot points along the seismic deep-refraction line* [continued]

SP1-8		SP1- 9		SP1-11		SP1-12		SP1-13	
DEPTH M	TEMP. DEG.C	DEPTH M	TEMP. DEG.C	DEPTH M	TEMP. DEG.C	DEPTH M	TEMP. DEG.C	DEPTH M	TEMP. DEG.C
12.2	28.140	12.2	28.279	12.2	28.377	12.2	28.379	9.1	28.669
15.2	28.282	15.2	28.301	15.2	28.374	15.2	28.383	12.2	28.392
18.3	28.303	18.3	28.315	18.3	28.384	18.3	28.394	15.2	28.387
21.3	28.325	21.3	28.334	21.3	28.404	21.3	28.419	18.3	28.397
24.4	28.347	24.4	28.364	24.4	28.425	24.4	28.442	21.3	28.419
27.4	28.374	27.4	28.391	27.4	28.445	27.4	28.463	24.4	28.444
30.5	28.399	30.5	28.419	30.5	28.463	30.5	28.474	27.4	28.466
33.5	28.436	33.5	28.456	33.5	28.487	33.5	28.496	30.5	28.480
36.6	28.481	36.6	28.511	36.6	28.513	36.6	28.534	33.5	28.497
39.6	28.516	39.6	28.536	39.6	28.530	39.6	28.558	36.6	28.526
42.7	28.556	42.7	28.576	42.7	28.558	42.7	28.574	39.6	28.558
45.7	28.595	45.7	28.614	45.7	28.577	45.7	28.587	42.7	28.582
48.8	28.629	48.8	28.644	48.8	28.614	48.8	28.618	45.7	28.603
51.8	28.676	51.8	28.683	51.8	28.651	51.8	28.665	48.8	28.631
54.9	28.725	54.9	28.730	54.9	28.698	54.9	28.711	51.8	28.686
57.9	28.781	57.9	28.780	57.9	28.739	57.9	28.778	54.9	28.727
61.0	28.834	61.0	28.836	61.0	28.782	61.0	28.820	57.9	28.776
64.0	28.885	64.0	28.885	64.0	28.823	64.0	28.862	61.0	28.823
67.0	28.941	67.1	28.920	67.1	28.854	67.1	28.907	64.0	28.863
				69.5	28.925			67.1	28.913

Appendix.–*Borehole depth and temperature measurement data at shot points along the seismic deep-refraction line* [continued]

SP1-14		SP1-15		SP1-16		SP2- A		SP2- 1	
DEPTH M	TEMP. DEG.C	DEPTH M	TEMP. DEG.C	DEPTH M	TEMP. DEG.C	DEPTH M	TEMP. DEG.C	DEPTH M	TEMP. DEG.C
9.1	28.722	12.2	28.328	10.8	28.414	24.4	30.095	21.3	30.039
12.2	28.385	15.2	28.335	12.2	28.374	27.4	30.133	24.4	30.083
15.2	28.378	18.3	28.356	15.2	28.379	30.5	30.158	27.4	30.127
18.3	28.393	21.3	28.392	18.3	28.395	33.5	30.191	30.5	30.152
21.3	28.417	24.4	28.426	21.3	28.413	36.6	30.223	33.5	30.184
24.4	28.444	27.4	28.466	24.4	28.435	39.6	30.252	36.6	30.215
27.4	28.469	30.5	28.479	27.4	28.459	42.7	30.278	39.6	30.244
30.5	28.484	33.5	28.495	30.5	28.480	45.7	30.306	42.7	30.271
33.5	28.498	36.6	28.533	33.5	28.486	48.8	30.335	45.7	30.300
36.6	28.526	39.6	28.566	36.6	28.504	51.8	30.364	48.8	30.328
39.6	28.558	42.7	28.600	39.6	28.538	54.9	30.395	51.8	30.353
42.7	28.586	45.7	28.633	42.7	28.573	57.9	30.425	54.9	30.371
45.7	28.600	48.8	28.665	45.7	28.602	61.0	30.456	57.8	30.411
48.8	28.634	51.8	28.710	48.8	28.635	64.0	30.484		
51.8	28.683	54.9	28.751	51.8	28.670	67.1	30.509		
54.9	28.731	57.9	28.802	54.9	28.726	68.1	30.527		
57.9	28.788	61.0	28.845	57.9	28.771				
61.0	28.843	64.0	28.883	61.0	28.828				
64.0	28.886	67.1	28.948	64.0	28.873				
67.1	28.935			66.5	28.917				

Appendix.--*Borehole depth and temperature measurement data at shot points along the seismic deep-refraction line* [continued]

SP2- 2		SP2- 3		SP2- 4		SP2- 5		SP2- 6	
DEPTH M	TEMP. DEG.C	DEPTH M	TEMP. DEG.C	DEPTH M	TEMP. DEG.C	DEPTH M	TEMP. DEG.C	DEPTH M	TEMP. DEG.C
24.4	30.098	24.4	30.100	24.4	30.069	15.2	29.971	9.1	29.861
27.4	30.137	27.4	30.143	27.4	30.113	18.3	30.015	12.2	30.064
30.5	30.164	30.5	30.172	30.5	30.140	21.3	30.046	15.2	30.005
33.5	30.195	33.5	30.204	33.5	30.172	24.4	30.090	18.3	30.033
36.6	30.222	36.6	30.235	36.6	30.200	27.4	30.131	21.3	30.062
39.6	30.252	39.6	30.264	39.6	30.232	30.5	30.157	24.4	30.105
42.7	30.281	42.7	30.295	42.7	30.263	33.5	30.189	27.4	30.149
45.7	30.306	45.7	30.322	45.7	30.296	36.6	30.218	30.5	30.175
48.8	30.355	48.8	30.352	48.8	30.326	39.6	30.247	33.5	30.205
51.8	30.376	51.8	30.383	51.8	30.353	42.7	30.283	36.6	30.230
54.9	30.400	54.9	30.406	54.9	30.377	45.7	30.314	39.6	30.261
57.9	30.418	57.9	30.426	57.9	30.418	48.8	30.343	42.7	30.298
61.0	30.456	60.2	30.461	58.9	30.430	51.8	30.371	45.7	30.327
61.1	30.458					54.9	30.401	48.8	30.359
						57.9	30.420	51.8	30.389
						61.0	30.466	54.9	30.418
						61.4	30.471	57.9	30.447
								59.7	30.468

Appendix.–*Borehole depth and temperature measurement data at shot points along the seismic deep-refraction line* [continued]

SP2- 7		SP2- 8		SP2- 9		SP3- 1		SP3- 2	
DEPTH M	TEMP. DEG.C	DEPTH M	TEMP. DEG.C	DEPTH M	TEMP. DEG.C	DEPTH M	TEMP. DEG.C	DEPTH M	TEMP. DEG.C
21.3	30.007	24.4	30.085	25.9	30.129	21.3	29.438	24.4	29.460
24.4	30.057	25.9	30.105	27.4	30.153	24.4	29.492	27.4	29.493
27.4	30.099	26.8	30.139	30.5	30.182	27.4	29.533	30.5	29.531
30.5	30.128	27.4	30.139	33.5	30.213	30.5	29.555	33.5	29.574
33.5	30.163	30.5	30.163	36.6	30.244	33.5	29.602	36.6	29.617
36.6	30.194	33.5	30.194	39.6	30.273	36.6	29.631	39.6	29.651
39.6	30.223	36.6	30.221	42.7	30.307	39.6	29.662	42.7	29.686
42.7	30.255	39.6	30.248	45.7	30.335	42.7	29.694	45.7	29.720
45.7	30.284	42.7	30.273	48.8	30.364	45.7	29.728	48.8	29.756
48.8	30.316	45.7	30.300	51.8	30.392	48.8	29.757	51.8	29.790
51.8	30.348	48.8	30.323	54.9	30.419	51.8	29.791	54.9	29.822
54.9	30.374	51.8	30.346	57.9	30.446	54.9	29.815	57.9	29.849
57.9	30.392	54.9	30.369	61.0	30.462	55.0	29.826	61.0	29.900
60.0	30.430	57.9	30.390	61.5	30.480			61.7	29.909
		61.0	30.421						
		61.3	30.425						

Appendix.–*Borehole depth and temperature measurement data at shot points along the seismic deep-refraction line* [continued]

SP3- 3		SP3- 4		SP3- 5		SP3- 6		SP3- 7	
DEPTH M	TEMP. DEG.C	DEPTH M	TEMP. DEG.C	DEPTH M	TEMP. DEG.C	DEPTH M	TEMP. DEG.C	DEPTH M	TEMP. DEG.C
6.1	28.569	21.3	29.393	24.4	29.423	21.3	29.408	12.2	29.513
15.2	29.581	24.4	29.446	27.4	29.451	24.4	29.460	21.3	29.448
21.3	29.450	27.4	29.472	30.5	29.483	27.4	29.499	24.4	29.495
24.4	29.500	30.5	29.497	33.5	29.526	30.5	29.531	27.4	29.521
27.4	29.528	33.5	29.561	36.6	29.564	33.5	29.573	30.5	29.560
30.5	29.567	36.6	29.605	39.6	29.599	36.6	29.613	33.5	29.598
33.5	29.602	39.6	29.636	42.7	29.631	39.6	29.648	36.6	29.636
36.6	29.640	42.7	29.674	45.7	29.659	42.7	29.683	39.6	29.669
39.6	29.667	45.7	29.714	46.8	29.692	45.7	29.719	42.7	29.703
42.7	29.699	48.8	29.757			48.8	29.752	45.7	29.734
45.7	29.731	51.8	29.788			51.8	29.778	48.8	29.770
48.8	29.767	54.9	29.827			54.9	29.822	51.8	29.809
51.8	29.800	55.4	29.835			56.1	29.836	54.9	29.839
54.9	29.829							57.9	29.868
56.3	29.859							61.0	29.885
								61.3	29.905

Appendix.–*Borehole depth and temperature measurement data at shot points along the seismic deep-refraction line* [continued]

SP3- 8		SP4- 1		SP4- 3		SP4- 4		SP4- 5	
DEPTH M	TEMP. DEG.C	DEPTH M	TEMP. DEG.C	DEPTH M	TEMP. DEG.C	DEPTH M	TEMP. DEG.C	DEPTH M	TEMP. DEG.C
21.3	29.404	12.2	29.627	15.2	29.530	12.2	29.549	15.2	29.522
24.4	29.450	15.2	29.606	18.3	29.554	15.2	29.544	18.3	29.552
27.4	29.484	18.3	29.635	21.3	29.593	18.3	29.561	21.3	29.589
30.5	29.530	21.3	29.666	24.4	29.632	21.3	29.585	24.4	29.631
33.5	29.561	24.4	29.697	27.4	29.661	24.4	29.621	27.4	29.669
36.6	29.594	27.4	29.733	30.5	29.699	27.4	29.663	30.5	29.708
39.6	29.625	30.5	29.770	33.5	29.740	30.5	29.704	33.5	29.749
42.7	29.656	33.5	29.815	36.6	29.783	33.5	29.749	36.6	29.797
45.7	29.692	36.6	29.858	39.6	29.818	36.6	29.786	39.6	29.839
48.8	29.733	39.6	29.897	42.7	29.856	39.6	29.824	42.7	29.879
51.8	29.766	42.7	29.937	45.7	29.895	42.7	29.849	45.7	29.916
54.9	29.795	45.7	29.979	48.8	29.929	45.2	29.902	48.3	29.941
55.5	29.797	48.8	30.013	50.9	29.967			50.4	29.981
		51.8	30.046						
		54.9	30.079						
		57.9	30.124						
		59.9	30.152						

Appendix.–*Borehole depth and temperature measurement data at shot points along the seismic deep-refraction line* [continued]

SP4- 9		SP4-10		SP5- 1		SP5- 2		SP5- 3	
DEPTH M	TEMP. DEG.C	DEPTH M	TEMP. DEG.C	DEPTH M	TEMP. DEG.C	DEPTH M	TEMP. DEG.C	DEPTH M	TEMP. DEG.C
9.1	29.527	15.2	29.530	21.3	36.788	21.3	36.738	18.3	36.620
12.2	29.538	18.3	29.543	24.4	36.836	24.4	36.799	21.3	36.697
15.2	29.510	21.3	29.572	27.4	36.880	27.4	36.849	24.4	36.747
18.3	29.534	24.4	29.605	30.5	36.924	30.5	36.896	27.4	36.800
21.3	29.567	27.4	29.645	33.5	36.977	33.5	36.949	30.5	36.855
24.4	29.601	30.5	29.680	36.6	37.027	36.6	37.004	33.5	36.913
27.4	29.642	33.5	29.714	39.6	37.075	39.6	37.058	36.6	36.971
30.5	29.679	36.6	29.750	42.7	37.125	42.7	37.113	39.6	37.028
33.5	29.718	39.6	29.786	45.7	37.177	45.7	37.163	42.7	37.076
36.6	29.752	42.7	29.818	48.8	37.225	48.8	37.217	45.7	37.130
39.6	29.789	45.7	29.852	52.0	37.300	51.8	37.269	48.8	37.178
42.7	29.827	48.8	29.895			54.9	37.323	51.8	37.230
45.7	29.861	51.8	29.928			57.7	37.381	54.4	37.292
48.8	29.892	54.9	29.969						
51.8	29.929								
54.9	29.968								
58.0	30.013								

Appendix.–*Borehole depth and temperature measurement data at shot points along the seismic deep-refraction line* [continued]

SP5- 4		SP5- 5		SP5- 6		SP5- 7	
DEPTH M	TEMP. DEG.C	DEPTH M	TEMP. DEG.C	DEPTH M	TEMP. DEG.C	DEPTH M	TEMP. DEG.C
18.3	36.605	18.3	36.318	21.3	36.502	21.3	36.566
21.3	36.681	21.3	36.468	24.4	36.601	24.4	36.659
24.4	36.732	24.4	36.530	27.4	36.667	27.4	36.728
27.4	36.784	27.4	36.609	30.5	36.738	30.5	36.795
30.5	36.836	30.5	36.681	33.5	36.810	33.5	36.866
33.5	36.885	33.5	36.760	36.6	36.878	36.6	36.930
36.6	36.940	36.6	36.830	39.6	36.947	39.6	36.989
39.6	36.989	39.6	36.897	42.7	37.006	42.7	37.052
42.7	37.050	42.7	36.967	45.7	37.064	45.7	37.106
45.7	37.103	45.7	37.034	48.8	37.126	48.8	37.169
48.8	37.167	48.8	37.094	51.8	37.177	51.8	37.234
51.8	37.197	51.8	37.149	54.3	37.250	54.9	37.288
53.8	37.253	54.6	37.215			58.0	37.369